Fundamental Studies of Bitumen Aeration

Juan Ma

Dissertation submitted to the faculty of the

Virginia Polytechnic Institute and State University

in partial fulfillment of the requirements for the degree of

Doctor of Philosophy

in

Mining Engineering

Roe-Hoan Yoon, Chair

Gregory T. Adel

Gerald H. Luttrell

William A. Ducker

Alan R. Esker

February 9, 2015

Blacksburg, Virginia

Keywords: wetting film, bitumen, air bubble, thinning, disjoining pressure

Fundamental Studies of Bitumen Aeration

Juan Ma

ABSTRACT

In the oil sand industry, bitumen is separated from sands by aerating the heavy oil so that it can float out of a flotation vessel, leaving the unaerated sands behind. A bubble-against-plate apparatus equipped with a high-speed camera has been developed to record the optical interference patterns of the wetting films formed on a flat surface and subsequently obtain the temporal and spatial profiles of the films offline using the Reynolds lubrication theory. The technique has been used to study the interaction mechanisms between air bubbles and bitumen. It has been found that the film thinning kinetics increases in the order of asphaltene, bitumen, and maltene, and that the kinetics increases sharply with increasing temperature.

In addition to obtaining kinetic information, the temporal and spatial profiles of the wetting films have been used to derive appropriate hydrodynamic information that can be used to determine the disjoining pressures (Π) in the wetting films. The results obtained in the present work show that $\Pi < 0$ for maltene and bitumen, while $\Pi > 0$ for asphaltene at temperatures in the range of 22 to 80 °C. The disjoining pressure data have been analyzed by considering the contributions from the hydrophobic and steric forces in addition to the classical DLVO forces. It has been found that the hydrophobic force increases with increasing temperature, which corroborates well with contact angle data. Dynamic contact angle measurements show that air bubbles attach on bitumen with relatively small contact angles initially but increase sharply to $>90^{o}$. The extent and the kinetics of contact angle change increase sharply with increasing temperature. These findings suggest that the primary role of temperature may be to increase

bitumen hydrophobicity and hence hydrophobic force, which is the driving force for bubble-bitumen interaction. A thermodynamic analysis carried out on the basis of the Frumkin-Derjaguin isotherm suggests that the disjoining pressure will remain positive (and hence no flotation) until the hydrophobic force becomes strong enough (due to temperature increase) to overcome the positive disjoining pressure created during the course of bitumen liberation.

Dedication

To Hongbo and Xuekai, for their love and support.

Acknowledgements

My most sincere gratitude goes to my dear advisor, Dr. Roe-Hoan Yoon, for his support and guidance throughout the course of my Ph.D. program; for his inspiration, suggestion, and encouragement in my research; and for sharing his philosophy in life.

Sincere thanks are also due to Dr. Gerald H. Luttrell, Dr. Gregory T. Adel, Dr. William A. Ducker, and Dr. Alan R. Esker for their valuable suggestions and guidance throughout the entire program.

Special acknowledgements go to Mr. Peter Cleyle and his associates at Suncor Energy, Inc., Alberta, Canada, who provided bitumen samples and technical guidance during the course of the project; and Prof. Zhenghe Xu and his colleagues at the University of Alberta for providing useful information, including sample preparation methods.

The financial support from the CONRAD Bitumen Production Fundamental Research Group in Canada is deeply appreciated.

I would like to extend my gratitude to colleagues and staffs of the Center for Advanced Separation Technologies (CAST), especially to Drs. Lei Pan and Zuoli Li for their advice, cooperation and training on how to use the equipment in our lab.

Finally, I would like to express my eternal gratitude to my parents, husband and son for their love and support.

Table of Contents

List of Figures

List of Tables

Chapter 1

Introduction

1.1 Background

Canadian oil sands reserves are estimated to contain as much as 1.7 to 2.5 trillion barrels of crude oil, of which about 170 billion barrels are economically recoverable using existing technologies. These numbers make Canada the third-largest country in the world in proven oil reserves, after Saudi Arabia and Venezuela. This huge oil sands resource would be sufficient to meet Canada's need for crude oil for 186 years at an oil consumption rate of 2.5 million barrels per day. Canada's oil sands deposits, covering 141,000 square kilometers (54,132 square miles), are located in three main regions within the province of Alberta: Peace River, Athabasca (Fort McMurray area) and Cold Lake. Among them, the Athabasca area, which is located in the northeast of Alberta, has the world's largest oil sands deposit.[1]

Oil sand, also known as tar sand, bituminous sand, or bitumen-impregnated sandstone/rock, is a type of unconventional petroleum deposit that contains a carbonaceous material with a high viscosity at reservoir temperature. This carbonaceous material is normally referred to as bitumen. At room temperature, bitumen, like cold molasses, is so viscous and difficult to flow that it must be treated to reduce its viscosity before it can be transported. In the upgraders and refineries, bitumen is further treated to produce usable fuels such as gasoline, jet fuel, heating oil and diesel fuel.

Formed 50 to100 million years ago and first discovered in 1715, Alberta's oil sands occur naturally as a mixture of sands, fines (- 44μm particles including silt, clay and other minerals), water and bitumen. It typically contains 7 to 14 wt.% bitumen, 3 to 5 wt.% water, and 83 to 88

wt.% solids. In an oil sand matrix, a film of water surrounds the sand grains, which in turn is surrounded by bitumen. A portion of the clays and fines are associated with the bitumen at the bitumen-water interface.[2]

Two predominant methods currently exist to extract bitumen from oil sands: surface mining followed by bitumen extraction and *in-situ* extraction. Surface mining, or open-pit mining, is used when oil sands are close to the surface, for deposits at a depth of less than 75 meters. Surface mining represents the most significant source for bitumen production and is currently the main extraction method. The problem, however, is that only about 20% of the oil sands are shallow enough to be recovered by surface mining. The other method, *in-situ* extraction, is used to recover oil sands that are hundreds of meters underground. Approximately, 80% of oil sands deposits are situated deeply underground and are only recoverable through *in-situ* technologies. Most *in-situ* methods involves injecting steam into the oil sands deposits to heat and soften the bitumen so that it can be pumped to the surface through wells. Steam-Assisted Gravity Drainage (SAGD) and Cyclic Steam Stimulation (CSS) are the two main *in-situ* methods. The present work is related to surface mining, which is detailed in the following sections.

1.2 Process Description

Numerous scientists and engineers have investigated economic and efficient ways to recover bitumen from oil sands. Among them, Dr. Karl Clark was the first to develop a successful extraction process in the 1920s.[3] His process, which is referred to as the Clark Hot Water Process, laid the foundation for today's oil sands extraction technologies. Despite some modifications over the ensuing decades, Clark's hot water process is still used in commercial operations by many oil sand operators.

Figure 1.1 shows a generic flow diagram of the bitumen recovery process.[4] The basic operations of bitumen production include mining, utilities, extraction, froth treatment, water management (tailings treatment) and upgrading, all of which are interrelated. For example, mining affects extraction and the extraction, in turn, affects upgrading. As shown in Figure 1.1, in commercial bitumen recovery, oil sands are mined in open-pit mines using large shovels and then carried by trucks to the crushers, where large clumps of oil sands are broken down into transportable sizes. The oil sands are then treated with a warm recycle process water to transform dry oil sands into a slurry in mixing boxes, stirred tanks, cyclo-feeders or rotary breakers. Initially, this slurry was then fed to tumblers; more recently, the tumblers have been replaced by pipelines, known as hydrotransport process, which helps reduce the cost of transporting ore from mine sites to processing plants. Whether in tumblers or hydrotransport pipelines, the lumps of oil sands are

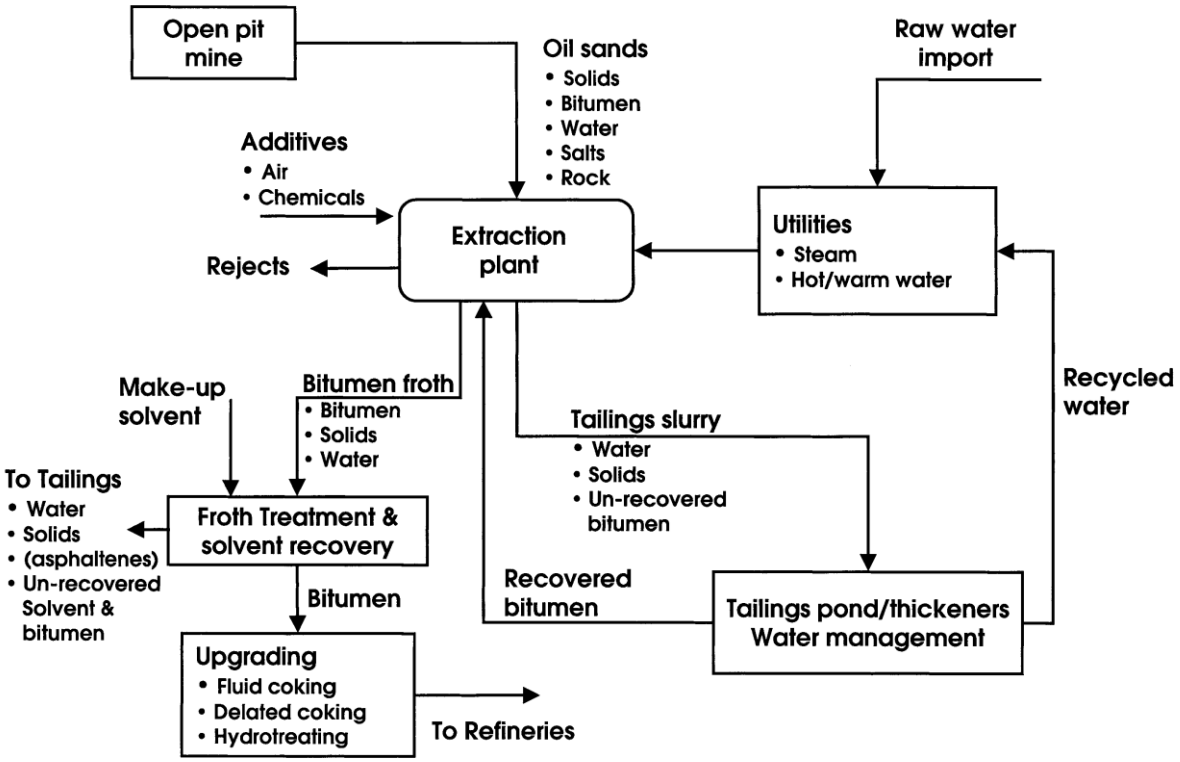

Figure 1.1 Generalized scheme for oil sands processing using water-based extraction processes.[4]

then broken and dispersed in water. While sand grains coated with bitumen are suspended in water, the bitumen is detached (or liberated), so that it can interact with air bubbles and become aerated. Chemical additives such as caustic soda can be added during the slurry conditioning stage.

The oil sand slurry is transported to large gravity separation vessels, known as primary separation vessels (PSV), in which the aerated bitumen float to the surface while unaerated sands sink to the bottom. The aerated bitumen floating to the top of the PSV is subsequently skimmed off from the slurry. Small amounts of bitumen (or middlings) not recovered via the PSV are recovered in a bank of mechanical flotation cells or cyclo-separators.[5]

The bitumen froth product, normally containing 60% bitumen, 30% water and 10% solids, is de-aerated, diluted with hydrocarbon solvents (usually naphtha) to reduce bitumen density and viscosity, and subsequently separated from the water and solids using centrifuge, cyclones, and/or lamella thickener in the froth treatment process. Naphtha is recovered so that it can be used again. Later, the diluted bitumen containing 1.5 to 2.5% water and ~0.4 to 0.6% solids is upgraded via a combination of thermal cracking and catalytic hydrocracking processes to obtain synthetic crude oils (SCO) and hydrocarbon gases. An alternative is to use a paraffinic solvent (mainly hexane) at a sufficiently high diluent-to-bitumen ratio to precipitate asphaltenes, forming composite aggregates that trap the water and solids in the diluted bitumen froth. In this way diluted bitumen with less than ~0.5% solids plus water can be obtained.[6]

Tailings from the extraction plant, which is a process byproduct composed of water, clay, sand, and small amount of residual bitumen, are then pumped to the tailings pond where water is recycled to be used in the extraction plant. At Sunsor and Syncrude (the two major oil sand companies in Canada), gypsum is added to mature fine solids to consolidate the fines together with coarse sands into a non-segregating mixture that is subsequently disposed of in a geotechnical

manner. At Albian (a relatively new oil sand company), cyclones are used, with the underflow (coarse tailings) being directly pumped into a tailings pond, while the overflow (fine tailings) pumped to thickeners where they are treated with flocculants, then thickened and finally discharged into a tailings pond.

The industrial bitumen-extraction process described above entails two fundamental steps: the liberation of bitumen from sand grains, and the aeration of liberated bitumen to air bubbles. Both steps are very important for the success of bitumen flotation. The bitumen liberation and subsequent stabilization against heterocoagulation between the released bitumen and sand or clay particles are prerequisites for bitumen flotation. NaOH is added to the slurry to create a weakly alkaline environment that favors the liberation of bitumen from oil sands. There is an optimum amount of added NaOH that leads to maximum bitumen recovery.[2] The role of added NaOH was reported to ionize organic acids in bitumen to generate natural surfactants, which are surface active species that facilitate bitumen liberation.[7]

Once the bitumen is liberated, bitumen aeration, which involves the attachment and engulfment of liberated bitumen to air bubbles, is critical to bitumen flotation since bitumen has almost the same density as water over the temperature ranges used in the extraction process. The attachment/engulfment of bitumen to air bubbles decreases the apparent density of bitumen so that it can float to the top of the separation cell and be collected.[1] Bitumen aeration occurs in the oil sand slurry conditioning stage, at which point liberated bitumen attaches to air bubbles entrained in oil sands or extra air bubbles added to the slurry, and in flotation cells used to extract remaining bitumen in the middlings from the primary separation cell. Research shows that the aeration of bitumen can also enhance the effective release of bitumen from sand grains.[8]

Despite the importance of bitumen aeration, several fundamental mechanisms involved in this process are still not fully understood. For example, what is the driving force for the attachment and subsequent engulfment of bitumen onto air bubbles? Does attachment have the same driving force as engulfment? Will the conditions favorable for bitumen liberation enhance bitumen aeration? What role will each bitumen component play in bitumen aeration? To answer these questions, the present work focuses on studies of bitumen aeration—mainly the thinning of the wetting film of water formed between bitumen and air bubble. Additionally, the engulfment of bitumen over air bubbles is described.

1.3 Bitumen Composition

The fact that so many chemicals are present in bitumen makes its chemistry complex. The elemental composition of bitumen differs from the crude source. Typically, bitumen contains carbon (80 to 88 wt.%) and hydrogen atoms (8 to 12 wt.%), affording a hydrogen-to-carbon (H/C) molar ratio of around 1.5, which is intermediate between that of aromatic structures and saturated alkanes.[9] In addition, bitumen contains heteroatoms such as sulphur (0 to 9 wt.%), nitrogen (0 to 2 wt.%), oxygen (0 to 2 wt.%), as well as trace metals such as vanadium (up to 2000 ppm) and nickel (up to 200 ppm). Sulfur, generally the most ubiquitous polar atom, appears in the form of sulfides, thiols, and to a lesser extent, sulfoxides; oxygen exists in the form of ketones, phenols and, to a lesser extent, carboxylic acids; and nitrogen in the form of pyrrolic and pyridinic structures. Most metals appear in the form of complexes such as metalloporphyrins.

Constituents of bitumen include maltenes and asphaltenes. Asphaltenes are defined as the insoluble part of bitumen in low molecular weight paraffins (*i.e.*, heptane, pentane, and hexane), but soluble in light aromatic hydrocarbons (*i.e.*, toluene and benzene). Maltenes are defined as the soluble part of bitumen in both types of solvents, which can be further separated into saturates,

aromatics, and resins. At present, the composition of bitumen is usually given in so-called SARA fractions, which refers to Saturates, Aromatics, Resins and Asphaltenes, as shown in Figure 1.2.

1.3.1 Maltenes

1.3.1.1 Saturates

Saturates have a H/C ratio close to 2, usually accounting for 5 to 15 wt.% of the total bitumen.[10] They contain a few crystalline n-alkanes, with a number-average molecular weight of about 600 g/mol. Fourier-Transform Infra-Red spectroscopy (FTIR) shows that different branching structures and some long aliphatic chains are present in saturates. At room temperature, they appear as a colorless or lightly colored liquid. Their density at 20 °C is around 0.9 g/cm^3.

1.3.1.2 Aromatics

Aromatics, also referred to as naphthene aromatics, are the most abundant components of bitumen; in fact, they account for 30 to 45 wt.% of the total bitumen. The carbon skeleton of an aromatic is slightly aliphatic with lightly condensed aromatic rings. Aromatics have a number-average molecular weight of about 800 g/mol, and at room temperature they form a yellow to red liquid. They are more viscous than saturates at the same temperature. They have a density close (inferior) to 1 g/cm^3 at 20 °C.[10]

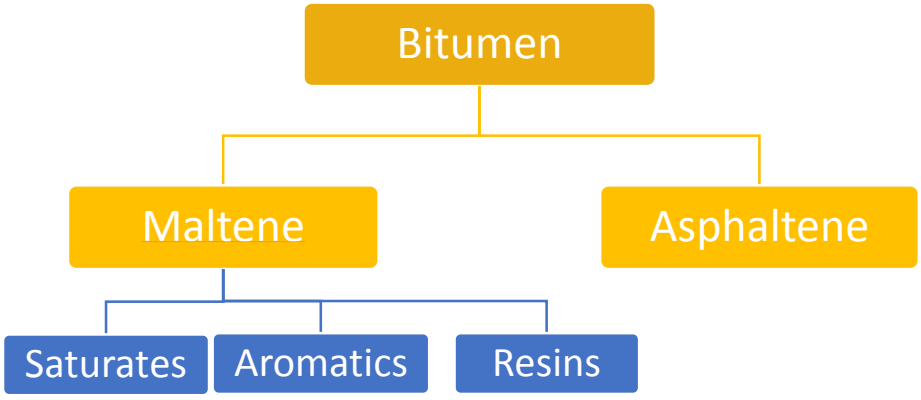

Figure 1.2 Separation of bitumen into its various components

1.3.1.3 Resins

Resins also account for 30 to 45 wt.% of the total bitumen; moreover, depending on choice of solvent they could even outnumber the percentage of aromatics. Resins have a H/C ratio between 1.38 and 1.69, with a number-average molecular weight of about 1100 g/mol.[10] It has been shown that resins have a similar composition to that of asphaltene, but exhibit a less condensed aromatic structure and a lower molar mass. They typically contain fused aromatic rings, with a most probable structure corresponding to 2 to 4 fused rings, and a few polar groups. When saturates and aromatics are oily liquids at room temperature, the resins form a black solid. Their density at 20 °C is close to 1.07 g/cm^3.

1.3.2 Asphaltenes

Asphaltenes represent a solubility class of macromolecules present in crude oil and bitumen. They have a H/C ratio between 0.98 and 1.56 depending on the asphaltene source, and usually gather traces of transition metals of the whole bitumen (*e.g.*, Ni, Va, Fe), thereby forming complexes such as metallo-porphyrins.[9] They account for 5 to 20 wt.% of the total bitumen. The molecular weight of asphaltenes has been controversial for decades, with estimates ranging from 700 to 3500 g/mol.[11] Some estimates of the average molecular weight of asphaltene are as high as 9500 g/mol.[12] Asphaltenes are by far the most studied bitumen fraction due to their viscosity-building role and their importance in the processing of crude oil. They exist as a black powder at room temperature and are largely responsible for the black color of bitumen. They have a density of about 1.15 g/cm^3 at 20 °C. Moreover, asphaltenes contain fused aromatic rings, most probably 4 to 10 fused rings, together with some pending aliphatic chains and polar groups such as carboxyl, amide, thiol, and hydroxyl groups.[9] In comparison to other bitumen molecules, asphaltenes contain

more condensed aromatic rings and more polar groups. Because of their many condensed aromatic rings, asphaltenes form almost planar molecules.

1.4 Thin Liquid Film

A thin liquid film (TLF) is formed when two interfaces of a liquid are brought into close proximity, normally a few hundred nanometers or less. TLFs are ubiquitous in industrial processes and among scholarly researchers, and also play a vital role in our daily lives. There are six types of TLF, which are categorized according to the phases of the interface:

1) Solid/liquid/solid film: A film confined between two solid surfaces, which is very common in colloidal chemistry. For instance, a water film between two quartz or mica surfaces is often studied as a model system by atomic force microscopy (AFM) to investigate surface forces. Another example is the oil film between rocks in an oil reservoir, which is of interest to the oil and gas industry.
2) Liquid/liquid/liquid film: A film between two liquid droplets that is immiscible with the liquid in between. This type of TLF is common in emulsions, such as milk (an emulsion of fat in water and proteins).
3) Gas/liquid/gas film: A foam lamella separating gas phases, which is frequently found in soap, shampoo, and the froth flotation industry.
4) Solid/liquid/liquid film: A film between a solid surface and a liquid surface. For instance, the water film between rock and oil in an oil reservoir.
5) Solid/liquid/gas film: A film between a solid and a gas bubble—*i.e.*, a wetting film. For example, the water film between a mineral particle and an air bubble in flotation.
6) Liquid/liquid/gas film: A film between a liquid surface and a gas bubble, such as the water film between an oil and air bubble.

There are many different types of TLFs associated with the bitumen extraction process: those between bitumen and air bubble, between bitumen and sand grain, between bitumen and clay particle such as kaolinite, illite or montmorillonite, between air bubble and sand grain, between air bubble and clay particle, between sand grain and clay particle, between two bitumen droplets, between two air bubbles, between two sand grains, and between two similar or different clay particles. In the present work, we focus on the wetting film between bitumen and air bubble. Other types of TLFs will only be discussed briefly (or not included in this study).

1.4.1 Disjoining Pressure

TLFs are known to be unstable and seek to thicken or thin themselves depending on the pressure in the film (P_{film}) relative to that in the adjacent bulk (P_{bulk}) of the same fluid under the same thermodynamic conditions. Such a difference is defined, originally by Derjaguin in 1955, as the "disjoining pressure" $\Pi(h)$,[13] h being the thickness of the TLF,

$$\Pi(h) = P_{film} - P_{bulk} \qquad [1.1]$$

Thermodynamically, disjoining pressure can be defined as the change in excess Gibbs free energy per unit area of a flat TLF (G) with the film thickness (h),[14, 15]

$$\Pi(h) = -(\partial G / \partial h)_{P,T,\mu_S} \qquad [1.2]$$

at constant pressure (P), temperature (T), and chemical potential of solutes (μ_s).

Disjoining pressure quantifies the driving force for spontaneous thinning or thickening of a film. With a positive disjoining pressure, *i.e.*, $\Pi > 0$, the film thickens; with a negative disjoining pressure, *i.e.*, $\Pi < 0$, it thins. When $\Pi = 0$, it is in an equilibrium state. The process of thickening is equivalent to separating (or "disjoining") its bounding surfaces, hence its name. When h becomes sufficiently large that the liquid in the film behaves the same as in the bulk, Π tends to be zero.

Disjoining pressure determines the stability of a TLF. A TLF should be stable thermodynamically when the disjoining pressure derivative is negative, *i.e.*, $\partial\Pi/\partial h < 0$. In other words, the disjoining pressure *vs. h* curve should have a negative slope. When the disjoining pressure derivative is positive, *i.e.*, $\partial\Pi/\partial h > 0$, a TLF should be unstable, thin by itself, and rupture catastrophically, such as the wetting film between a hydrophobic particle and an air bubble in flotation.

The most common method for measuring a film with a thinning thickness is to use optical interference techniques in conjunction with microscopy, which was originally developed by Derjaguin and Kusakov[16] to measure $\Pi > 0$. In 1967, Laskowski and Kitchener[17] recognized that the disjoining pressure in wetting films must be negative for bubble-particle attachment to occur in flotation. However, the authors recognized the difficulty of measuring negative disjoining pressure due to several reasons—principally fast kinetics of film thinning, deformation of the air/water interface, and complex interactions between hydrodynamic and surface forces. It was only recently that CAST developed a technique for measuring negative disjoining pressure using a modified thin film pressure balance (TFPB) technique with high-speed video microscopy.[18, 19] This new method is based on monitoring the profiles of the wetting films in nanoscale, and then analyzing the profiles using the Reynolds lubrication theory to determine various pressures. Such a technique is possible because bubbles deform in response to changes in pressure.

1.4.2 Disjoining Pressure Isotherm

As indicated in Eqs. [1.1] and [1.2], disjoining pressure Π is a function of the film thickness *h*. $\Pi(h)$, called the disjoining pressure isotherm, depends on the makeup of the film, the adjoining bulk phases and the interfaces between them.

There are many contributors to disjoining pressure. The classical Derjaguin-Landau-Verwey-Overbeek (DLVO) theory is based on the contribution from the van der Waals force present in a TLF (Π_d) and the electrostatic force between overlapping electrical double layers (Π_e), as shown below,

$$\Pi = \Pi_d + \Pi_e \qquad [1.3]$$

DLVO theory is used to explain the stability of a colloidal system, but only to a limited degree. Specifically, discrepancies between DLVO theory and experimental results have been reported in a number of cases,[20, 21] indicating that other contributions must also be considered, as shown in the following equation,

$$\Pi = \Pi_d + \Pi_e + \Pi_h + \Pi_s + \Pi_{hydration} + \Pi_H \ldots \qquad [1.4]$$

where Π_h, Π_s, $\Pi_{hydration}$, Π_H, represent the contribution from hydrophobic force, steric force, hydration force, and hydrogen bonding, respectively. There might be other forces as well, such as supramolecular structuring forces.

1.4.2.1 Van der Waals Force

Van der Waals dispersion forces are ever-present between two macroscopic objects and can be important both for both small and large separations. There are three origins for Van der Waals forces: 1) electrostatic interactions between permanent charge distributions in the molecules, such as dipoles, quadrupoles, *etc*. (Keesom's dipole – dipole interaction); 2) electrostatic interactions between permanent charge distributions and induced charge distributions (Debye's dipole – induced dipole interaction); and 3) the dispersion forces associated with the oscillations of the orbital electrons and interactions with the synchronous induced dipoles in neighboring molecules (London's fluctuating dipole-induced dipole interaction).[22]

Hamaker,[23] who was responsible for elucidating the mechanisms of the van der Waals interaction, suggested that the van der Waals force between two macroscopic objects could be obtained by adding up the forces acting between all the molecules in one body and all those in the other body. The Hamaker constant, *A*, which is often used in interaction laws, is conventionally defined as

$$A = \pi^2 C \rho_1 \rho_2 \qquad [1.5]$$

where ρ_1 and ρ_2 are the number of atoms per unit volume (number density) in the two bodies, and *C* is the coefficient in the atom-atom pair potential. Typical values for the Hamaker constants of condensed phases, either solid or liquid, are about 10^{-19} or 10^{-20} J for interactions in a vacuum or air. For gas phases, the Hamaker constant is generally taken to be zero due to the low molecular density in such media.

The pairwise additivity assumptions in Eq. [1.5] ignore the influence of neighboring atoms on the interaction between any pair of atoms. The Lifshitz theory[24] avoided the additivity problem and provided an alternative way to calculate the nonretarded Hamaker constant macroscopically for the interaction of material (1) and (2) in the medium (3), as shown below

$$A_{132} = \frac{3}{4} kT \left(\frac{\varepsilon_1 - \varepsilon_3}{\varepsilon_1 + \varepsilon_3}\right)\left(\frac{\varepsilon_2 - \varepsilon_3}{\varepsilon_2 + \varepsilon_3}\right) + \frac{3h_p \upsilon_e}{8\sqrt{2}} \frac{(n_1^2 - n_3^2)(n_2^2 - n_3^2)}{(n_1^2 + n_3^2)^{1/2}(n_2^2 + n_3^2)^{1/2}\left[(n_1^2 + n_3^2)^{1/2} + (n_2^2 + n_3^2)^{1/2}\right]} \qquad [1.6]$$

where *k* is Boltzmann constant, *T* is the absolute temperature (in Kelvin), h_p is the Planck's constant (6.63×10^{-34}J·s), υ_e is main electronic adsorption frequency (3×10^{15} Hz), n_1, n_2 and n_3 represent the refractive indices of the three media, and ε_1, ε_2, and ε_3 refer to the static dielectric constants of the three media. Eq. [1.6] is an approximate expression based on the assumption that the absorption frequencies of all three media are the same.

For the symmetric case of two surfaces composed of the same material (1) in a medium (3), one obtains

$$A_{131} = \frac{3}{4} kT\left(\frac{\varepsilon_1 - \varepsilon_3}{\varepsilon_1 + \varepsilon_3}\right)^2 + \frac{3h_p \upsilon_e}{16\sqrt{2}} \frac{(n_1^2 - n_3^2)^2}{(n_1^2 + n_3^2)^{3/2}} \quad [1.7]$$

Hamaker constant is often used to calculate the disjoining pressure in a TLF,

$$\Pi_d = -\frac{A_{132}}{6\pi h^3} \quad [1.8]$$

It is useful to consider the general situation of two different materials (1) and (2) in a liquid film (3). The former may be solids, liquids immiscible with (3) or gases, or any combination thereof. The Hamaker constant of the film for computation of the disjoining pressure isotherm is[25]

$$A_{132} = A_{12} + A_{33} - A_{13} - A_{23} \quad [1.9]$$

The first two terms consider the interactions of the adjoining phases with each other and the film molecules with themselves, while the last two consider the interaction of the film with its adjoining phases.

When dispersion forces dominate the interactions between two materials, the geometric mean combining rule is applicable, as shown below

$$A_{ij} = \sqrt{A_{ii} A_{jj}} \quad [1.10]$$

where *i* and *j* mean different materials. It should be noted that when the medium between two materials is with high dielectric constants, the use of combining rules is not recommended.

Substituting Eq. [1.10] to Eq. [1.9], one can obtain

$$A_{132} = (\sqrt{A_{11}} - \sqrt{A_{33}})(\sqrt{A_{22}} - \sqrt{A_{33}}) \quad [1.11]$$

From Eq. [1.11], one can easily find that for different materials, the Hamaker constant could be either positive or negative. According to Eq. [1.8], positive values suggest van der Waals

attraction, while negative values suggest van der Waals repulsion. If A_{33} is intermediate in value between A_{11} and A_{22}, the Hamaker constant will be negative, which is the case for flotation.

If the materials separating the liquid film are the same,

$$A_{131} = (\sqrt{A_{11}} - \sqrt{A_{33}})^2 \qquad [1.12]$$

A_{131} is thus always positive in spite of the relative values of A_{11} and A_{33}. Therefore, van der Waals interactions are always attractive for like materials, such as foam films and films between two like particles or liquid droplets. The greater the difference between Hamaker constants of the material and the medium, the greater the van der Waals attraction.

In bitumen flotation, where the case is bubble (1)-bitumen (2) interaction in the medium of water (3), the Hamaker constant of air bubble tends to zero ($A_{11} = 0$), as mentioned earlier, and the Hamaker constant of bitumen is greater than that of water ($A_{22} > A_{33}$). Therefore, the Hamaker constant of the film is negative ($A_{132} < 0$) according to Eq. [1.11], indicating repulsive van der Waals interactions between air bubbles and bitumen in flotation.

1.4.2.2 Electrostatic Force

Interfaces rarely carry a net charge. They are normally charged because of following mechanisms: 1) preferential adsorption/desorption of lattice ions, 2) specific adsorption of ions, 3) ionization of surface functional groups, 4) isomorphic substitution, and 5) depletion of electrons. When a surface acquires a charge, counterions gather in the vicinity of the charged surface and neutralize the charge, forming an "electric double layer." If two surfaces bearing an electric double layer approach one another, their overlap can contribute to the total disjoining pressure.

The electrical double-layer interaction between a particle and an air bubble can be determined from the Poisson-Boltzmann equation, as shown below:

$$\varepsilon\varepsilon_0\nabla^2\psi = -e\sum z_i n_i(\infty)\exp\left(-\frac{ez_i\psi}{kT}\right) \qquad [1.13]$$

where ε is the dielectric constant of the solution, ε_0 is the permittivity of vacuum, ψ is the potential, e is the charge on electron, $n_i(\infty)$ is the number per unit volume of the electrolyte ions of type i with valence z_i. Two boundary conditions are needed to solve the Poisson-Boltzmann equation.

The electrical double-layer interaction also depends on the charging mechanisms at the surfaces. Three cases are considered:

1) Both surfaces at constant surface potentials.

In this case, the surface potentials are known and remain the same for all separations. Zeta potential is often used rather than surface potential. The disjoining pressure between a particle and an air bubble can be calculated using the Hogg-Healey-Fuerstenau (HHF) approximation:[26, 27]

$$\Pi_e = -\frac{\varepsilon\varepsilon_0\kappa^2}{2\sinh(\kappa h)}\left[(\psi_1^2+\psi_2^2)\cos ech(\kappa h) - 2\psi_1\psi_2\coth(\kappa h)\right] \qquad [1.14]$$

where κ is the reciprocal Debye length, ψ_1 and ψ_2 are the zeta potentials at the solid/water and air/water interfaces, respectively. Eq. [1.14] holds exactly for surface potentials less than $25/z_i$ mV (the condition of the Debye-Hückel linearization) and for small-scaled separations (the condition of the Derjaguin approximation). A comparison between the HHF expression and the exact solution of the Poisson-Boltzmann equation shows that even at 75 to 100 mV the divergence is not excessive except for very short distances between the surfaces.[26]

For two surfaces with potentials of the unlike sign, the interaction is attractive to each other at all separation distances, as expected. For two surfaces with potentials of the same sign but of unequal magnitude, the interaction is repulsive at large separations, but attractive at small

separations. When the surfaces have potentials of the same sign and of equal magnitude, the interaction is repulsive at all separations.[27]

2) Both surfaces at constant surface charges.

If a system cannot regulate its charge during the interaction, a constant charge interaction is appropriate. In this case, charge per unit area on the surfaces (charge densities) remains constant. The disjoining pressure is given by[28]

$$\Pi_e = \frac{\varepsilon\varepsilon_0\kappa^2}{2}\frac{2\psi_{1\infty}\psi_{2\infty}\cosh(\kappa h)+\psi_{1\infty}^2+\psi_{2\infty}^2}{\sinh^2(\kappa h)} \qquad [1.15]$$

Where $\psi_{1\infty}$ and $\psi_{2\infty}$ are the zeta potentials at the isolated solid/water and air/water interfaces before the interaction, respectively.

When the two surfaces have unlike sign charges of unequal magnitude, the interaction is attractive at large separations, but becomes repulsive at small separations. When the two surfaces are of unlike sign charges with equal magnitude, the interaction is attractive at all separations. When the two surfaces have the same sign charges, the interaction is repulsive at all separation distances.[29]

3) One surface at constant potential and the other at constant charge.

In this case, one surface has constant potential at all separations while the other has constant surface charge. The disjoining pressure can be obtained by[29]

$$\Pi_e = \frac{\varepsilon\varepsilon_0\kappa^2}{2}\frac{2\psi_1\psi_{2\infty}\sinh(\kappa h)+(\psi_1^2-\psi_{2\infty}^2)}{\cosh^2(\kappa h)} \qquad [1.16]$$

The electrical double-layer interaction in this case falls between that at constant potential and at constant charge. As shown above, for two surfaces having the same initial potential, the electrostatic interactions are different for systems due to the differences in the charging mechanisms of their surfaces.

Given the fact that the third case is complicated, the first and second cases have been favored in scholarly research. The constant potential case (#1) represents an ideal regulation of the surface charge. When the surface charge cannot be regulated during the interaction, a constant charge model should be used. In flotation, if a particle slides over an air bubble, the location of the particle-bubble interaction sites changes continuously, making it difficult to achieve a perfect regulation of the surface charge. In such cases the interaction at constant surface charge is more appropriate than at constant surface potential. If the location of the particle-bubble interaction does not change over the bubble surface, constant surface potential interaction may occur.

According to Eqs. [1.14] to [1.16], one must know surface potential to calculate the electrostatic double-layer interaction. Surface potential is often substituted by zeta potential, which can be measured by electrokinetic methods such as electrophoresis, electroosmosis, or streaming potential. In bitumen flotation, the zeta potential of bitumen emulsion is mainly measured using electrokinetic methods. Research shows that the bitumen zeta potential becomes increasingly more negative when the solution pH increases from 4 to 6, but then levels off at pH>8.[30, 31] The iso-electric point of bitumen in water has been reported to be about pH = 3.

Measuring the zeta potential of gas bubbles is more difficult than that of solid particles due to the inconveniencies associated with the generation of gas bubbles in the measuring cells and the rise of bubbles in liquid solutions. Different values have been reported depending on the solution pH, electrolyte concentration, surfactant addition, *etc*.[32-37] In general, gas bubbles are negatively charged in pure water and inorganic solutions such as NaCl and KCl at pH > 2-3. The magnitude of the zeta potential decreases with increasing salt concentration, suggesting that Na^+, K^+, Cl^- ions act as indifferent ions that control the effective diffuse layer thickness, but do not specifically adsorb on the gas-water interface. When surfactants are present in the solution, the zeta potential

of gas bubbles is determined by the type of surfactant—specifically, negative for an anionic surfactant and positive for a cationic surfactant.

1.4.2.3 Steric Force

Although DLVO theory can be applied to many systems, the situation becomes more complicated when considering flotation. In this case, non-DLVO forces such as steric force and hydrophobic force must also be considered. When bitumen is in contact with water, asphaltene is extracted from bitumen and deposited on the bitumen/water interface. The polar groups of asphaltene are exposed toward the aqueous phase.[38] In this manner, the bitumen surface would become relaxed or swelled, forming brush-like structures. It has been reported that asphaltene is responsible for the steric repulsion in bitumen flotation systems.[38-41]

The steric interaction has been studied both theoretically and experimentally.[42-44] Normally, stabilizing polymers contain anchor groups and buoy groups. Anchor groups are components that are attached either chemically or physically to a surface to prevent the escape of polymers as polymer-coated surfaces approach each other. Buoy groups, or stabilizing moieties, are the adsorbed layers that are as solvent-compatible as possible and have sufficient molar mass to provide needed adlayer thickness. Anchor groups usually account 10 to 25% of the total adsorbing macromolecule, with the remaining volume occupied by the buoy groups.

When two polymer-coated surfaces are brought into contact and start to interpenetrate, the potential energy of the steric interaction may be comprised of: 1) mixing effect — the excess chemical potential of the adsorbate and solvent due to overlapping of layers; 2) volume restriction effect — elastic energy arising from compression of the polymer layers, which makes it difficult to press two polymer layers together; or 3) changes in surface free energy, which could occur from moving polymers laterally away from the surface or because of the desorption of polymers.[45] The

third factor, however, can be discarded since typically the adsorbed molecules are assumed to be anchored irreversibly and locally.

The most important properties of the system in terms of steric repulsion are 1) the adlayer thickness or the polymer tail length L, and 2) the solvency of the buoy blocks of the polymer in the medium. These two properties are related to each other. While the adlayer thickness depends primarily on the molar mass of the buoy groups of the polymer, solvency can also play a role. In a good solvent, interactions between buoy groups of polymers and solvent molecules are energetically favorable; thus, the polymer coils will expand or extend. In a poor solvent, polymers prefer to interact with themselves and the polymer coils will shrink. The length of polymer tails is roughly equivalent to the end-to-end distance of these free polymer segments under the same conditions as the system. At low surface coverage and in a good solvent, the thickness of the adsorbed polymer layer should be roughly equal to the Flory radius (R_F):

$$R_F = n^{3/5} l \qquad [1.17]$$

where l and n are the length and the number of the monomers, respectively.

At higher coverage, the grafted chains are so close to each other that they are forced to extend away from the surface much farther than R_F, thereby forming a "brush layer." For a brush in a good solvent, L becomes:[46]

$$L = s\left(\frac{R_F}{s}\right)^{5/3} \qquad [1.18]$$

where s is the mean distance between attachment points.

Once two brush-bearing surfaces are within a distance of $2L$ from each other, there will be a repulsive pressure between them. According to the Alexander-de Gennes theory,[44] the disjoining pressure is given by:

$$\Pi_s = \frac{kT}{s^3}\left[(\frac{2L}{h})^{4/9} - (\frac{h}{2L})^{3/4}\right] \quad [1.19]$$

1.4.2.4 Hydrophobic Force

In addition to steric force, another non-DLVO force—namely, the hydrophobic force—is also critical for bitumen flotation because both bitumen and air bubble surfaces are hydrophobic. Israelachvili and Pashley[47] were the first to directly measure the short-range attractive hydrophobic force between two curved mica surfaces using surface force apparatus (SFA). The researchers rendered the mica surfaces moderately hydrophobic using a cationic surfactant hexadecyltrimethylammonium bromide (CTAB), having an advancing water contact angle of about 60°.[48] Since then, many other investigators have measured both short- and long-range hydrophobic forces between two solid surfaces using SFA and atomic force microscopy (AFM).[49-52] All results indicate the presence of an attractive hydrophobic force between hydrophobic solid surfaces.

Measuring the surface forces between a solid surface and an air bubble were made possible by AFM.[53] Assessing particle-bubble interactions using AFM was first reported by Ducker *et al.*[54] and Butt[55] in 1994; other related studies soon followed.[56-62] Attractive forces were observed between a hydrophobized silica particle and an air bubble in water.

The hydrophobic forces (F_h) measured in experiments are commonly represented using the following form,[47]

$$\frac{F_h}{R} = C\exp(-\frac{h}{D}) \quad [1.20]$$

where *R* is the radius of curvature of the hydrophobic surfaces interacting with each other, *C* and *D* (decay length) are fitting parameters.

According to the Derjaguin approximation,[63] which is shown in the following equation,

$$\frac{F_h}{R} = 2\pi \int_h^\infty \Pi_h dh \qquad [1.21]$$

one can obtain Eq. [1.22] to calculate the disjoining pressure contributed by hydrophobic force:

$$\Pi_h = \frac{C}{2\pi D} \exp(-\frac{h}{D}) \qquad [1.22]$$

The origin of the hydrophobic force is still controversial. Some believe it is of entropic origin, arising from the rearrangement of water molecules at hydrophobic surfaces.[64-66] When water molecules come into contact with a small nonpolar molecule or bubble, they re-orientate or re-structure to form "clathrate cages" or "gas hydrates."[67] When water molecules are in contact with a hydrophobic-water interface, including the air-water interface, they also form clathrate-like structures.[68, 69] When two hydrophobic surfaces approach each other, the water structure changes in the overlapping boundary layers of water.[70] Based on this concept, Eriksson *et al.*[66] derived a theoretical model for hydrophobic force, which assumes that the intervening water between two surfaces is progressively more ordered with decreasing *h*. Most recently, Yoon and coworkers[71-73] determined the thermodynamic functions of hydrophobic interactions by conducting surface force measurements at several different temperatures. The researchers showed that macroscopic hydrophobic interactions entail decreases in both the excess entropy (S^f) and the excess enthalpy (H^f) of thin liquid films (TLF) of water confined between hydrophobic surfaces.

Other investigators believe that hydrophobic force is due to the bridging of nanoscopic bubbles preexisting on the hydrophobic force. This theory is supported by three important observations: 1) discontinuities (or "steps") on force *vs.* distance curves,[52, 74] 2) the disappearance of attractive forces in deaerated water,[75] and 3) the presence of nanobubbles on hydrophobic surfaces detected by AFM imaging.[76] In contrast, other researchers argue that 1) steps on the force curve can be avoided by modifying the conditions and procedures involved in force

measurement,[77] 2) long-range attractions still exist in degassed solutions,[78, 79] and 3) AFM studies do not show nanobubbles on hydrophobic surfaces;[80] rather, optical measurements confirm that water between two hydrophobic surfaces has the same refractive index as the bulk water.[81]

There are other possibilities for the origin of hydrophobic force, including electrostatic origin,[82] separation-induced cavitation,[83] hydrodynamic fluctuating correlation,[84] *etc.*

In bitumen flotation, all Π_d , Π_e and Π_s are positive (or repulsive); therefore, the total disjoining pressure does not afford a negative value that is required for bitumen-bubble attachment. Adding a hydrophobic component to the disjoining pressure allows the total disjoining pressure to be negative when Π_h is negative.

1.5 Dissertation Outline

Despite the importance of bitumen aeration in water-based bitumen extraction processes, some of the fundamental mechanisms involved in bitumen aeration are still not fully understood. Thus, the principal objective of this thesis work is to investigate the thinning of wetting films formed between bitumen and air bubbles. To facilitate this objective, we developed a bubble-against-plate apparatus equipped with a high-speed camera to record the optical interference patterns of the wetting films formed on a flat bitumen surface. It is necessary to use a high-speed camera as the wetting films formed on hydrophobic surfaces are unstable and hence thin fast. The recorded interference patterns were then used to obtain the temporal and spatial profiles of the films offline. The film profiles were then analyzed to determine the disjoining pressure (Π) using the method and algorithms developed by Pan, *et al.*[18] These authors derived the following expression for disjoining pressure,

$$\Pi = \frac{2\gamma}{R} - \frac{\gamma}{r}\frac{\partial}{\partial r}\left(r\frac{\partial h}{\partial r}\right) - 12\mu\int_{r=\infty}^{r}\frac{1}{rh^3}\left[\int_{r=0}^{r} r\frac{\partial h}{\partial t}dr\right]dr \qquad [1.23]$$

where γ is the air/water interfacial tension, R the bubble radius, r the radial position, h the wetting film thickness, and μ the fluid viscosity.

Chapter 1 gives an overview of the state-of-the-art oil sands extraction process and a brief review of the recent scientific research conducted on the role of colloidal forces in the extraction processes.

Chapter 2 describes the temperature effect on the kinetics of the thinning of wetting films of water on bitumen. A modified thin film pressure balance (TFPB) technique has been used to monitor the changes in the profiles of the TLFs between an air bubble and a flat substrate coated by bitumen, maltene, or asphaltene at temperatures ranging from 22 to 80 °C. The kinetic information in the vertical and radial directions, *i.e.*, $\partial h/\partial t$ and $\partial h/\partial r$, respectively, have been derived from the film profiles to determine the disjoining pressure (Π) in the TLFs. In addition, water contact angles on bitumen surfaces at temperatures in the range of 22 to 80 °C have been measured using captive bubble method. Based on these results and the thermodynamic data available in the literature, a model for bitumen aeration is proposed.

Chapter 3 studies the role of colloidal forces in bitumen aeration. The thin film pressure balance (TFPB) technique has been used i) to study the kinetics of thinning of the wetting films formed on bitumen and its hydrophilic and hydrophobic components, *i.e.*, asphaltene, and maltene, and ii) to determine the disjoining pressures (Π) in the films from the curvature changes recorded during the process of film thinning. The results will be analyzed in view of the extended DLVO theory, which includes the contributions from the electrical double-layer force, van der Waals force, hydrophobic force, and steric force that may be present in the TLFs.

Chapter 4 deals with the effects of solution chemistry on the stability of wetting films on bitumen. A new bubble-against-plate apparatus has been developed and used to study effects of immersion time, pH, KCl, Ca^{2+}, Mg^{2+} ion concentrations, and the approach speed on bubble-surface interactions.

Chapter 5 includes the summary of the present work and suggestions for future work.

References

1. Masliyah, J.H., Z. Xu, and J.A. Czarnecki, *Handbook on Theory and Practice of Bitumen Recovery from Athabasca Oil Sands*, Kingsley Publishing Services, 2011.
2. Sanford, E.C., *Processibility of athabasca oil sand: Interrelationship between oil sand fine solids, process aids, mechanical energy and oil sand age after mining,* The Canadian Journal of Chemical Engineering. 61(4), p. 554-567, 1983.
3. Clark, K. and D. Pasternack, *Hot Water Seperation of Bitumen from Alberta Bituminous Sand,* Industrial & Engineering Chemistry. 24(12), p. 1410-1416, 1932.
4. Masliyah, J., et al., *Understanding Water‐Based Bitumen Extraction from Athabasca Oil Sands,* The Canadian Journal of Chemical Engineering. 82(4), p. 628-654, 2004.
5. Cymerman, G.J. and T. Kwong, *Improvements in the Oil Recovery Flotation Process at Syncrude Canada Ltd.*, in *Processing of Hydrophobic Minerals and Fine Coals: Proceedings of the 1st UBSMcGill Bi-Annual International Symlposium on Fundamentals of Mineral Processing,* CIM, Vancouver, BC, 1995.
6. Tipman, R.N. and Y.-C. Long, patent US 5876492, 1999.
7. Sanford, E.C. and S. F.A., *Processability of Athabasca Tar Sand Using a Batch Extraction Unit: The Role of NaOH,* CIM Bull. 72(803), p. 164-169, 1979.

8. Drelich, J., et al., *The role of gas bubbles in bitumen release during oil sand digestion,* Fuel. 74(8), p. 1150-1155, 1995.

9. Lesueur, D., *The colloidal structure of bitumen: Consequences on the rheology and on the mechanisms of bitumen modification,* Advances in colloid and Interface Science. 145(1), p. 42-82, 2009.

10. Corbett, L.W., *Composition of asphalt based on generic fractionation, using solvent deasphaltening, elution-adsorption chromatography, and densimetric characterization,* Analytical Chemistry. 41(4), p. 576-579, 1969.

11. Peramanu, S., B.B. Pruden, and P. Rahimi, *Molecular Weight and Specific Gravity Distributions for Athabasca and Cold Lake Bitumens and Their Saturate, Aromatic, Resin, and Asphaltene Fractions,* Industrial & Engineering Chemistry Research. 38(8), p. 3121-3130, 1999.

12. Leon, O., et al., *Electrophoretic mobility and stabilization of asphaltenes in low conductivity media,* Petroleum science and technology. 18(7-8), p. 913-927, 2000.

13. Derjaguin, B.V., Kolloid Zh. 17(205), 1955.

14. Derjaguin, B.V., *Theory of stability of colloids and thin films,* Consultants Bureau New York, 1989.

15. Eriksson, J.C. and R.H. Yoon, *Role of Surface Forces - Part I, Colloid and Interface Science Series*, T.F. Tadros, Editor, p. 99, Wiley-VCH, 2007.

16. Derjaguin, B.V. and M.M. Kusakov, *An experimental investigation of polymolecular solvate (adsorbed) films as applied to the development of a mathematical theory of stability of colloids,* Acta Physicochim. URSS. 10 p. 25, 1939.

17. Laskowski, J. and J. Kitchener, *The hydrophilic—hydrophobic transition on silica,* J. of Colloid and Interface Sci. 29(4), p. 670-679, 1969.

18. Pan, L., S. Jung, and R.H. Yoon, *Effect of hydrophobicity on the stability of the wetting films of water formed on gold surfaces,* Journal of colloid and interface science. 361(1), p. 321-330, 2011.

19. Pan, L., S. Jung, and R.H. Yoon, *A fundamental study on the role of collector in the kinetics of bubble–particle interaction,* International Journal of Mineral Processing. 106 p. 37-41, 2012.

20. Tchaliovska, S., et al., *Interactions in Equilibrium Free Films of Aqueous Dodecylammonium Chloride Solutions,* Journal of Colloid and Interface Science. 168(1), p. 190-197, 1994.

21. Lyklema, J. and K.J. Mysels, *A Study of Double Layer Repulsion and van der Waals Attraction in Soap Films,* Journal of the American Chemical Society. 87(12), p. 2539-2546, 1965.

22. Berg, J.C., *An introduction to interfaces & colloids: the bridge to nanoscience*, World Scientific, 2010.

23. Hamaker, H., *The London—van der Waals attraction between spherical particles,* physica. 4(10), p. 1058-1072, 1937.

24. Lifshitz, E.M., J. Exp. Theoret. Phys. (USSR). 29(94), 1955.

25. Israelachvili, J.N., *Intermolecular and Surface Forces*, 2nd ed, Academic press, London, 1992.

26. Hogg, R., T.W. Healy, and D.W. Fuerstenau, *Mutual coagulation of colloidal dispersions,* Transactions of the Faraday Society. 62(0), p. 1638-1651, 1966.

27. Nguyen, A. and H.J. Schulze, *Colloidal science of flotation*, p. 332, CRC Press, 2003.

28. Nguyen, A. and H.J. Schulze, *Colloidal science of flotation*, p. 334, CRC Press, 2003.

29. Nguyen, A. and H.J. Schulze, *Colloidal science of flotation*, p. 337, CRC Press, 2003.

30. Liu, J., et al., *Bitumen–clay interactions in aqueous media studied by zeta potential distribution measurement,* Journal of colloid and interface science. 252(2), p. 409-418, 2002.

31. Hall, A., S. Collins, and J. Melrose, *Stability of aqueous wetting films in Athabasca tar sands,* Society of Petroleum Engineers Journal. 23(2), p. 249-258, 1983.

32. McShea, J.A. and I. Callaghan, *Electrokinetic potentials at the gas-aqueous interface by spinning cylinder electrophoresis,* Colloid & Polymer Science. 261(9), p. 757-766, 1983.

33. Yoon, R.-H. and J.L. Yordan, *Zeta-potential measurements on microbubbles generated using various surfactants,* Journal of Colloid and Interface Science. 113(2), p. 430-438, 1986.

34. Li, C. and P. Somasundaran, *Reversal of bubble charge in multivalent inorganic salt solutions—Effect of magnesium,* Journal of Colloid and Interface Science. 146(1), p. 215-218, 1991.

35. Li, C. and P. Somasundaran, *Reversal of bubble charge in multivalent inorganic salt solutions—Effect of aluminum,* Journal of Colloid and Interface Science. 148(2), p. 587-591, 1992.

36. Graciaa, A., et al., *The ζ-Potential of Gas Bubbles,* Journal of Colloid and Interface Science. 172(1), p. 131-136, 1995.

37. Creux, P., et al., *Specific Cation Effects at the Hydroxide-Charged Air/Water Interface,* The Journal of Physical Chemistry C. 111(9), p. 3753-3755, 2007.

38. Yoon, R.H., D. Guzonas, and B.S. Aksoy, *Role of Surface Forces in Tar Sand Processing*, in *Proceeding of the 1st UBC-McGill Bi-Annual International Symposium* Vancouver, BC, Canada, 1995.

39. Yoon, R.H. and Y.I. Rabinovich, *Role of Asphaltene in the Processing of Tar Sand*, in *Proceeding of the 3rd UBC-McGill Bi-Annual International Symposium*, CIM, Montreal, Quebec, Canada, 1999.

40. Abraham, T., et al., *Asphaltene-silica interactions in aqueous solutions: direct force measurements combined with electrokinetic studies,* Industrial & engineering chemistry research. 41(9), p. 2170-2177, 2002.

41. Liu, J., et al., *Colloidal interactions between asphaltene surfaces in aqueous solutions,* Langmuir. 22(4), p. 1485-1492, 2006.

42. De Gennes, P.-G., *Scaling concepts in polymer physics*, Cornell university press, 1979.

43. Patel, S.S. and M. Tirrell, *Measurement of forces between surfaces in polymer fluids,* Annual Review of Physical Chemistry. 40(1), p. 597-635, 1989.

44. De Gennes, P., *Polymers at an interface; a simplified view,* Advances in Colloid and Interface Science. 27(3), p. 189-209, 1987.

45. Berg, J.C., *An introduction to interfaces & colloids: the bridge to nanoscience*, p. 583, World Scientific, 2010.

46. Alexander, S., *Adsorption of chain molecules with a polar head a scaling description,* Journal De Physique. 38(8), p. 983-987, 1977.

47. Israelachvili, J. and R. Pashley, *The hydrophobic interaction is long range, decaying exponentially with distance,* Nature. 300(5890), p. 341-342, 1982.

48. Pashley, R.M. and J.N. Israelachvili, *A comparison of surface forces and interfacial properties of mica in purified surfactant solutions,* Colloids and Surfaces. 2(2), p. 169-187, 1981.

49. Yoon, R.-H., D.H. Flinn, and Y.I. Rabinovich, *Hydrophobic interactions between dissimilar surfaces,* Journal of colloid and interface science. 185(2), p. 363-370, 1997.

50. Parker, J.L., et al., *Surface Forces between Plasma Polymer Films,* Langmuir. 10(8), p. 2766-2773, 1994.

51. Yoon, R.-H. and S.A. Ravishankar, *Long-Range Hydrophobic Forces between Mica Surfaces in Alkaline Dodecylammonium Chloride Solutions,* Journal of Colloid and Interface Science. 179(2), p. 403-411, 1996.

52. Ishida, N., et al., *Effects of Hydrophobizing Methods of Surfaces on the Interaction in Aqueous Solutions,* Journal of Colloid and Interface Science. 216(2), p. 387-393, 1999.

53. Binnig, G., C.F. Quate, and C. Gerber, *Atomic force microscope,* Physical review letters. 56(9), p. 930, 1986.

54. Ducker, W.A., Z. Xu, and J.N. Israelachvili, *Measurements of Hydrophobic and DLVO Forces in Bubble-Surface Interactions in Aqueous Solutions,* Langmuir. 10(9), p. 3279-3289, 1994.

55. Butt, H.-J., *A Technique for Measuring the Force between a Colloidal Particle in Water and a Bubble,* Journal of Colloid and Interface Science. 166(1), p. 109-117, 1994.

56. Fielden, M.L., R.A. Hayes, and J. Ralston, *Surface and Capillary Forces Affecting Air Bubble−Particle Interactions in Aqueous Electrolyte,* Langmuir. 12(15), p. 3721-3727, 1996.

57. Gillies, G., M. Kappl, and H.-J. Butt, *Direct measurements of particle–bubble interactions,* Advances in Colloid and Interface Science. 114–115(0), p. 165-172, 2005.

58. Johnson, D.J., N.J. Miles, and N. Hilal, *Quantification of particle–bubble interactions using atomic force microscopy: A review,* Advances in Colloid and Interface Science. 127(2), p. 67-81, 2006.

59. Ishida, N., *Direct measurement of hydrophobic particle–bubble interactions in aqueous solutions by atomic force microscopy: Effect of particle hydrophobicity,* Colloids and Surfaces A: Physicochemical and Engineering Aspects. 300(3), p. 293-299, 2007.

60. Nguyen, A.V., J. Nalaskowski, and J.D. Miller, *A study of bubble–particle interaction using atomic force microscopy,* Minerals Engineering. 16(11), p. 1173-1181, 2003.

61. Englert, A., et al., *Interaction forces between a deformable air bubble and a spherical particle of tuneable hydrophobicity and surface charge in aqueous solutions,* Journal of colloid and interface science. 379(1), p. 121-129, 2012.

62. Ren, S., J. Masliyah, and Z. Xu, *Studying bitumen–bubble interactions using atomic force microscopy,* Colloids and Surfaces A: Physicochemical and Engineering Aspects. 444 p. 165-172, 2014.

63. Derjaguin, B.V., *Friction and adhesion IV. The theory of adhesion of small particles.,* Kolloid Z. 69 p. 155-164, 1934.

64. Israelachvili, J.N. and R.M. Pashley, *Measurement of the hydrophobic interaction between two hydrophobic surfaces in aqueous electrolyte solutions,* Journal of Colloid and Interface Science. 98(2), p. 500-514, 1984.

65. Claesson, P.M., et al., *Interactions between water—stable hydrophobic Langmuir—Blodgett monolayers on mica,* Journal of Colloid and Interface Science. 114(1), p. 234-242, 1986.

66. Eriksson, J.C., S. Ljunggren, and P.M. Claesson, *A phenomenological theory of long-range hydrophobic attraction forces based on a square-gradient variational approach,* Journal of the Chemical Society, Faraday Transactions 2: Molecular and Chemical Physics. 85(3), p. 163-176, 1989.

67. Israelachvili, J.N., *Intermolecular and surface forces: revised third edition*, p. 158, Academic press, 2011.

68. Nguyen, A. and H.J. Schulze, *Colloidal science of flotation*, p. 360, CRC Press, 2003.

69. Drost-Hansen, W., Ind. Eng. Chem. 61 p. 10, 1978.

70. Rabinovich, Y.I. and B. Derjaguin, *Interaction of hydrophobized filaments in aqueous electrolyte solutions,* Colloids and Surfaces. 30(3), p. 243-251, 1988.

71. Li, Z. and R.H. Yoon, *Thermodynamics of hydrophobic interaction between silica surfaces coated with octadecyltrichlorosilane,* Journal of colloid and interface science. 392 p. 369-375, 2013.

72. Wang, J., R.H. Yoon, and J.C. Eriksson, *Excess thermodynamic properties of thin water films confined between hydrophobized gold surfaces,* Journal of colloid and interface science. 364(1), p. 257-263, 2011.

73. Li, Z. and R.-H. Yoon, *Thermodynamics of Solvophobic Interaction between Hydrophobic Surfaces in Ethanol,* Langmuir. 2014.

74. Parker, J.L., P.M. Claesson, and P. Attard, *Bubbles, cavities, and the long-ranged attraction between hydrophobic surfaces,* The Journal of Physical Chemistry. 98(34), p. 8468-8480, 1994.

75. Stevens, H., et al., *Effects of Degassing on the Long-Range Attractive Force between Hydrophobic Surfaces in Water,* Langmuir. 21(14), p. 6399-6405, 2005.

76. Tyrrell, J.W. and P. Attard, *Images of nanobubbles on hydrophobic surfaces and their interactions,* Physical Review Letters. 87(17), p. 176104, 2001.

77. Wang, J. and R.-H. Yoon, *AFM Forces Measured between Gold Surfaces Coated with Self-Assembled Monolayers of 1-Hexadecanethiol,* Langmuir. 24(15), p. 7889-7896, 2008.

78. Zhang, J.H., et al., *Effects of degassing and ionic strength on AFM force measurements in octadecyltrimethylammonium chloride solutions,* Langmuir. 21(13), p. 5831-5841, 2005.

79. Meyer, E.E., Q. Lin, and J.N. Israelachvili, *Effects of Dissolved Gas on the Hydrophobic Attraction between Surfactant-Coated Surfaces,* Langmuir. 21(1), p. 256-259, 2004.

80. Tsao, Y.H., et al., *Interactions between hydrophobic surfaces. Dependence on temperature and alkyl chain length,* Langmuir. 7(12), p. 3154-3159, 1991.

81. Kekicheff, P. and O. Spalla, *Refractive Index of Thin Aqueous Films Confined between Two Hydrophobic Surfaces,* Langmuir. 10(5), p. 1584-1591, 1994.

82. Tsao, Y.H., D.F. Evans, and H. Wennerstroem, *Long-range attraction between a hydrophobic surface and a polar surface is stronger than that between two hydrophobic surfaces,* Langmuir. 9(3), p. 779-785, 1993.

83. Christenson, H.K. and P.M. Claesson, *Cavitation and the interaction between macroscopic hydrophobic surfaces,* Science. 239(4838), p. 390-392, 1988.

84. Ruckenstein, E. and N. Churaev, *A possible hydrodynamic origin of the forces of hydrophobic attraction,* Journal of Colloid and Interface Science. 147(2), p. 535-538, 1991.

Chapter 2

Temperature Effect on the Stability of Wetting Films of Water on Bitumen

Abstract

For air bubbles to attach on mineral (or bitumen) particles, the wetting films of water formed on the surfaces must rupture. Thermodynamically, the films can rupture when the disjoining pressures (Π) of the films are negative. In the present work, the disjoining pressures of the wetting films formed on bitumen have been measured at temperatures in the range of 22 to 80 °C. The results show that Π becomes less negative with decreasing temperature. However, it remains negative until the temperature is decreased to 35 °C, but becomes positive at 22 °C. These results are consistent with the industrial experiences in bitumen flotation.

2.1 Introduction

In 2012, Canada produced 1.8 million bbl/day of oil from the oil sands resources in Alberta, which is expected to grow to 5.2 million bbl/day by 2030, according to the projections from the Canadian Association of Petroleum Producers (CAPP). The amount of heavy oil (bitumen) deposited in the form of oil sands is estimated to be 2.5 trillion bbls, which is five-times larger than the conventional oil reserves in Saudi Arabia. At present, approximately 55% of the bitumen

is produced from mining followed by flotation, with the rest produced by *in-situ* extraction methods, *e.g*., cycle steam stimulation (CSS) and steam-assisted gravity drainage (SAGD).

The oil sands ores are composed of sand grains with a median size of 65 mesh (208 μm) and a top size of 14 mesh (1,168 μm), a layer of hydrated water (or innate water), and bitumen that forms a continuous phase between sand grains.[3] The innate water contains ultrafine clay particles such as kaolinite and illite. The ores containing typically 7 to 14% by weight of bitumen are processed by flotation, with recoveries usually in the range of ~93%, while those of the *in situ* processes are much lower (40 to 70%). In general, the ores containing large amounts of ultrafine particles are of low grades and suffer from low recoveries. Also, the ores containing divalent cations such as Ca^{2+} and Mg^{2+} ions are difficult to process.[5]

The basic bitumen extraction processes used today are the same as the original hot-water processing method developed by Clark in the 1920s.[7] In this process, bitumen is detached (or liberated) from sand grains by agitating an aqueous ore slurry in hot water (~80 °C) in the presence of caustic soda to raise the pH to 8.0 – 8.5. Initially, the agitation was provided by a tumbler along with steam injection. In early 1990's, the tumblers have been replaced by pipelines, in which bitumen is liberated and aerated in transit. The aerated bitumen droplets float in a primary separation vessel (PSV) to be separated from the sand grains and clays. The middlings that are insufficiently aerated are directed to a bank of conventional and/or column flotation cells to recover additional bitumen. The froth products, containing typically 60% bitumen, 30% water and 10% solids, are de-aerated, diluted in naphtha (or *n*-alkane), and centrifuged to remove solids. The clean bitumen is then upgraded by a combination of thermal and catalytic hydrocracking processes to obtain synthetic crude oils (SCO).

Much work has been done to lower operating temperatures to reduce the energy consumption. In 1990, Sury[9] developed a cold water process for bitumen extraction, in which an oil sand matrix was attrition-scrubbed in water in the presence of appropriate conditioning agents to achieve liberation and disperse the liberated bitumen. The aqueous slurry was then subjected to flotation. The conditioning agents included typical flotation reagents such as kerosene, diesel oil, and frother, *e.g.*, methyl-isobutyl-carbinol (MIBC). Bitumen recoveries were ~90 % at 5 to 10 °C and ~95% at 15 to 35 °C. In 2000, a similar process was tested at the Aurora plant, Syncrude Canada, Ltd., at ~25 °C.[10] In 2002, the operating temperature was raised to 35 to 40 °C to obtain higher and more consistent recoveries.

Despite the simplicity in the extraction process and the significant improvement achieved in recent years, some of the mechanisms involved in the different steps of the extraction process are not fully understood. Contrary to the general belief that bitumen-in-water emulsions are stabilized by the surfactants that are naturally present in bitumen (*e.g.*, naphthenate), it has been shown that the emulsions are stabilized by the asphaltene polymers present in bitumen.[11] This mechanism was proposed on the basis of the surface forces measured between two bitumen-coated mica surfaces using a surface force apparatus (SFA). Recognizing the role of asphaltene as an emulsifier may help explain the long conditioning times and high temperatures required for bitumen extraction.

In general, the bubble-bitumen attachment (or aeration) requires long induction times usually in the range of seconds, while the bubble-particle attachment in mineral flotation occurs in milliseconds.[11-13] Further, air bubbles attach on mineral surfaces, forming finite contact angles, while in bitumen flotation small bubbles are engulfed into bitumen droplets. Despite the differences noted above, the fundamental mechanisms are the same in that the wetting films of

water formed on the substrates (mineral and bitumen) must be broken for the flotation to occur. It is more difficult for air bubbles to break the wetting films formed on bitumen than those formed on mineral most probably due to the presence of asphaltene polymers exposed on the former.

When an air bubble is pressed against the surface of a bitumen droplet (or a mineral particle) under turbulent conditions, it deforms; and the curvature change associated with the deformation creates an excess pressure (p), which is equal to $2\gamma/R$, where γ is the surface tension and R is the radius of curvature. The excess (or Laplace) pressure causes the thin liquid film (TLF) of water (or wetting film) formed between the two macroscopic surfaces to thin. As the film thins further, the surface forces in the film come into play and create a disjoining pressure (Π) at h < 200 to 300 nm, in which case the excess pressure should become,

$$p = \frac{2\gamma}{R} - \Pi \qquad [2.1]$$

Eq. [2.1] shows that the excess pressure becomes large when $\Pi < 0$, which will accelerate the film thinning and cause the film to rupture at a critical thickness (h_{cr}). This will result in bubble-bitumen attachment and subsequent engulfment. If $\Pi > 0$, however, the wetting film is stable and the bubble-particle attachment becomes difficult.

The highest value of Π in a disjoining pressure isotherm (Π *vs.* h curve) may represent the energy barrier (E_1) for bubble-particle attachment. In bitumen flotation, E_1 is high most probably due to the repulsive steric force created by the asphaltene exposed on bitumen surface[11] and due to the high negative ζ-potentials created by the alkali (KOH) added to the system to help liberate the bitumen from sand grains. According the bubble-particle attachment model proposed by Luttrell and Yoon (1992),[9]

$$P_a = \exp\left(-\frac{E_1}{E_k}\right) \qquad [2.2]$$

it is necessary to apply a high kinetic energy (E_k) to overcome the energy barrier and achieve a high probability of attachment (P_a). An alternative to applying a high E_k would be a long conditioning time, which may be provided by the pipeline transport (or hydrotransport) system used in industry today.

Still another alternative is to reduce the energy barrier (E_1) by appropriate means. It has been shown that the induction time for bubble-bitumen interaction decreases at lower pH,[11] suggesting a corresponding decrease in E_1. However, flotation at low pH is impractical in a sense that bitumen liberation requires a high pH. In the present work, the effects of temperature on E_1 have been studied by measuring Π at temperatures in the range of 22 to 80 °C. The measurements were conducted using the modified thin film pressure balance (TFPB) technique described previously.[10,11] Since this technique is capable of measuring pressures in unstable films, the measurements have been extended to the TLFs of water formed on hydrophobic substrates such as maltene and bitumen at elevated temperatures of up to 80 °C. The results are in good agreement with industry practice in terms of temperature effect on bitumen extraction. It is hoped that the results of the present work will be useful for better understanding the role of temperature in bitumen extraction by flotation.

2.2 Experimental

2.2.1 Materials

A sample of bitumen (99 wt.%) was provided by Suncor Energy, Inc. Reagent grade toluene (>99.5% purity) was purchased from Spectrum Chemical Mfg. Corp., and HPLC grade n-heptane (99.3% purity) was obtained from Fisher Scientific. Millipore ultrapure water with a resistivity of 18.2 MΩ·cm was obtained using a Direct Q3 water purification system. Silicon wafers (100 crystal planes, University Wafer) were used as the substrates for coating bitumen,

asphaltene and maltene. Sulfuric acid (H_2SO_4, 98% purity, VMR international) and hydrogen peroxide (H_2O_2, 29.0–32.0% purity, Alfa Aesar) were used to clean the silicon substrates.

2.2.2 Separation of Asphaltene and Maltene

The bitumen sample was dissolved in toluene at a toluene/bitumen ratio of 5:1 by volume. The solution was then stirred using a magnetic stirrer for 2 hr, centrifuged for 30 min to remove the solids, and subsequently put under a fume hood to allow the toluene to naturally evaporate. After the toluene evaporation was complete, n-heptane was added to the toluene- and solids-free bitumen at a heptane/bitumen ratio of 40:1 by volume. The n-heptane and bitumen mixture were stirred by means of a magnetic stirrer for 2 hr, during which time maltene dissolved into n-heptane while asphaltene precipitated out. The mixture was left overnight for the asphaltene to settle at the bottom. The supernatant n-heptane was carefully removed by means of a pipette and placed under a fume hood to let the n-heptane naturally evaporate, leaving maltene behind. The amount of the evaporated n-heptane was small.

The asphaltene precipitate was repeatedly washed for 17 times with an excess amount (~1L) of n-heptane to remove any maltene that may have co-precipitated. In each washing step, the mixture was agitated for 2 hr and left to stand overnight to allow the asphaltene to precipitate and the supernatant was carefully removed. After the last washing step, the supernatant n-heptane became colorless. The asphaltene precipitate was left under a fume hood to allow n-heptane to evaporate and thereby obtain a sample of purified asphaltene.

2.2.3 Preparation of Bitumen-, Maltene-, and Asphaltene-coated Surfaces

Silicon wafer was first oxidized in an oxidation furnace at 1070 °C for ~40 min using wet oxidation procedure. The oxidized silicon wafers were then cut into 12x12 mm pieces and used as substrates for bitumen, asphaltene, and maltene. Before the coating, the silicon substrates were put

in an ultrasonic bath of water for ~1 hr and then cleaned by immersing in a Piranha solution (3:7 by volume of H_2O_2/H_2SO_4) at 120 °C for 1 hr, followed by rinsing with an adequate amount of ultrapure water and pure nitrogen (N_2) blow-drying. The silicon substrate was placed in a spin-coater (Laurell, WS-400-6NPP), rinsed with toluene, and then spun at 6,000 rpm for 30 s to dry off the toluene. When the substrate was free of toluene, a small amount of (2 or 3 drops) of a bitumen-in-toluene solution (2.5 mg/mL) was placed on the substrate and let it stand for 10 s. The substrate was then spun at 3,500 rpm for 20 s before placing another drop of the bitumen solution and continuing spinning for additional 10 s. The spinning continued for an additional 1 minute at 6,000 rpm to evaporate the solvent and obtain a smooth and uniform bitumen coating. The spin-coated bitumen was then placed in a particulate matter-free laminar hood for ~30 min to ensure maximum removal of toluene from the coating. The procedure described above was also employed for the preparation of asphaltene- and maltene-coated silicon surfaces.

2.2.4 Measurement of Film Thinning Kinetics

Figure 2.1 shows the modified thin film pressure balance (TFPB) apparatus used in the present work to study the kinetics of film thinning. The original TFPB apparatus was designed for the study of foam films (or the water films between two air bubbles) by Scheludko and Exorowa.[14] The equipment was modified to study the kinetics of film thinning for wetting films.[15] As shown in the inset, a flat surface of interest is placed on the top of a film holder (2.0 mm diameter glass tubing) with its surface facing downward, so that the surface is in contact with the water in the film holder. In the present work, the flat silicon wafers coated with bitumen, asphaltene, or maltene were used as samples of interest.

In a given experiment, the silicon wafer-glass tubing assembly was inserted in a glass cell surrounded by a water jacket, in which water of known temperature was circulated. The film

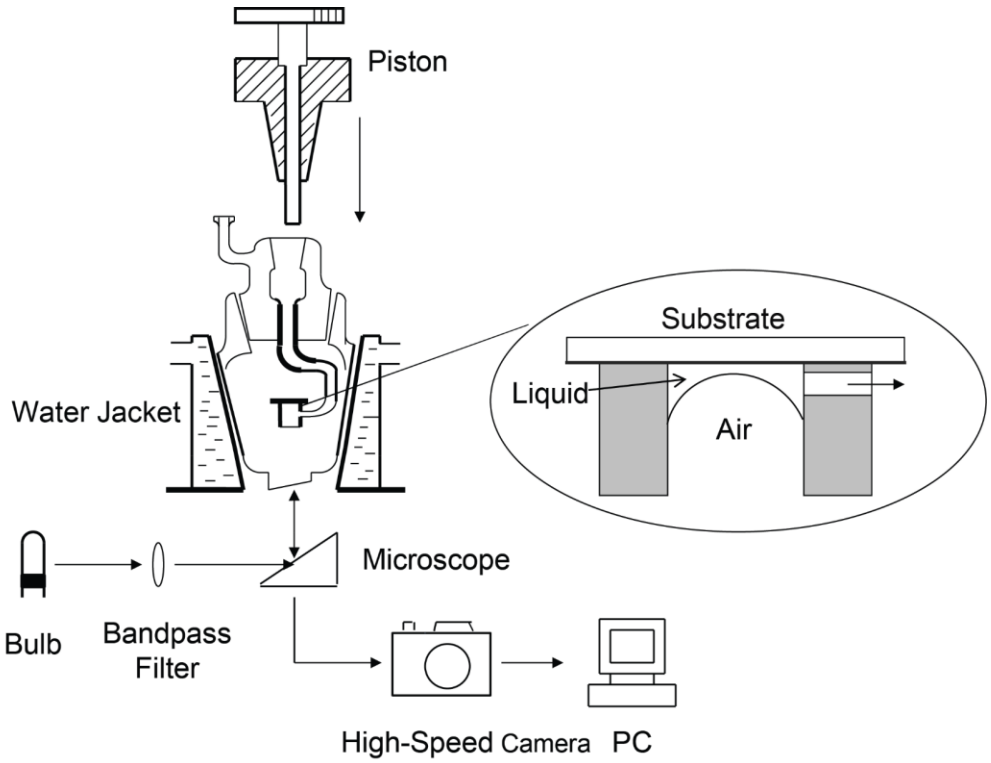

Figure 2.1 Schematics of the modified TFBC apparatus used for the study of wetting films.

holder-water jacket assembly was placed on an inverted microscopic stage (Olympus IX51) to monitor the changes in film thicknesses as a function of time. A mercury arc short lamp (100 W, Olympus) was used as a light source with a bandpass interference filter (#65-643, Edmund Optics) to produce a monochromatic green light source (λ=546 nm). In a given experiment, the liquid in the film holder is slowly withdrawn by turning the knob of the piston. Once the interference patterns (Newton rings) began to appear in the microscopic field of view, the film was allowed to thin spontaneously while recording the images by means of a high-speed camera (Fastec Imaging, HS400115). The interference patterns recorded were used to reconstruct timed thickness profiles of a wetting film across the entire film holder with a nanometer resolution. The spatial and temporal film profiles of the wetting film were then used to monitor the changes in film thicknesses (h) as a function of time and radial distance of the film at any point of the film. The experimental

data were used to obtain information on the film thinning kinetics and calculate the disjoining pressure (Π) in the thin liquid films (TLFs) according to Eq. [2.3], as derived by Pan. *et.al.*,[16]

$$\Pi = \frac{2\gamma}{R} - \frac{\gamma}{r}\frac{\partial}{\partial r}\left(r\frac{\partial h}{\partial r}\right) - 12\mu\int_{r=\infty}^{r}\frac{1}{rh^3}\left[\int_{r=0}^{r} r\frac{\partial h}{\partial t}dr\right]dr \qquad [2.3]$$

where γ is the air/water interfacial tension, R the bubble radius, r the radial position, h the wetting film thickness, and μ the fluid viscosity. The experiments were conducted at temperatures in the range of 22 to 80 °C.

2.2.5 Contact Angle Measurements on Bitumen Film

Flat plates of silicon wafers were coated with bitumen using the spin-coating technique described in the previous section (2.2.3). The thicknesses of the coatings were approximately 11 nm. The hydrophobicity of the bitumen-coated surfaces were determined by measuring water contact angles using the captive bubble technique. For each measurement, an air bubble was brought to a bitumen-coated surface from underneath. The measurements were conducted using a Ramé-Hart contact angle goniometer, Model 250, F4 series. The measurements were conducted in a double-jacketed rectangular glass cell with optical windows filled with ultrapure water. The measurements were conducted at different temperatures in the range of 22 to 80 ^{o}C under controlled temperature conditions.

Effect of temperature was also studied by measuring contact angles on relatively thick (~0.5 mm) films of bitumen formed on clean Teflon plates. Several bitumen-coated Teflon plates were placed in an oven for 3 to 4 min at ~120 °C to soften the bitumen and obtain flat surfaces, which were subsequently cooled at room temperature in a dust-free cabinet. To measure contact angles at an elevated temperature, a bitumen-coated Teflon plate was placed in an oven at a desired temperature for a few minutes and then placed in ultrapure water at approximately the same

temperature. The water temperature was controlled by circulating the water from a constant temperature bath through a double-walled glass cell that was designed for captive bubble contact angle measurement. The Ramé-Hart contact angle goniometer was used to record the images of air bubbles interacting with bitumen-coated surfaces at a speed of 30 fps and to determine dynamic contact angles offline using a protractor.

2.3 Results and Discussion

2.3.1 Temperature Effect on the Film Thinning Kinetics

Figure 2.2 shows the changes in Newton rings (or interference patterns) of the wetting films formed on bitumen-, asphaltene-, and maltene-coated silicon surfaces obtained at 80 °C. As shown, the Newton rings changed with time due to film thinning until the film ruptured. From the light intensities of the interference patterns, one can calculate the film thickness (*h*) using the micro-interferometric technique and obtain temporal and spatial profiles of the wetting films, as shown

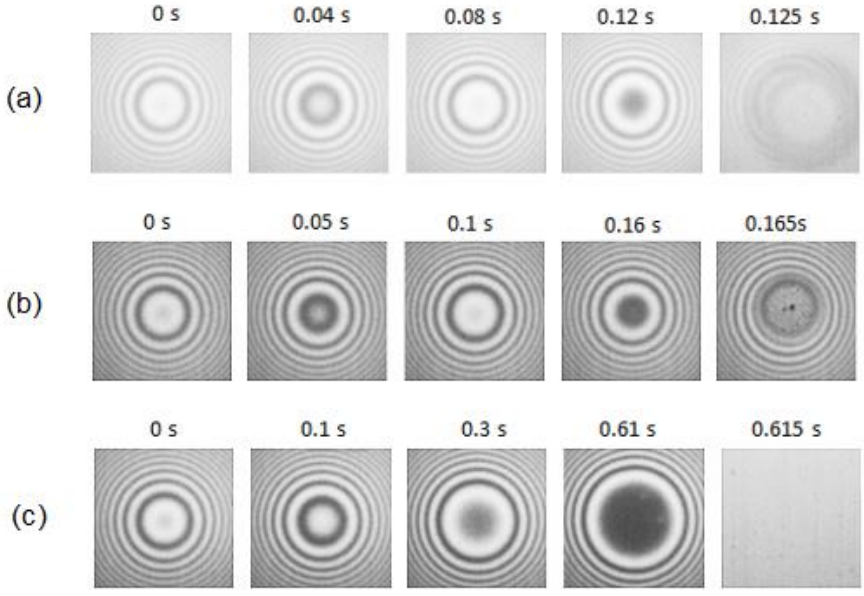

Figure 2.2 Changes of Newton rings with time due to the decrease in the thickness of the wetting film of water formed on maltene (a), bitumen (b) and asphaltene (c) surface, while the air bubble was approaching the substrate at 80 °C.

in Figure 2.3. The arrow in each profile represents the film thickness at which the wetting film ruptured catastrophically.

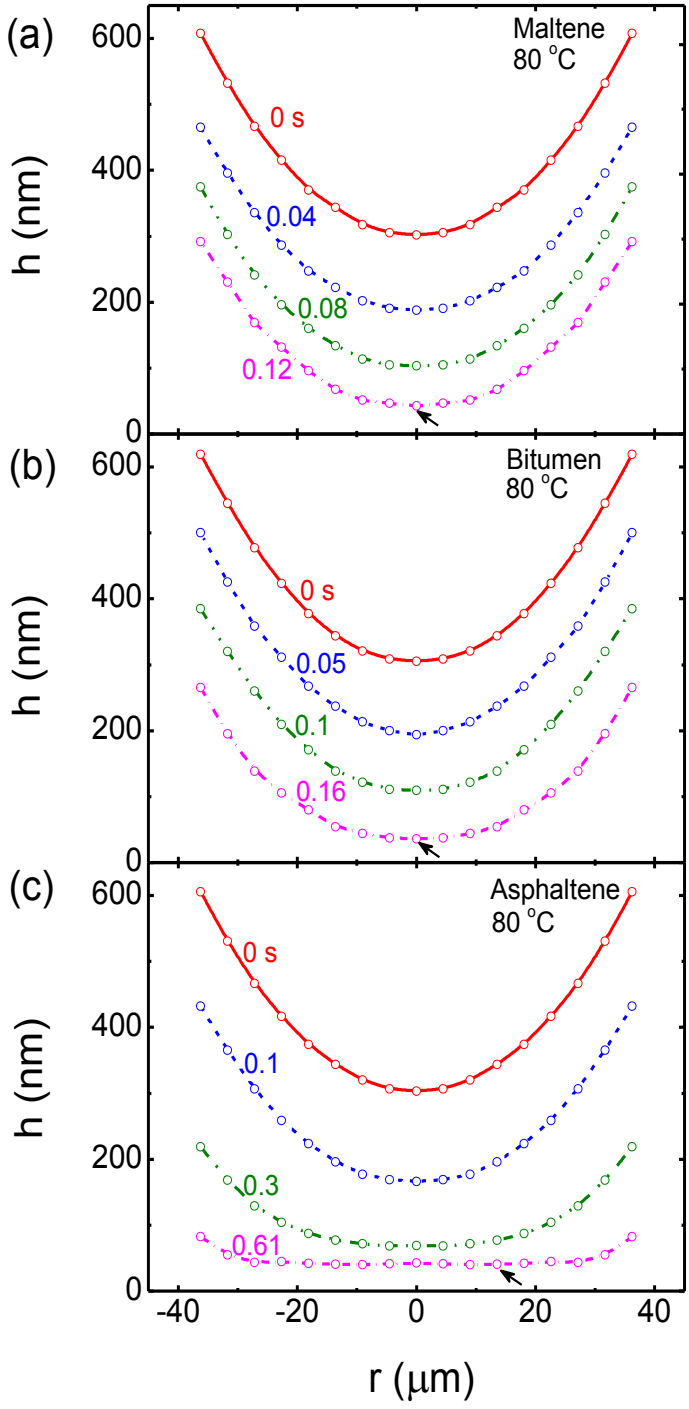

Figure 2.3 Spatial and temporal profiles of the wetting films of water formed on maltene, bitumen, and asphaltene surface, respectively, at 80 °C. The arrows represent the critical thicknesses where the films rupture.

As shown in Figure 2.3, the films formed on maltene and bitumen surfaces thinned fast and ruptured at 0.12 and 0.16 s, respectively. On asphaltene, the film thinned substantially slower, with the rupture occurring at 0.615 s. Note here that the wetting film before rupture formed on asphaltene were flatter than those formed on the other two substrates most probably due to the presence of a greater resistance force to film thinning.

Figure 2.4 shows the effect of temperature on the kinetics of film thinning on bitumen. The film thicknesses (h) measured at the film centers, *i.e.*, r = 0, are plotted *vs.* time (t) at different temperatures. As shown, the film thinning kinetics represented by the slope of the h *vs.* t curves increased with increasing temperature, which explains the advantage of floating bitumen at higher temperatures. According to the kinetics curves presented in Figure 2.4, bitumen flotation would be possible at temperatures as low as 35 °C. At 22 °C, it took >80 s for the wetting film to rupture,

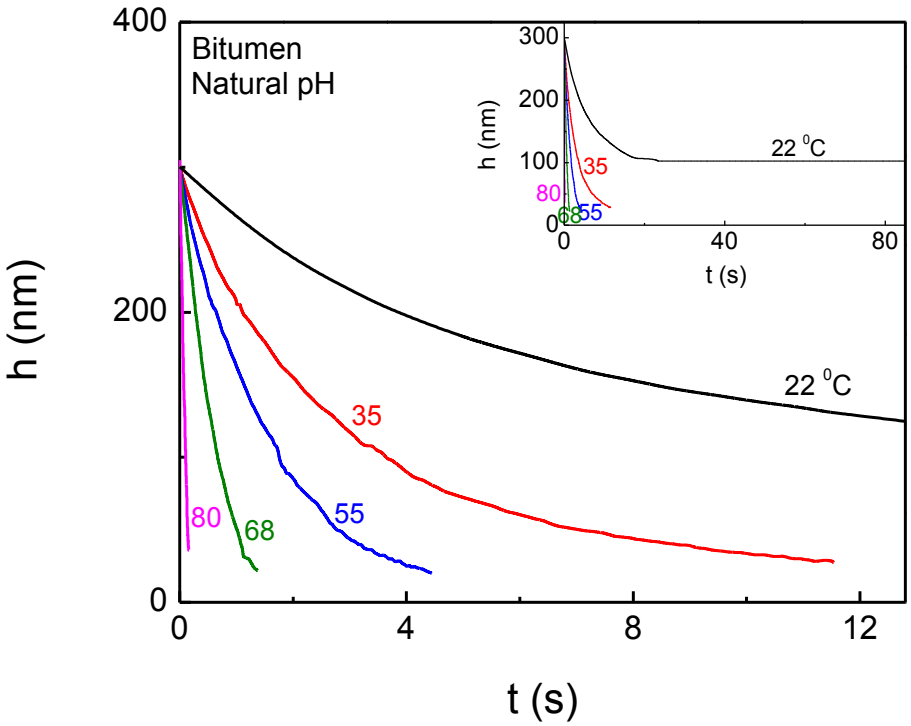

Figure 2.4 Effect of temperature on the kinetics of film thinning on bitumen in water at natural pH of about 5.7.

which would make it difficult to float bitumen at such a low temperature. The results presented in Figure 2.4 are consistent with the industrial experiences reported in the literature. The original hot water extraction process was designed to work at 80 to 85 °C. During the 1990s, the operating temperatures were reduced to 70 to 80 °C to save energy. In 2000, the Aurora plant of Syncrude Canada, Ltd., tested the cold water processing at approximately 25 °C.[10] However, the operating temperature has been increased to 35 to 40 °C, which is consistent with the results obtained in the present work. At present, most plants operate at temperatures in the range of 40 to 55 °C to ensure operation reliability and high bitumen recovery. The results that the film thinning became faster at higher temperatures are also in agreement with the induction time measurements reported by Gu *et al.*,[12, 17] who found that the induction time of bubble-bitumen attachment decreased greatly with increasing temperature.

Figures 2.5 and 2.6 show the *h vs. t* curves for the wetting films formed on maltene and asphaltene, respectively, at temperatures in the range of 35 to 80 °C. As shown, the kinetics of film thinning increased with increasing temperature. Also, the thin liquid film of water thins much faster on maltene than on asphaltene at a given temperature, indicating a greater resistance on asphaltene surface.

Comparison of the results presented in Figures 2.4, 2.5, and 2.6 shows that the kinetics of film thinning increased in the order of asphaltene, bitumen, and maltene, which in turn suggests that the hydrophobicity of the three different materials increases in the same order. This finding is in good agreement with the work by Yoon and Rabinovich,[18] who conducted direct force measurements using an atomic force microscope (AFM) between bitumen, asphaltene and maltene surfaces in water and found that there was a long-range attractive force between maltene surfaces

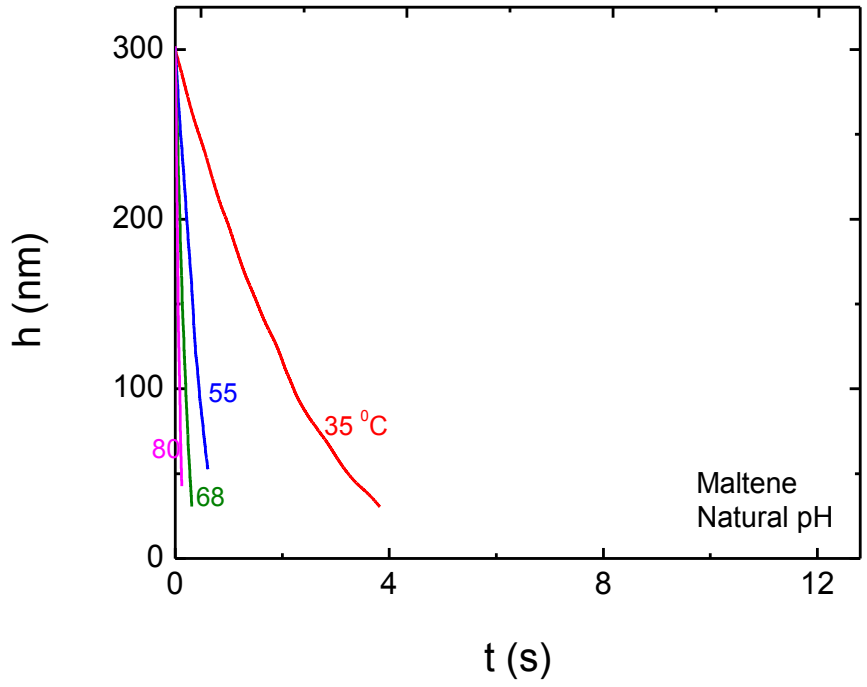

Figure 2.5 Effect of temperature on the kinetics of film thinning on maltene.

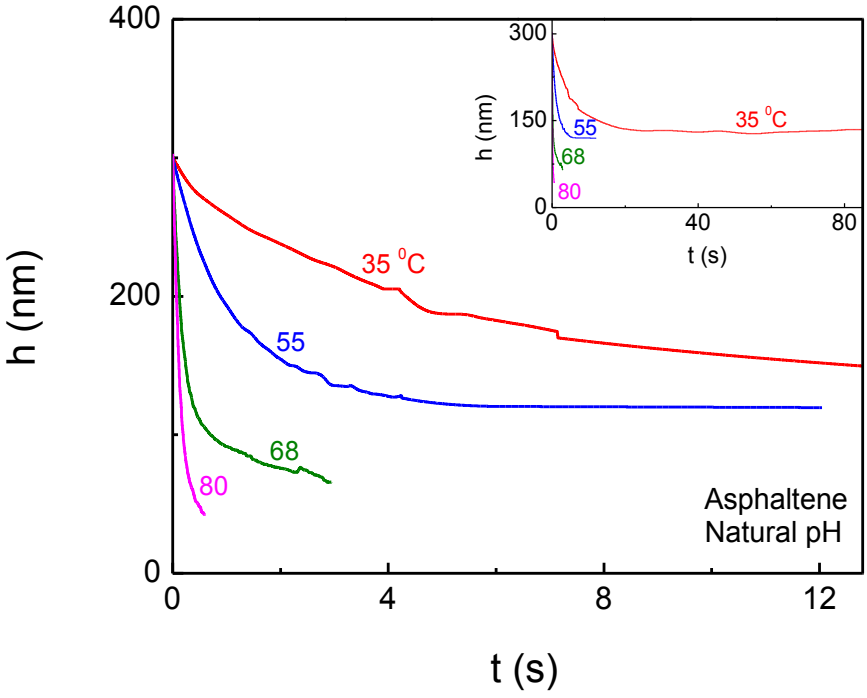

Figure 2.6 Effect of temperature on the kinetics of film thinning on asphaltene

while a strong repulsive steric force between asphaltene surfaces. The steric force may be responsible for the slow kinetics of film thinning on asphaltene-coated surfaces.

2.3.2 Temperature Effet on Disjoning Pressure

Figure 2.7 shows the disjoining pressure (Π) in the wetting films of water formed on maltene, asphaltene, and bitumen surface at temperatures in the range of 20 to 80 °C. The disjoining pressure was calculated using a spatial and temporal profile obtained in the present work. Figure 2.3 shows the data obtained at 80 °C, while the profiles obtained at other temperatures are not shown in this communication. The film profiles were used to derive the kinetic information on film thinning, *i.e.*, $\partial h/\partial t$ and $\partial h/\partial r$, which were then substituted into Eq. [2.3] and obtain Π. As shown in Figure 2.7, both maltene and bitumen exhibited negative disjoining pressures ($\Pi < 0$) at temperatures between 35 to 80 °C. On asphaltene, $\Pi > 0$ at all temperatures except at 80 °C. These results suggest that maltene and bitumen can be more readily floated than asphaltene. In general, Π decreases with increasing temperature, which is consistent with the industrial experience that bitumen flotation becomes easier at higher temperatures.

2.3.3 Contact Angle Measurements at Different Temperatures

The results obtained in the present work suggest that the hydrophobicity of bitumen increased with increasing temperature. In order to better understand this observation, the contact angles of water on bitumen-coated surfaces, on both thin and thick bitumen films, were measured at different temperatures using the captive bubble method. Figure 2.8 shows the dynamic contact angles measured on thin bitumen films (~11 nm thick) formed on silicon wafer at different temperatures. At a given temperature, the contact angle decreased with time, as was also observed by others.[19] Note here that contact angles decreased with increasing temperature, which is contrary

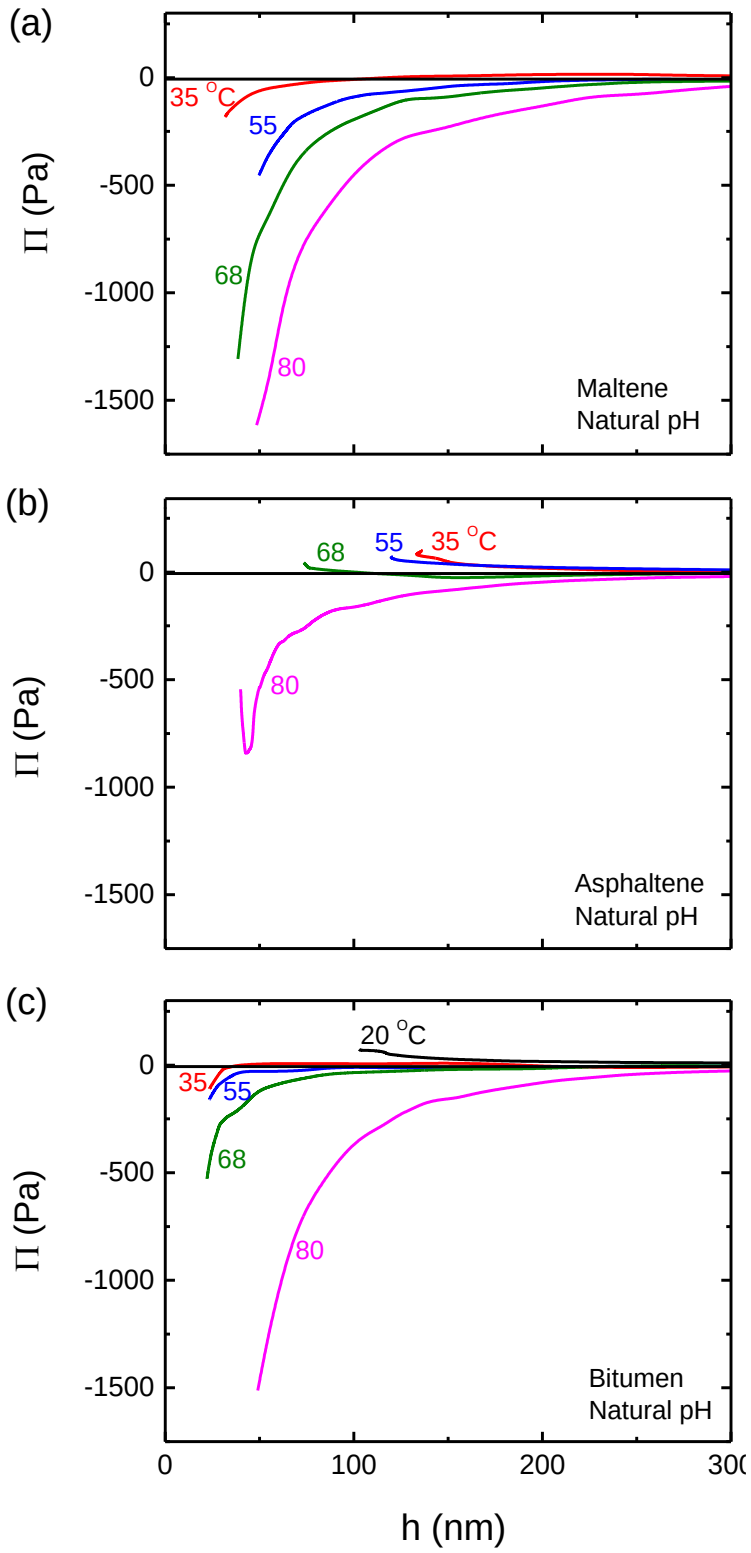

Figure 2.7 Effect of temperature on the disjoining pressure isotherms (Π(h)) in the thin films of water formed on maltene (a), asphaltene (b), and bitumen (c). The data have been collected at the center of films.

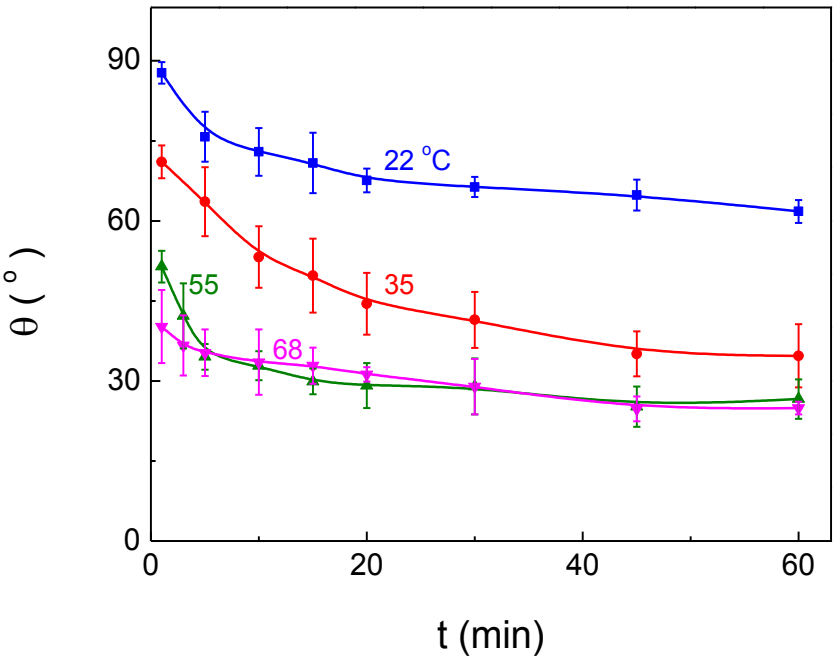

Figure 2.8 Dynamic water contact angles measured on the thin bitumen films at different temperatures. The thickness of the bitumen films were ~11 nm.

to what is expected in view of increasing flotation recovery with temperature.[20] It is also contrary to our findings that film thinning kinetics on bitumen increased with temperature and the disjoining pressure became more negative at a higher temperature.

The decrease in contact angle with time may be attributed to changes in the orientation of the surfactants present in bitumen, as suggested by Ren, *et al.*[19] It is more likely, however, that the bitumen films used for the contact angle measurement were so thin that parts of the films dissolved away into water and, thereby, exposed the hydrophilic silicon dioxide substrates. The higher the temperature, the faster and more bitumen would dissolve into the solution. Therefore, a series of contact angle measurements were conducted on a thick bitumen film of ~0.5 mm to avoid the exposure of silicon dioxide substrates toward water. Figure 2.9 shows the images of the air bubbles adhering on bitumen surfaces at different temperatures, while Figure 2.10 shows the dynamic contact angles measured from the images by extrapolating the curvatures of the bubbles. A close

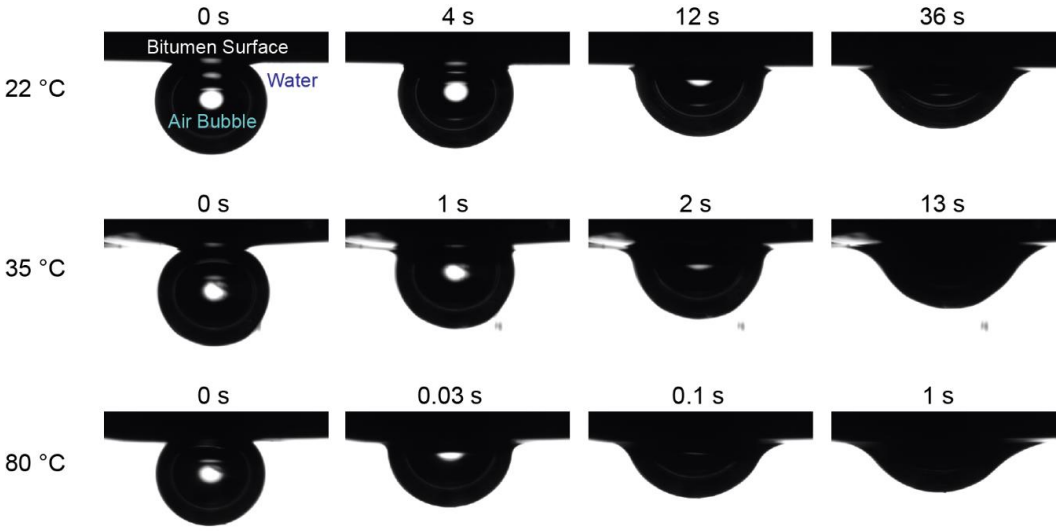

Figure 2.9 The kinetics of bubble-bitumen interactions at 22, 35, and 80 ºC. The thickness of the film was about 0.5 mm.

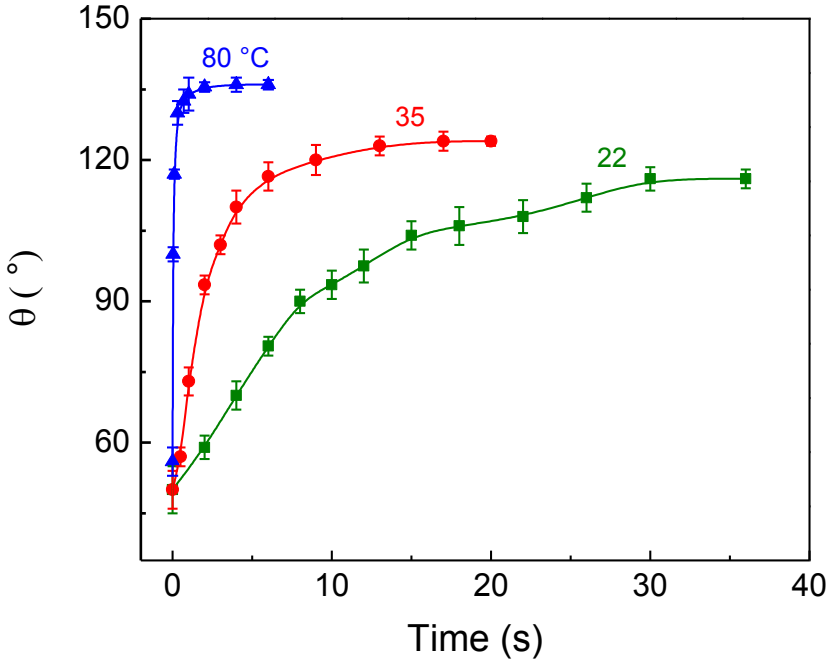

Figure 2.10 Dynamic contact angles on the thick bitumen films at different temperatures in water. The measurement was difficult due to the liquid (oil) collecting around the three-phase contact lines as shown in Figure 2.9. Therefore, the contact angles were measured by extending the bubble surface along the curvatures.

examination of the images shows that a type of liquid, most probably maltene, collects near the three-phase contact points, and the amount of the liquid increases with temperature.

When bitumen is exposed to water, asphaltene (or the surfactant naturally present in bitumen) may be exposed to the surface, rendering the surface less hydrophobic. As the temperature increases, maltene will diffuse through the asphaltene layer and restore the hydrophobicity of the bitumen surface, causing the contact angle to increase, as shown in Figure 2.10. Furthermore, part of the air bubble may be covered by maltene. As shown, the contact angles increased with time and temperature, indicating that the diffusion of maltene is slow at room temperature, but the rate of diffusion increases with temperature due to a corresponding decrease in viscosity.

Figure 2.11 depicts a model showing how bitumen contact angles increase with time at a high temperature. Initially, the contact angle is relatively low due to the presence of asphaltene on the surface, which is hydrophilic at an alkaline pH in the range of 8 to 10. At a pH close to its pK_a, its functional groups are ionized and strongly interact with water (or become hydrophilic). At an elevated temperature, maltenes diffuse into the asphaltene layer on the surface and increase its

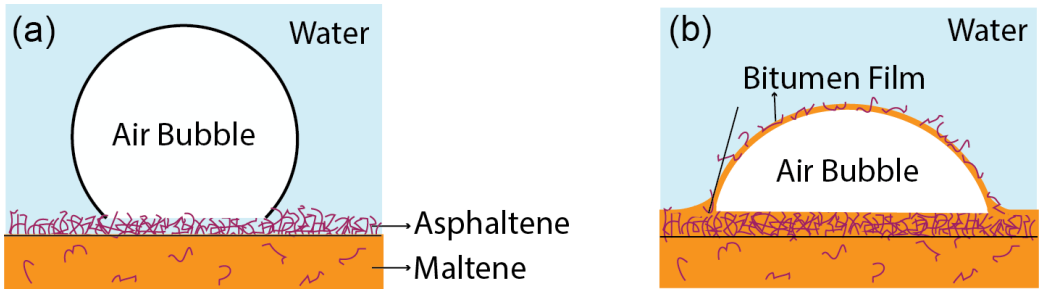

Figure 2.11 A model for the attachment of air bubble to the surface of bitumen at a high temperature: a) initially, an air bubble attaches to a bitumen surface coated by asphaltene with a low contact angle; b) maltene diffuses into the asphaltene layer on the surface and increases the hydrophobicity and hence the contact angle. This is possible due to the low viscosity of maltene at higher temperatures. Eventually, the bitumen layer saturated with maltene begins to cover the bubble surfaces.

Table 2.1 Dynamic Viscosity Data for Bitumen, Maltene, *n*-Dodecane, Hexacane and Naphthalene.

	Viscosity (mPa·s)					
	20 °C	30 °C	40 °C	50 °C	60 °C	75 °C
Athabasca bitumen[1]	$7x10^5$	$\sim10^5$	$\sim4x10^4$	$\sim10^4$	$\sim5x10^3$	$\sim10^3$
Lloydmin bitumen[2]	38601	11591	3999	1604	746	
Maltene extracted from Lloydmin bitumen[2]	2585	1017	431	219	119	
n-Dodecane ($C_{12}H_{26}$)[4]	~1.344			0.911		0.659
Hexadecane ($C_{16}H_{34}$)[6]	~3.061			1.829		1.231
Naphthalene ($C_{10}H_8$)[8]	2.483			1.422		

hydrophobicity, causing the contact angle to increase, as shown. (Recall that in the present work the contact angle measurements began as soon as a sample was placed in water.) When the asphaltene layer is saturated with maltene, an oily substance begins to coat the bubble surface, as shown in the images of the dynamic contact angle measurements (see Figure 2.9). At the same time, the contact angles increase, and the profiles of the bubbles change accordingly. As the bubble profiles become flat, the bubble-bitumen contact area increases, which may facilitate the diffusion of air into bitumen underneath through the asphaltene layer. The time it takes for the contact angle to increase and reach an equilibrium decreases with increasing temperature most probably due to the decrease in viscosity. It can be seen from Table 2.1 that the dynamic viscosity of bitumen and maltene decreased dramatically with temperature. For example, the viscosity of Athabasca bitumen decreases by nearly three orders of magnitude as temperature increases from 20 to 75 °C. The viscosity data presented in Table 2.1 were experimentally measured using different types of

viscometers by previous researchers. Details about the viscometers used could be found in the cited papers.[1, 2, 4, 6, 8] The increase in contact angle with time and temperature, as shown in Figure 2.10, may be attributed qualitatively to the increased saturation of the asphaltene layer with maltene at longer contact times and higher temperatures. Furthermore, the hydrophobicity of maltene itself increases with temperature, as shown in the disjoining pressure measurements (see Figure 2.7a).

2.3.4 Thermodynamic Analysis Based on Acid-base Theory

As noted in the foregoing paragraph, it appears that the oily substance coats the bubble when the asphaltene layer is saturated with maltene. It was thought first that maltene could readily coat bubble surface due to the hydrophobic interaction between maltene and air bubble as both are hydrophobic. A simple thermodynamic analysis suggests, however, that maltene is less likely to coat the bubble than the asphaltene saturated with maltene (or bitumen). The free energy change associated with the spreading of an oily substance on an air bubble (ΔG_s) can be obtained using the following relation,

$$\Delta G_s = \gamma_o + \gamma_{o/w} - \gamma_w \qquad [2.4]$$

where γ_o is the surface tension of oil, $\gamma_{o/w}$ is the interfacial tension between oil and water, and γ_w is the surface tension of water. Eq. [2.4] shows that the spreading of an oily substance on an air bubble entails the expansion of the oil/air and oil/water interfaces at the expense of the air/water interface of the bubble. In the present work, maltene may be considered the oily substance.

According to the acid-base theory,[21]

$$\gamma_{o/w} = \gamma_o + \gamma_w - 2\sqrt{\gamma_o^d \gamma_w^d} - 2\sqrt{\gamma_o^+ \gamma_w^-} - 2\sqrt{\gamma_o^- \gamma_w^+} \qquad [2.5]$$

where γ_o^d and γ_w^d are the dispersion components of the oil and water interfaces, respectively; γ_o^+ and γ_w^+ are the acidic components of oil and water, respectively; γ_o^- and γ_w^- are the basic components of oil and water, respectively.

Substituting Eq. [2.5] into Eq. [2.4], one obtains,

$$\Delta G_s = 2\gamma_o - 2\sqrt{\gamma_o^d \gamma_w^d} - 2\sqrt{\gamma_o^+ \gamma_w^-} - 2\sqrt{\gamma_o^- \gamma_w^+} \qquad [2.6]$$

If maltene is as hydrophobic as other hydrocarbon oils , γ_o and γ_o^d should be in the range of 17 to 25 mJ/m^2, while γ_w^d = 21.8 mJ/m^2, $\gamma_w^+ = \gamma_w^-$ = 25.5 mJ/m^2, and γ_o^+ and γ_o^- are approximately zero, assuming maltene is completely apolar.[22] Assuming also that γ_o = 17 mJ/m^2 for maltene, Eq. [2.6] gives ΔG_s = -4.5 mJ/m^2, suggesting that maltene can coat the bubble surface. If γ_o = 25 mJ/m^2 rather than 17 mJ/m^2, the free energy change becomes positive, and thus maltene cannot coat air bubbles. Since the surface tensions of oils decrease with increasing temperature in general, it is thermodynamically possible that maltene can coat air bubbles at relatively high temperatures. It is unfortunate that detailed thermodynamic information for maltene is not available in the literature. The authors contacted the University of Alberta looking for a correct value of γ_o for maltene to no avail. The data do not exist as yet. It would be fruitful to determine the missing thermodynamic data in the future.

The surface tension data for bitumen are better known than those for maltene. According to the data reported by Moran *et al.*,[23] γ_o = 30 mJ/m^2 for bitumen, and $\gamma_{o/w}$ are in the range of 11 to 20 mJ/m^2. Substituting these values into Eq. [2.4] along with γ_w = 72 mJ/m^2, one obtains that ΔG_s is in the range of -22 to -31 mJ/m^2. It appears, therefore, that bitumen (or asphaltene saturated with maltene) is more likely to coat air bubbles during bitumen flotation. The reason for this is that

the polar groups of asphaltene can interact with the surrounding water molecules and give rise to a more negative free energy of spreading (ΔG_s), as is obvious from Eq. [2.6]. Conceptually, a hydrophobic oil will not spread at the air/water interface or bubble surface because it cannot interact with the water surrounding bubbles. If a surfactant is added to the oil, however, it can spread because the polar heads of the surfactant molecules interact with the surrounding water molecules and reduce free energy. Asphaltene acts effectively as a surfactant in the bitumen extraction system and facilitates the spreading of bitumen (or maltene) on bubble surfaces. As mentioned earlier, asphaltene contains polar groups such as carboxyl, sulfide, amide, and hydroxyl groups. In the spreading process, asphaltene molecules in bitumen tend to adsorb at the air/water interface because of these polar groups, lowering the bitumen/water interfacial tension and hence the Gibbs free energy change for spreading. Asphaltene acts as a spreading agent for bitumen.

It should be noted here that maltene is not completely apolar because one of its components, resin, contains polar groups such as carboxylates and sulfates.[24] Compared to asphaltene, however, resin is less polar.[25] Asphaltene still plays a major role in facilitating the spreading of bitumen onto air bubbles.

2.3.5 A Bitumen Aeration Model

Based on the contact angle measurements shown in Figures 2.9 and 2.10 and the thermodynamic considerations discussed above, a conceptual model for bitumen aeration may be suggested as depicted in Figure 2.12. When a small air bubble collides with a bitumen droplet in a hydrotransport pipeline or in a secondary flotation cell, the bubble will deform and create an excess pressure (p) in the wetting film of water formed in between the bitumen droplet and the air bubble. At this point in time, the film will thin due to the curvature pressure (p_{cur}). When the thickness reaches the range of 250 to 300 nm, the film thinning process may encounter a resistance from the

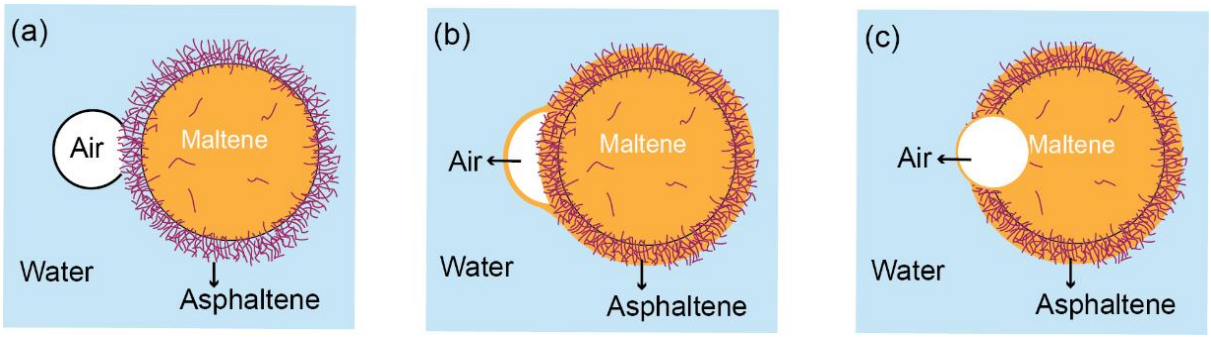

Figure 2.12 A dynamic bitumen aeration model: a) an air bubble attaches to an asphaltene-coated bitumen surface, forming a low contact angle; b) maltene diffuses into the asphaltene layer on the surface and increases the contact angle of the layer, and subsequently covers bubble surface; c) when the air bubble is covered by the maltene-saturated asphaltene, the bubble enters bitumen droplet, completing aeration. Thermodynamically, maltene-saturated asphaltene (or bitumen) spreads on air bubble better than maltene. Thus, asphaltene may act as a spreading agent for maltene.

colloidal forces in the form of a positive disjoining pressure ($\Pi > 0$). The film thinning will stop when $p_{cur} = \Pi$, because the excess pressure in the film becomes zero. If $\Pi < 0$, on the other hand, the excess pressure will increase, as $p = p_{cur} - \Pi$, and hence accelerate the film thinning process and eventually rupture the wetting film. Once the film has ruptured, a contact angle is formed.

Initially, the contact angle is small as depicted in Figure 2.12a. The experimental data presented in Figures 2.9 and 2.10 show actually that initial contact angles are less than 90°. In time, however, contact angles increase above 90°, as depicted in Figure 2.12b. According to the Young's equation,

$$\cos\theta = \frac{\gamma_b - \gamma_{b/w}}{\gamma_w} \qquad [2.7]$$

the contact angle increase should be due to the changes in interfacial tensions involved, Eq. [2.7] suggests that contact angle (θ) should be less than 90° when $\gamma_b > \gamma_{b/w}$. The contact angle should increase above 90° when $\gamma_b < \gamma_{b/w}$. Therefore, the dynamic contact angle behavior of bitumen as manifested in Figures 2.9 and 2.10 must be due to the changes in interfacial tensions. It should be

noted also that the secret of achieving high contact angles, which is essential for successful aeration, is to increase the bitumen/water interfacial tension ($\gamma_{b/w}$).

As has already been noted, it is necessary to increase the disjoining pressure for bitumen liberation, which can be achieved by agitating a bitumen slurry at a reasonably high temperature in the presence of an alkali (KOH). Under this condition, the basic functional groups of asphaltene, which includes carboxylic acids, carbonyls, phenols, pyroles, and pyridinic functional groups, dissociate and become polar.[26-29] As a result, highly-charged asphaltene molecules are exposed on bitumen surface and create steric and electrical double-layer forces to create a highly-positive disjoining pressure in the wetting films of water between bitumen and silica sands. At the same time, the exposure of the polar asphaltene should render the bitumen surface polar by increasing the acidic and basic components of surface tensions, *i.e.*, γ_b^+ and γ_b^-. This should in turn decrease the bitumen/water interfacial tension ($\gamma_{b/w}$) according to the acid-base theory,

$$\gamma_{b/w} = \gamma_b + \gamma_w - 2\sqrt{\gamma_b^d \gamma_w^d} - 2\sqrt{\gamma_b^+ \gamma_w^-} - 2\sqrt{\gamma_b^- \gamma_w^+} \qquad [2.8]$$

After bitumen is liberated from sand grains, bitumen aeration is desired. The aeration of bitumen consists of two substeps: 1) the attachment of bitumen droplets to air bubbles and 2) the subsequent engulfment of air bubbles by bitumen. The bubble-bitumen attachment, like in the case of mineral flotation, involves the thinning of the wetting film of water formed between bitumen droplets and air bubbles and the subsequent film rupture at a critical thickness forming a three phase contact line. The bubble engulfment involves the spreading of the bitumen onto air bubbles. Attachment (or film rupture) is the prerequisite of the engulfment. Without the film rupture, engulfment will not happen and the bitumen flotation is not possible. If a bitumen droplet and an

air bubble collide, their mutual attachment is thermodynamically favorable if the Gibbs free energy change associated in the attachment (ΔG_a) is negative. ΔG_a can be given as the following equation,

$$\Delta G_a = \gamma_b - (\gamma_{b/w} + \gamma_w) \quad [2.9]$$

which represents a process of a new air/bitumen interface being created at the expense of the air/water and bitumen/water interfaces. If ΔG_a is negative, the attachment is favored and spontaneous. If ΔG_a is positive, the bitumen should not attach. From Eq. [2.9], one can see that high bitumen/water interfacial tension ($\gamma_{b/w}$) will favor the bitumen-air attachment

For bitumen-bubble attachment, it is necessary to render the disjoining pressure in the wetting films formed between air bubble and bitumen negative, for which the asphaltene molecules exposed on bitumen surface need to become less polar so that the bitumen/water interfacial tension is increased. The most likely way to achieve this goal will be to allow the maltene at the interior of a bitumen-in-water emulsion droplet to diffuse out to the exterior through the asphaltene layer exposed on the surface and render the droplet surface hydrophobic. According to Eq. [2.8], one must reduce the acidic and basic components of bitumen surface tension, which can be readily accomplished when the maltene exposed on the surface masks the polar groups of the asphaltene on the surface. Once this has been accomplished, air bubble begins to penetrate the asphaltene droplet, as shown in Figure 2.12b, with the asphaltene acting effectively as an emulsifier for maltene, as has already been discussed.

In effect, bitumen droplets rendered hydrophilic during the liberation step are rendered hydrophobic in a hydrotransport pipeline prior to aeration. The hydrophilic-to-hydrophobic transition is induced by the diffusion of maltene through the asphaltene layer. Most of the diffusion-controlled processes are slow. One way to expedite the diffusion is to reduce the viscosity of maltene, which can be accomplished by increasing temperature. It appears, therefore,

that the role of temperature in bitumen aeration may be to decrease the viscosity of maltene. That contact angle data obtained at different temperatures and presented in Figures 2.9 and 2.10 may support this view.

After the bitumen-bubble attachment has occurred, bitumen would spread spontaneously over an air bubble (Figure 2.12b and 2,12c) if the Gibbs free energy change associated in spreading is negative ($\Delta G_s < 0$), as discussed previously. (ΔG_s) can be calculated as

$$\Delta G_s = \gamma_b + \gamma_{b/w} - \gamma_w \qquad [2.10]$$

Eq. [2.10] is essentially the same as Eq. [2.4]. Contrary to bitumen-air attachment, low bitumen/water interfacial tension ($\gamma_{b/w}$) will favor the bitumen spreading over air bubbles.

Figure 2.12c shows that an air bubble enters a bitumen droplet and remains spherical. The air bubble may form a coaxial interlayer between the maltene core and the layer of bitumen exposed on the surface. According to Eq. [2.4], however, ΔG_s will become more negative if γ_o is small, which can be achieved if the bubble remains spherical so that the air/oil (or air/maltene) interfacial area remains small.

Eqs. [2.9] and [2.10] give the following relation,

$$\Delta G_a = \Delta G_s - 2\gamma_{b/w} \qquad [2.11]$$

which shows that ΔG_a is always more negative than or equal to ΔG_s. Based on Eq. [2.11], there are three possibilities, representing three possible cases in bitumen aeration. First, if ΔG_a is positive, ΔG_s has to be positive too. In this case, bitumen will neither attach nor spread on air bubble surfaces and therefore flotation won't occur. Second, if ΔG_a is negative, but ΔG_s is positive, in which case bitumen will attach but won't spread on air bubbles. This case will occur when the processing temperature of the bitumen extraction is low, *e.g.*, < 35 °C, and bitumen droplets will attach to air bubbles as discrete particles.[30, 31] In this case, the success of flotation depends on whether the slurry

is sufficiently quiescent that the attached bitumen won't be sheared away from the bubble. Finally, if both ΔG_a and ΔG_s are negative, then bitumen will attach and engulf air bubbles, which happens at high processing temperatures, *e.g.*, > 45 °C. Once the bitumen engulfs an air bubble, only very high mechanical shear would cause it to be stripped away. Therefore, this is the best condition for successful bitumen aeration.[31]

Our thermodynamic analysis shows that bitumen/water interfacial tension ($\gamma_{b/w}$) plays an important role in bitumen extraction form oil sands. Low bitumen/water interfacial tension will be favorable for bitumen liberation from oil sands as well as the engulfment of bitumen over air bubbles. On the other hand, high bitumen/water interfacial tension is beneficial for the attachment between bitumen and air bubble. Therefore, our analysis suggests that an optimum bitumen/water interfacial tension is needed for bitumen extraction in industrial operations. Bitumen/water interfacial tension could be controlled by the slurry pH. A high pH will facilitate the ionization of polar molecules at the bitumen/water interface and therefore reduce the bitumen/water interfacial tension. It was reported that an optimum amount of NaOH was needed to achieve a maximum bitumen recovery.[32] An over-dose of NaOH would cause a too low bitumen/water interfacial tension, making bitumen-bubble attachment difficult. It could also cause bitumen to emulsify, leading to small bitumen droplets that are undesirable for bitumen flotation.[33]

2.4 Summary and Conclusion

The wetting films of water formed on bitumen and its components (maltene and asphaltene) thin faster with increasing temperature, which provides an explanation for the improved bitumen extraction at higher temperatures. At a given temperature, the kinetics increase in the order of asphaltene, bitumen and maltene.

From the experimental data obtained in the film thinning kinetics studies, the disjoining pressures in the wetting films of water formed on bitumen, maltene, and asphaltene have been determined. The results show that $\Pi < 0$ for maltene and bitumen, while $\Pi > 0$ for asphaltene. In general, disjoining pressure decreases with temperature with all three substrates. That the disjoining pressure for bitumen decreases with temperature provides an explanation for the increased kinetics of bubble-bitumen interaction and hence improved extraction at higher temperatures.

The dynamic contact angle measurements conducted on bitumen show that, initially, contact angles are small but subsequently increase above 90^{o}, obviously due to changes in the interfacial tensions involved. It appears that the changes in interfacial tensions are brought about by the diffusion of maltene from underneath the asphaltene layer formed on the surface of bitumen, causing an increase in the surface hydrophobicity of bitumen.

References

1. Helper, L.G. and C. Hsi, *AOSTRA Technical Handbook on Oil Sands, Bitumen and Heavy Oils*, AOSTRA technical publication series 6, Alberta Oil Sands Technology and Research Authority, Edmonton, AB, 1989.
2. Luo, P. and Y. Gu, *Effects of asphaltene content on the heavy oil viscosity at different temperatures,* Fuel. 86(7), p. 1069-1078, 2007.
3. Plitt, L.R., *Athabasca Tar Sands*, in *Milling Practice in Canada*, p. 371-378, Harpell's Press Cooperative, Ste. Anne de Bellevue, Quebec, 1978.

4. Caudwell, D., et al., *The viscosity and density of n-dodecane and n-octadecane at pressures up to 200 MPa and temperatures up to 473 K,* International Journal of Thermophysics. 25(5), p. 1339-1352, 2004.

5. Zhao, H., et al., *Effect of divalent cations and surfactants on silica-bitumen interactions,* Industrial & engineering chemistry research. 45(22), p. 7482-7490, 2006.

6. Tanaka, Y., et al., *Viscosity and density of binary mixtures of cyclohexane with n-octane, n-dodecane, and n-hexadecane under high pressures,* International journal of thermophysics. 12(2), p. 245-264, 1991.

7. Clark, K. and D. Pasternack, *Hot Water Seperation of Bitumen from Alberta Bituminous Sand,* Industrial & Engineering Chemistry. 24(12), p. 1410-1416, 1932.

8. Evans, E., *The viscosity of hydrocarbons. Parts VII and VIII,* J. Inst. Pet. Technol. 24 p. 537, 1938.

9. Sury, K.N., *Low Temperature Bitumen Recovery Process,* patent US 4946597, August 7, 1990.

10. Mankowski, P., et al., *Syncrude's Low Energy Extraction Process: Commercial Implementation*, in *Proceedings of the 31st Annual Meeting of the Canadian Mineral Processors*, Canadian Mineral Processors, CIM, Ottawa, Canada, 1999.

11. Yoon, R.H., D. Guzonas, and B.S. Aksoy, *Role of Surface Forces in Tar Sand Processing*, in *Proceeding of the 1st UBC-McGill Bi-Annual International Symposium* Vancouver, BC, Canada, 1995.

12. Gu, G., et al., *Effects of physical environment on induction time of air–bitumen attachment,* International Journal of Mineral Processing. 69(1), p. 235-250, 2003.

13. Yoon, R.H. and J.L. Yordan, *Induction time measurements for the quartz—amine flotation system,* Journal of colloid and interface science. 141(2), p. 374-383, 1991.

14. Scheludko, A. and D. Exerowa, Kolloid-Z. 165 p. 148, 1959.

15. Scheludko, A., Dokl. Bolg. Akad. Nauk. 24 p. 47, 1971.

16. Pan, L., S. Jung, and R.H. Yoon, *Effect of hydrophobicity on the stability of the wetting films of water formed on gold surfaces,* Journal of colloid and interface science. 361(1), p. 321-330, 2011.

17. Gu, G., et al., *A novel experimental technique to study single bubble–bitumen attachment in flotation,* International Journal of Mineral Processing. 74(1), p. 15-29, 2004.

18. Yoon, R.H. and Y.I. Rabinovich, *Role of Asphaltene in the Processing of Tar Sand*, in *Proceeding of the 3rd UBC-McGill Bi-Annual International Symposium*, CIM, Montreal, Quebec, Canada, 1999.

19. Ren, S., et al., *Effect of weathering on surface characteristics of solids and bitumen from oil sands,* Energy & Fuels. 23(1), p. 334-341, 2008.

20. Long, J., et al., *Effect of Operating Temperature on Water‐Based Oil Sands Processing,* The Canadian Journal of Chemical Engineering. 85(5), p. 726-738, 2007.

21. Good, R.J. and L. Girifalco, *A theory for estimation of surface and interfacial energies. III. Estimation of surface energies of solids from contact angle data*, The Journal of Physical Chemistry. 64(5), p. 561-565, 1960.

22. Van Oss, C.J., *Interfacial Forces in Aqueous Media*, 2nd ed, CRC press, Taylor and Francis Group 2006.

23. Moran, K., J. Masliyah, and A. Yeung, *Factors affecting the aeration of small bitumen droplets,* The Canadian Journal of Chemical Engineering. 78(4), p. 625-634, 2000.

24. Lesueur, D., *The colloidal structure of bitumen: Consequences on the rheology and on the mechanisms of bitumen modification,* Advances in colloid and Interface Science. 145(1), p. 42-82, 2009.

25. Kokal, S., et al., *Electrokinetic and adsorption properties of asphaltenes,* Colloids and Surfaces A: Physicochemical and Engineering Aspects. 94(2), p. 253-265, 1995.

26. Barbour, R.V. and J.C. Petersen, *Molecular interactions of asphalt. Infrared study of the hydrogen-bonding basicity of asphalt,* Analytical Chemistry. 46(2), p. 273-277, 1974.

27. Boduszynski, M.M., J.F. McKay, and D.R. Latham, Proc. Assoc. Asphalt Paving Technol. 49 p. 123, 1980.

28. Moschopedis, S.E. and J.G. Speight, *Investigation of hydrogen bonding by oxygen functions in Athabasca bitumen,* Fuel. 55(3), p. 187-192, 1976.

29. Petersen, J.C., Fuel. 46 p. 295, 1967.

30. Masliyah, J., et al., *Understanding Water‐Based Bitumen Extraction from Athabasca Oil Sands,* The Canadian Journal of Chemical Engineering. 82(4), p. 628-654, 2004.

31. Schramm, L.L., E.N. Stasiuk, and D. Turner, *The influence of interfacial tension in the recovery of bitumen by water-based conditioning and flotation of Athabasca oil sands,* Fuel Processing Technology. 80(2), p. 101-118, 2003.

32. Sanford, E.C., *Processibility of athabasca oil sand: Interrelationship between oil sand fine solids, process aids, mechanical energy and oil sand age after mining,* The Canadian Journal of Chemical Engineering. 61(4), p. 554-567, 1983.

33. Liu, J., Z. Xu, and J. Masliyah, *Colloidal forces between bitumen surfaces in aqueous solutions measured with atomic force microscope,* Colloids and Surfaces A: Physicochemical and Engineering Aspects. 260(1), p. 217-228, 2005.

Chapter 3

Colloidal Forces in Bitumen Aeration

Abstract

The thin film pressure balance (TFPB) technique has been used to study the thinning kinetics of the wetting films formed on bitumen, asphaltene, and maltene and to determine the disjoining pressures (Π) in the films from the curvature changes recorded during the process of film thinning. It was found that film thinning kinetics decreased in the order of maltene, bitumen and asphaltene. The results also showed that $\Pi < 0$ on maltene and bitumen, while $\Pi > 0$ on asphaltene, indicating that asphaltene may serve as a kinetic barrier for bitumen aeration. The disjoining pressure data obtained in the present work have been analyzed in view of the extended DLVO theory. The results suggest that hydrophobic force is the driving force for bitumen aeration.

3.1 Introduction

In the water-based bitumen extraction from Athabasca oil sands, bitumen aeration is critically important. Without aeration bitumen would not float because it has almost the same density as water.[1] Bitumen aeration is one of the two fundamental steps in the extraction process, the other being bitumen liberation from sand grains. These two steps entails three-phase interactions involving bitumen-bitumen, bitumen-solids (silica and clays), and bitumen-bubble. It has been generally recognized that colloidal forces play a crucial role in controlling these interactions and thus the stability of the thin liquid films (TLFs) formed between the three macroscopic phases.

In the past two decades, several researchers have reported their investigations of colloidal forces between two bitumen surfaces.[2-8] They studied various factors affecting colloidal forces and some also investigated adhesion forces. In this work, we focus on the nature of colloidal forces. Yoon et. al.[2, 3] reported the first direct measurement of colloidal forces between two bitumen surfaces. They prepared bitumen-coated mica or silica surfaces by means of a Langmuir-Blodgett trough (L–B deposition) and conducted surface force measurements using SFA and AFM. They observed long-range repulsive electrostatic force at a separation distance above 70 nm and strong repulsive force at a shorter range that cannot be explained by the classical DLVO theory. The authors suggested that the non-DLVO repulsive forces were steric forces due to the asphaltenes exposed on the bitumen surface in an aqueous environment. Wu *et al.*[4-6] on the other hand, investigated the colloidal forces between two micron-sized bitumen droplets in water based on the collision trajectories of two colliding bitumen droplets and the hydrodynamic force applied to break up a bitumen doublet into two droplets. They suggested that the enhanced repulsion between bitumen was due to the heterogeneous protrusion structure on the bitumen surface. Laroche *et al.*[7] used the same techniques and compared colloidal forces between deasphalted bitumen (*i.e.* maltene) droplets and whole bitumen droplets and found that the repulsion increases in the presence of asphaltene. More recently, Liu *et al.*[8] measured colloidal forces between two bitumen surfaces also using AFM as Yoon did. The difference was that Liu *et al.* prepared the bitumen substrate using spin-coating method and the bitumen sphere using dip-coating technique. In addition to the repulsive long-range electrostatic force and short-range steric force, they also detected attractive hydrophobic force at a separation distance around 10 nm in the presence of 1mM KCl in the solution.

For bitumen-sand interaction, Liu *et al.*[9] were the first to directly measure the surface force between bitumen and silica with AFM and found that at long separation distances bitumen-silica repulsion could be described by DLVO theory while at shorter distance (< 2–3 nm) an additional repulsive force of steric origin was observed. Long *et. al.*[10] found that the repulsive force between bitumen and silica increases with increasing temperature. Later, Zhao *et al.*[11] measured the surface force between bitumen and silica also using AFM in synthetic plant solutions, actual plant water, and the foam and residue solutions. In the synthetic electrolyte solutions, they found similar results as Liu *et al.*[9]. While in plant process water and the foam and residue solutions, the measured forces were weaker than the DLVO forces. More recently, Hogshead *et al.*[12] used AFM to measure bitumen-silica interaction forces in both an aqueous solution and an ionic liquid. When Utah bitumen was used, colloidal forces collected in water and ionic liquid appeared similar. For the Alberta bitumen, the attractive force was longer-ranged and stronger in water than in the ionic liquid. For bitumen-clay interactions, Liu *et al.*[13] measured the surface forces between bitumen-kaolinite and bitumen-montmorillonite using AFM. Repulsive forces were detected for both systems.

Many researchers studied the bitumen-bubble interactions.[2, 14-24] As far as colloidal forces are concerned, only a couple papers have been published in the open literature. In these studies,[22, 23] the forces between an air bubble and a bitumen surface were measured with AFM, in which the air bubble was placed on a hydrophobic substrate, while bitumen was coated on silica spheres by dip-coating. Long range repulsive forces were initially observed due to electrostatic double layer forces. It was also reported that an external force applied to the AFM cantilever was needed to exceed a threshold value before the probe jumped into contact with the air bubble, forming stable three-phase contact line.

Studies of the wetting film formed between bitumen and air bubble can provide useful information for better understanding the colloidal forces acting between the two macroscopic surfaces. In 1967, Laskowski and Kitchener[25] recognized that the disjoining pressure (Π) in wetting films must be negative for bubble-particle attachment to occur in flotation. However, the authors recognized the difficulty in measuring the negative disjoining pressures because the wetting films with $\Pi < 0$ are unstable and rupture too quickly. It was only recently that CAST developed a technique to measure negative disjoining pressures using a modified thin film pressure balance (TFPB).[26, 27] This new method is based on monitoring the profiles of the wetting films in nanoscale and analyzing the profiles using the Reynolds lubrication theory to determine the excess pressure in the film. This was made possible by monitoring the deformation of bubbles during the course of bubble-particle interactions.

Bitumen is a colloidal dispersion of asphaltene micelles in maltenes.[28, 29] Asphaltenes are the insoluble part of a bitumen in low molecular weight paraffins (*e.g.*, heptane, pentane, and hexane) but soluble in light aromatic hydrocarbons (*e.g.*, toluene and benzene). Maltenes are the soluble part in both types of the solvents and consists of saturates, aromatics and resins. The polar components of a bitumen are asphaltenes and resins, but asphaltenes are more polar than resins. These polar molecules have strong affinity toward water and adsorb at oil/water interfaces, contributing to the stabilization of the emulsions formed in bitumen extraction process.[30] For the bitumen-in-water emulsions, some researchers[31-33] suggested that they are stabilized by natural surfactants, mainly carboxylates and sulfates, present in bitumen, while others[2, 3] proposed that asphaltenes are the stabilizers. For the water-in-bitumen emulsions, both asphaltenes and resins are responsible for the stabilization of the emulsions, but asphaltenes are the key stabilizer.[34-37] In these regards, one may expect that the asphaltenes and/or resins may play a significant role. It is,

therefore, the objective of this chapter to study the role and extent that asphaltenes play in bitumen aeration.

In the present study, asphaltenes and maltenes were separated from bitumen to determine the colloidal forces present in the wetting films of water formed on these substrates and to discuss their roles in bitumen aeration. The kinetics of thinning of the wetting films formed on bitumen, asphaltene, and maltene were monitored using the TFPB technique. The disjoining pressure was determined based on the temporal and spatial profiles of the wetting films by the method developed by Lei *et al.*[27] The disjoining pressure data obtained in the present work have been analyzed in the view of the extended DLVO theory.[3, 38]

3.2 Experimental

3.2.1 Materials

A sample of bitumen (99 wt%) was provided by Suncor Energy, Inc. Reagent grade toluene (>99.5% purity) was purchased from Spectrum Chemical Mfg. Corp., and HPLC grade n-heptane (99.3% purity) was obtained from Fisher Scientific. Millipore ultrapure water with a resistivity of 18.2 MΩ·cm was obtained using a Direct Q3 water purification system. Silicon wafers (100 crystal planes, University Wafer) were used as the substrates for coating bitumen, asphaltene and maltene. Sulfuric acid (H_2SO_4, 98% purity, VMR international) and hydrogen peroxide (H_2O_2, 29.0–32.0% purity, Alfa Aesar) were used to clean the silicon substrates.

3.2.2 Separation of Asphaltene and Maltene

The bitumen sample was dissolved in toluene at a toluene/bitumen ratio of 5:1 by volume. The solution was then stirred using a magnetic stirrer for 2 hr, centrifuged for 30 min to remove the solids, and subsequently put under a fume hood to allow the toluene to naturally evaporate. After the toluene evaporation was complete, n-heptane was added to the toluene- and solids-free

bitumen at a heptane/bitumen ratio of 40:1 by volume. The n-heptane and bitumen mixture were stirred by means of a magnetic stirrer for 2 hr, during which time maltene dissolved into n-heptane while asphaltene precipitated out. The mixture was left overnight for the asphaltene to settle at the bottom. The supernatant n-heptane was carefully removed by means of a pipette and placed under a fume hood to let the n-heptane naturally evaporate, leaving maltene behind. The amount of the evaporated n-heptane was small.

The asphaltene precipitate was repeatedly washed for 17 times with an excess amount (~1L) of n-heptane to remove any maltene that may have co-precipitated. In each washing step, the mixture was agitated for 2 hr and left to stand overnight to allow the asphaltene to precipitate and the supernatant was carefully removed. After the last washing step, the supernatant n-heptane became colorless. The asphaltene precipitate was left under a fume hood to let n-heptane to evaporate and thereby obtain a sample of purified asphaltene. The amount of the evaporated n-heptane was small.

3.2.3 Preparation of Bitumen-, Maltene-, and Asphaltene-coated Surfaces

Silicon wafers were first oxidized in an oxidation furnace at 1070 °C for ~40 min using wet oxidation procedure. The oxidized silicon wafers were then cut into 12x12 mm pieces and used as substrates for bitumen, asphaltene, and maltene. Before the coating, the silicon substrates were subjected to ultrasonic vibration in water for ~1 hr and then cleaned by immersing in a Piranha solution (3:7 by volume of H_2O_2/H_2SO_4) at 120 °C for 1 hr, followed by rinsing with an adequate amount of ultrapure water and pure nitrogen (N_2) blow-drying. The silicon substrate was placed in a spin-coater (Laurell, WS-400-6NPP), rinsed with toluene, and then spun at 6,000 rpm for 30 s to dry off the toluene. When the substrate was free of toluene, a small amount of (2 or 3 drops) of a bitumen-in-toluene solution (2.5 mg/mL) was placed on the substrate and let it stand

for 10 s. The substrate was then spun at 3,500 rpm for 20 s before placing another drop of the bitumen solution and continuing spinning for additional 10 s. The spinning continued for an additional 1 minute at 6,000 rpm to evaporate the solvent and obtain a smooth and uniform bitumen coating. The spin-coated bitumen was then placed in a particulate matter-free laminar hood for ~30 min to ensure maximum removal of toluene from the coating. The procedure described above was also employed for the preparation of asphaltene- and maltene-coated silicon surfaces.

3.2.4 Measurement of Film Thinning Kinetics

Figure 3.1 shows the modified thin film pressure balance (TFPB) apparatus used in the present work to study the kinetics of film thinning, which is the same as Figure 2.1. The original TFPB apparatus was designed for the study of foam films (or the water films between two air bubbles) by Scheludko and Exorowa.[39] The equipment was modified to study the kinetics of film

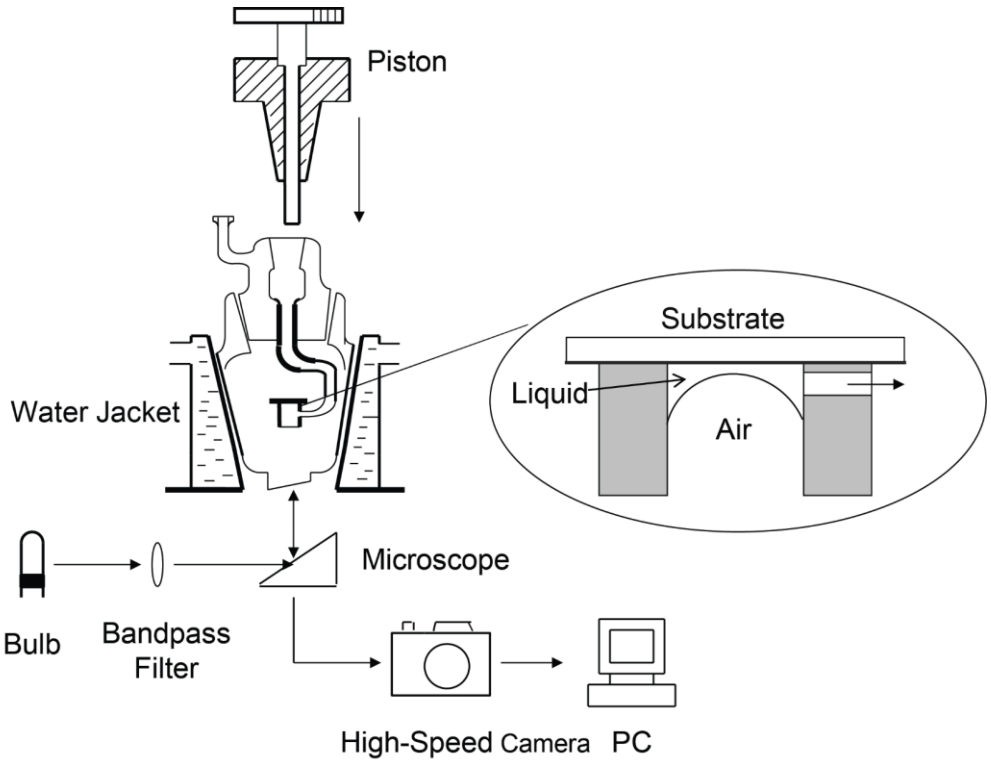

Figure 3.1 Schematics of the modified TFBC apparatus used for the study of wetting films.

thinning for wetting films.[40] As shown in the inset, a flat surface of interest is placed on the top of a film holder (2.0 mm diameter glass tubing) with its surface facing downward, so that the surface is in contact with the water in the film holder. In the present work, the flat silicon wafers coated with bitumen, asphaltene, or maltene were used as samples of interest.

In a given experiment, the silicon wafer-glass tubing assembly was inserted in a glass cell surrounded by a water jacket, in which water of known temperature was circulated. The film holder-water jacket assembly was placed on an inverted microscopic stage (Olympus IX51) to monitor the changes in film thicknesses as a function of time. A mercury arc short lamp (100 W, Olympus) was used as a light source with a bandpass interference filter (#65-643, Edmund Optics) to produce a monochromatic green light source (λ=546 nm). In a given experiment, the liquid in the film holder is slowly withdrawn by turning the knob of the piston. Once the interference patterns (Newton rings) began to appear in the microscopic field of view, the film was allowed to thin spontaneously while recording the images by means of a high-speed camera (Fastec Imaging, HS400115). The interference patterns recorded were used to reconstruct timed thickness profiles of a wetting film across the entire film holder with a nanometer resolution. The spatial and temporal film profiles of the wetting film were then used to monitor the changes in film thicknesses (h) as a function of time and radial distance of the film at any point of the film. The experimental data were used to obtain information on the film thinning kinetics and calculate the disjoining pressure (Π) in the thin liquid films (TLFs) according to Eq. [3.1], as derived by Pan. *et.al.*,[27]

$$\Pi = \frac{2\gamma}{R} - \frac{\gamma}{r}\frac{\partial}{\partial r}\left(r\frac{\partial h}{\partial r}\right) - 12\mu\int_{r=\infty}^{r}\frac{1}{rh^3}\left[\int_{r=0}^{r} r\frac{\partial h}{\partial t}dr\right]dr \qquad [3.1]$$

where γ is the air/water interfacial tension, R the bubble radius, r the radial position, h the wetting film thickness, and μ the fluid viscosity.

3.3 Results and Discussion

3.3.1 Film Thinning Kinetics and Disjoining Pressure

Figure 3.2 shows the spatial and temporal profiles of the wetting films formed between an

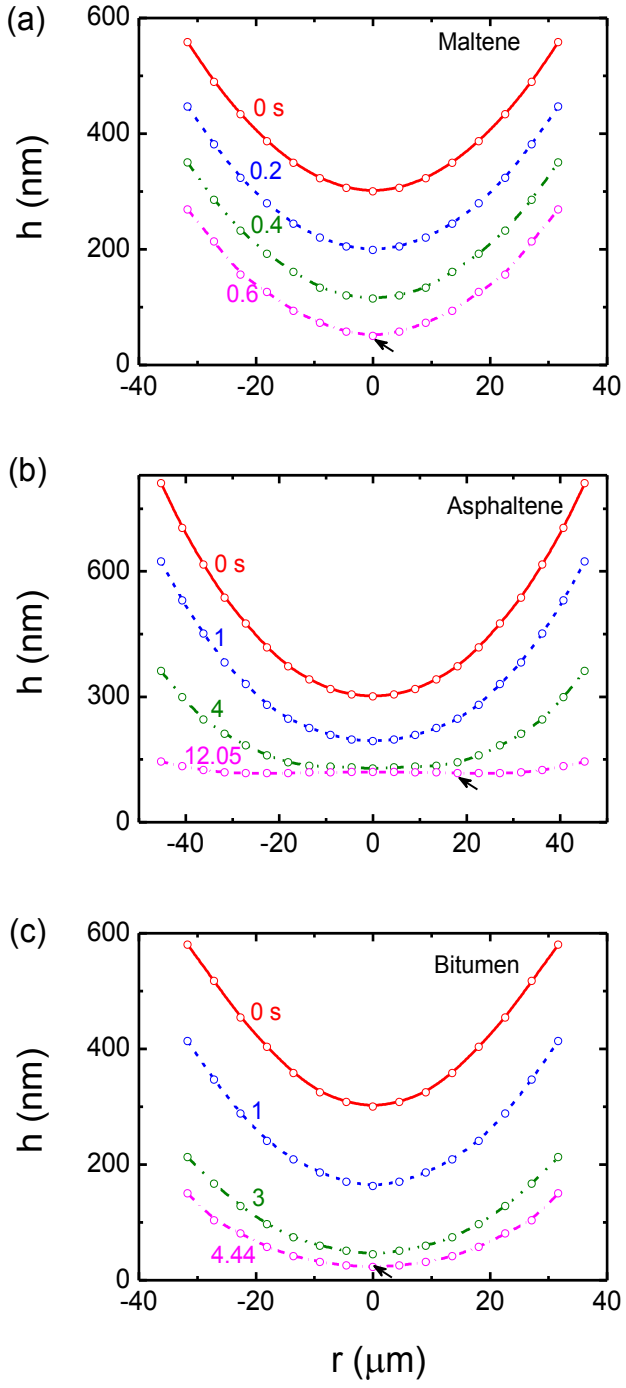

Figure 3.2 Spatial and temporal profiles of the wetting films of water formed on maltene (a), asphaltene (b), and bitumen (c) at 55 °C. The arrows represent the critical thicknesses (h_{cr}) where the films rupture.

air bubble and maltene, bitumen, and asphaltene surfaces in water at 55 °C. The profiles are similar to those obtained at 80 °C (see Figure 2.3 in Chapter 2). From a thickness of 300 nm, the films formed on maltene thinned fastest and ruptured at 0.6 s. On asphaltene, the film thinned 20 times slower than on maltene, with the rupture occurring at 12.05 s. On bitumen, which contains both maltene and asphaltene, the film thinned slower than on maltene and faster than on asphaltene. The film thickness (h) *vs.* time (t) plots in Figure 3.3 presents the kinetics of film thinning at the center of the wetting film, which increased in the order of asphaltene, bitumen, and maltene. It is obvious from Figure 3.3 that the film on asphaltene seemed "metastable" for about 3 s before its rupture, corresponding to the flattening of the film shown in Figure 3.2.

The film profiles presented in Figure 3.2 have been used to obtain kinetic information such as $\partial h/\partial t$ and $\partial h/\partial r$ (r is the radius position) that can be used to calculate the disjoining pressure (Π) according Eq. [3.1].[27]

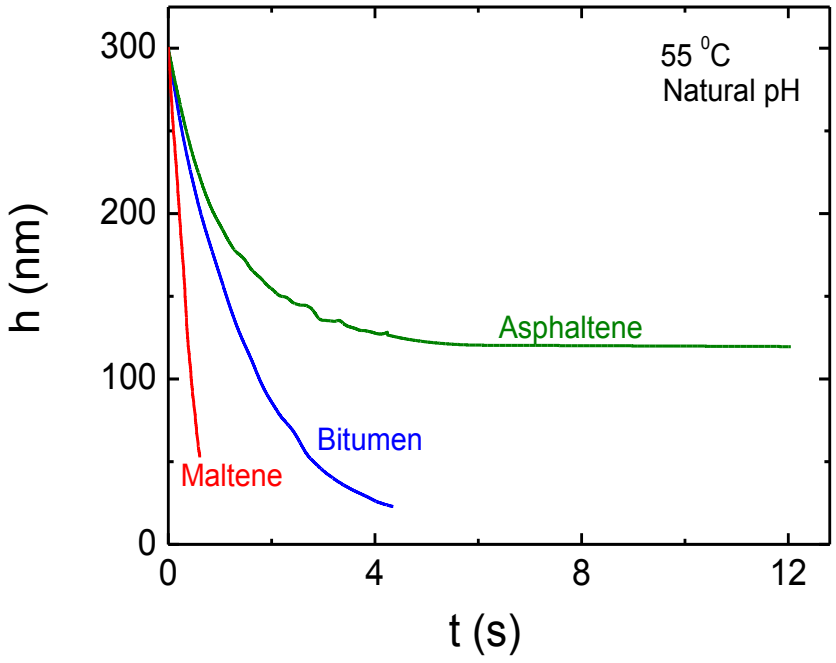

Figure 3.3 Kinetics of film thinning on maltene, bitumen, and asphaltene at 55 °C. It decreases in the order of maltene, bitumen and asphaltene.

Figure 3.4 shows the results of Π obtained for maltene, bitumen, and asphaltene at different time and radial positions. In these calculations, γ = 67.1 mN/m, μ = 0.5x10^{-3} Pa·s at 55 °C, and R = 2 mm were used. As shown, the disjoining pressures were negative in the wetting films formed on both maltene and bitumen, *i.e.*, Π < 0, while it is positive, *i.e.*, Π > 0, on asphaltene. A vertical pressure balance shows that

$$p = p_{cur} - \Pi \qquad [3.2]$$

where p is the pressure of the liquid in the wetting film and p_{cur} is the pressure due to curvature change and surface tension (Laplace pressure). Eq. [3.2] shows that a negative disjoining pressure helps increase the film thinning process, while a positive disjoining pressure causes retardation. Thus, the results presented in Figure 3.4 explain why the kinetics of film thinning increased in the order of asphaltene, bitumen, and maltene. The change in disjoining pressure with film thickness at the center of the films on maltene, bitumen, and asphaltene were shown in Figure 3.5. As shown, on maltene and bitumen, the disjoining pressure becomes increasingly negative as the film thickness decreases, while on asphaltene it becomes increasingly positive. Π = -450 Pa on maltene and Π = -160 Pa on bitumen were obtained just before the wetting films rupture. Therefore, the fast kinetics observed with maltene can be attributed to the highly negative disjoining pressure.

It has been shown that the hydrophobic force, and hence the magnitude of negative disjoining pressure, increase with increasing surface hydrophobicity.[41] The results obtained in the present work show, therefore, that maltene is the most hydrophobic, followed by bitumen. Asphaltene, on the other hand, is hydrophilic as shown by the positive disjoining pressures measured (see Figures 3.4b and 3.5). Asphaltene being least hydrophobic is understandable because its functional groups, such as carboxylic, amide, thiol, hydroxyl, and carbonyl, are

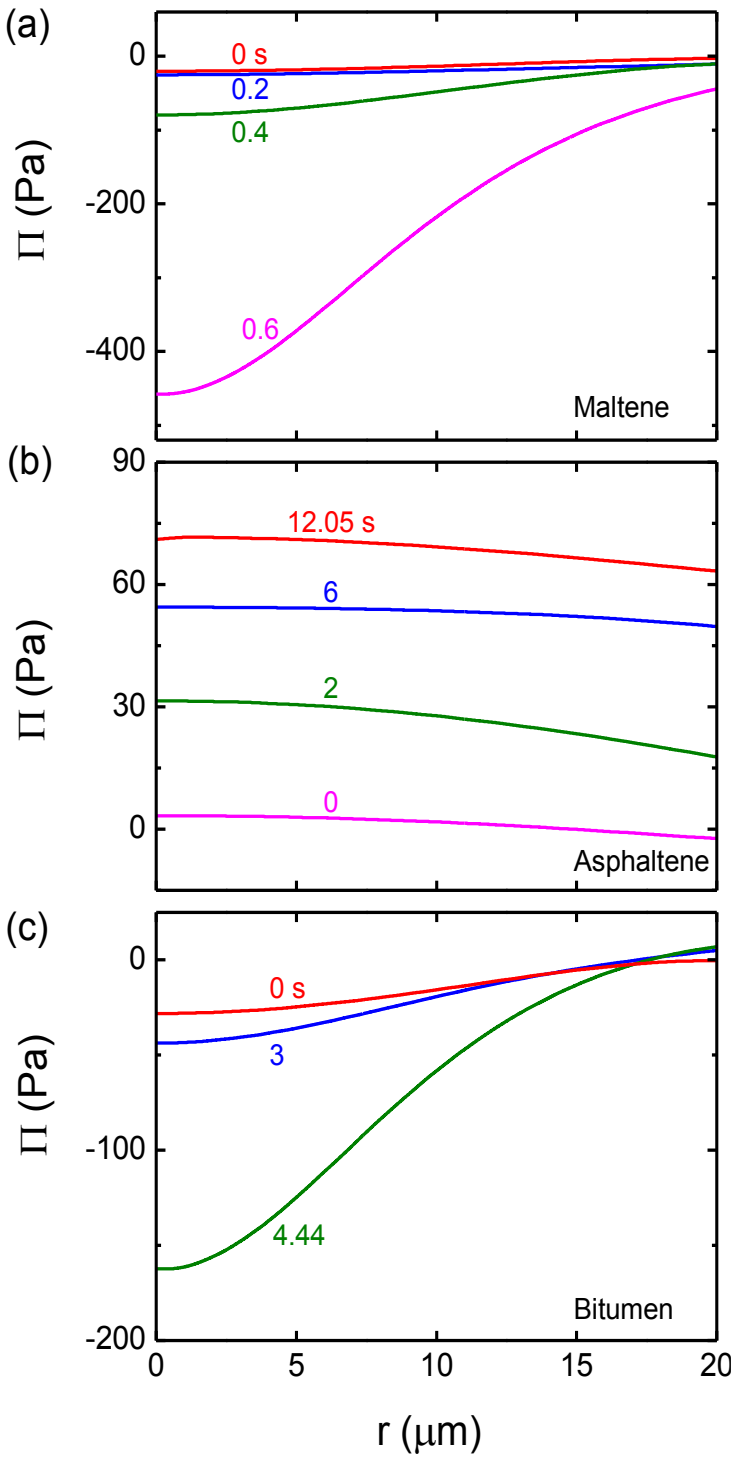

Figure 3.4 Changes in the disjoining pressure (Π) of the wetting films of water formed on maltene (a), asphaltene (b), and bitumen(c) as functions of time and radial distance (r) of the film from the film center at 55 °C.

hydrophilic. Maltene being the most hydrophobic is also understandable, because it contains hydrocarbons. The hydrophobicity of bitumen lies in between asphaltene and maltene, suggesting that asphaltene is exposed to the bitumen/water interface in aqueous.

The results obtained in the present work suggest that the hydrophobicity of maltene is compromised by the presence of asphaltene on the surface. It is likely that the hydrophilic groups of asphaltene are exposed to the aqueous phase, the extent of which will determine the hydrophobicity of bitumen and its floatability. That bitumen is still hydrophobic despite the likely exposure of asphaltene on the surface suggests that the surface may not be completely covered by the hydrophilic groups of asphaltene, which is very likely since more than 80% of bitumen is maltene. Further study is necessary to more fully understand the hydrophobicity of bitumen.

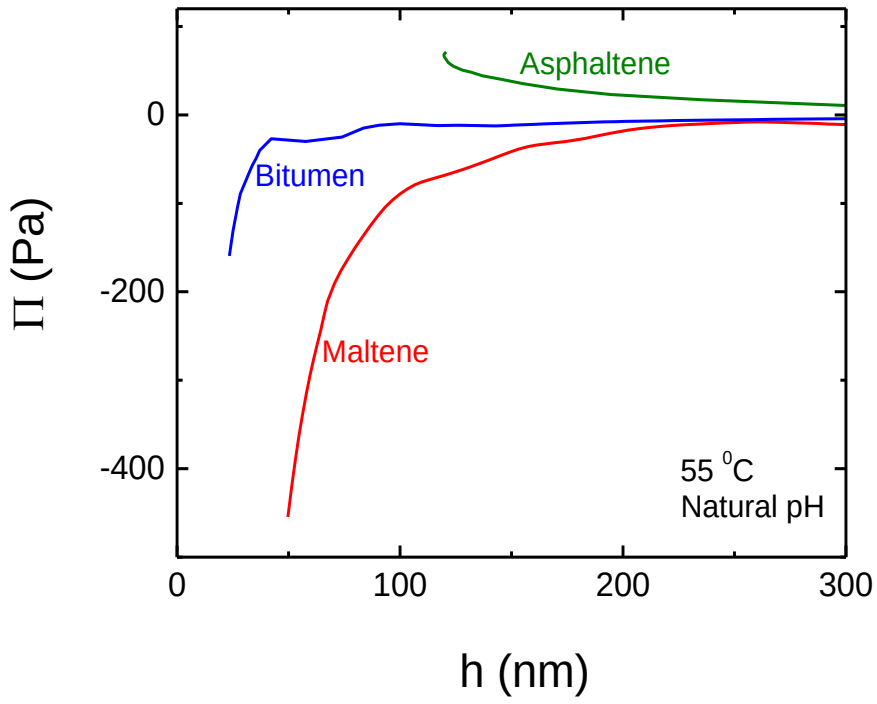

Figure 3.5 Changes in the disjoining pressure (Π) at the center of the wetting films of water formed on maltene, bitumen, and asphaltene at 55 °C. Thermodynamically, the film can rupture when $\Pi < 0$.

3.3.2 Extended DLVO Theory

It is well known that colloidal forces play an important role in bitumen extraction. The classical DLVO theory[42, 43] recognizes two colloidal (or surface) forces, which include the electrical double-layer force (F_e) and the van der Waals dispersion force (F_d). One can readily convert the forces to disjoining pressures (Π) or vice versa from the Derjaguin approximation,[44]

$$\frac{F}{R} = 2\pi G(h) \qquad [3.3]$$

and the definition of disjoining pressure,

$$\Pi(h) = -(\partial G / \partial h)_{P,T,\mu_s} \qquad [3.4]$$

in which F is the surface force, R is the radius of curvature of the macroscopic surface(s) involved, and $G(h)$ is the free energy of a wetting film which varies with film thickness h or the separation between two surfaces. According to the DLVO theory, the disjoining pressure of a thin liquid film (TLF) can be given by,

$$\Pi = \Pi_e + \Pi_d \qquad [3.5]$$

where the subscripts e and d represent the electrical double-layer and van der Waals dispersion forces, respectively.

The DLVO theory has long been used as the governing law in a wide range of industries, including the bitumen industry. The theory can predict the stability of the thin liquid films (TLFs) formed between any two surfaces involving macroscopic particles, air bubbles, oils, *etc*. For example, the disjoining pressure in the TLF between bitumen and an air bubble affects the bitumen aeration during the hydrotransport process.

When a particle approaches an air bubble, the TLF (or wetting film) formed in between them must be thinned quickly and rupture (or break) to form a finite contact angle (θ).

Thermodynamically, wetting films rupture when θ > 0, as is well known. The role of colloidal forces in bubble-particle interactions can be better appreciated using the Frumkin-Derjaguin isotherm,[45]

$$\cos\theta = 1 + (1/\gamma_{23})\int_{h_0}^{\infty} \Pi dh \qquad [3.6]$$

in which γ_{23} is the interfacial tension between air bubble and water (or surface tension of water), and Π is the disjoining pressure in a wetting film which varies with film thickness *h*. The integral of Π from $h = h_o$ to ∞ represents the Gibbs free energy change associated with bubble-particle interaction (ΔG). Here, the parameter h_o represents the thickness of the water film in equilibrium with the vapor phase inside an air bubble attached to a hydrophobic surface. The values of h_o are usually less than 1 nm.

The disjoining pressure in the wetting film due to the van der Waals force is given by,

$$\Pi_d = -\frac{A_{132}}{6\pi h^3} \qquad [3.7]$$

where A_{132} is the Hamaker constant, while the disjoining pressure due to the electrostatic double-layer force is given by

$$\Pi_e = \frac{\varepsilon\varepsilon_0\kappa^2}{2\sinh(\kappa h)}\left[(\psi_1^2 + \psi_2^2\right]\cos ech(\kappa h) - 2\psi_1\psi_2\coth(\kappa h) \qquad [3.8]$$

in which ε_0 is the permittivity in vacuum, ε the dielectric constant of water, ψ_1 and ψ_2 the double-layer potentials at the solid/water and air/water interfaces, respectively, and κ is the reciprocal Debye length. In this report, the subscripts 1, 2, and 3 represent solid, gas, and water phases, respectively.

Substituting Eqs. [3.7] and [3.8] into the DLVO theory (Eq. [3.5]) and subsequently into the Frumkin-Derjaguin isotherm (Eq. [3.6]), one obtains the following equation,

$$\cos\theta_0 = 1 + \frac{1}{\gamma_{23}}\left[-\frac{A_{132}}{12\pi h_0^2} + \varepsilon\varepsilon_0\kappa\frac{2\psi_1\psi_2\exp(\kappa h_0) - \psi_1^2 - \psi_2^2}{\exp(2\kappa h_0) - 1} \right] \quad [3.9]$$

In wetting films, both of the terms within the bracket are positive values, because A_{132} is negative and ψ_1 and ψ_2 are negative under most flotation conditions including bitumen aeration. Under these conditions, contact angles cannot be greater than zero and consequently $\Delta G > 0$ for the bitumen-bubble interaction. The only way to have $\theta > 0$ and $\Delta G < 0$, would be to create a hydrophobic force in wetting films, so that one can use the following relation,

$$\cos\theta = 1 + \frac{1}{\gamma_{23}}\left[-\frac{A_{132}}{12\pi h_0^2} + \varepsilon\varepsilon_o\kappa\frac{2\psi_1\psi_2\exp(\kappa h_0) - \psi_1^2 - \psi_2^2}{\exp(2\kappa h_0) - 1} + \frac{C}{2\pi}\exp(\frac{h_o}{D}) \right] \quad [3.10]$$

in which the third term in the bracket represents the contribution from the hydrophobic force (Π_h) to the total disjoining pressure (Π) in a wetting film.

According to Eq. [3.10], the hydrophobic force (and hence the negative disjoining pressure) must be large enough to overcome the sum of the repulsive van der Waals and double-layer forces in order to break the wetting film and form a finite contact angle that is greater than zero. The three terms within the bracket constitute the extended DLVO theory,[46]

$$\Pi = \Pi_e + \Pi_d + \Pi_h \quad [3.11]$$

where Π_h represents the disjoining pressure due to the hydrophobic force in a TLF, as proposed earlier by Yoon's group at Virginia Tech.[26, 27]

3.3.3 Disjoining Pressure Isotherms

According to the extended DLVO theory (Eq. [3.11]), the disjoining pressure (Π) in a wetting film has three components, *i.e.*, double-layer (Π_e), van der Waals dispersion (Π_d), and hydrophobic force (Π_h) components. It will be of interest to construct disjoining pressure isotherms, in which changes in the disjoining pressure components *vs*. film thickness are plotted.

a) Maltene

In Figure 3.6, the changes in Π_e, Π_d, and Π_h *vs. h* are plotted for the wetting film of water formed on maltene at 55 °C. The triangles represent the experimental data obtained in the present work, and the solid line represents a fit to the extended DLVO theory (Eq. [3.11]). There are three dashed lines, representing Π_d calculated using Eq. [3.7] with a A_{132} value of -1 x 10^{-20} J, and Π_e calculated using Eq.[3.8] with ψ_1 = - 65 mV for the surface potential of maltene, and ψ_2 = - 26 mV for that of air bubble, and κ^{-1} = 50 nm for the Debye length, and

$$\Pi_h = \frac{C}{2\pi D}\exp\left(-\frac{h}{D}\right) \qquad [3.12]$$

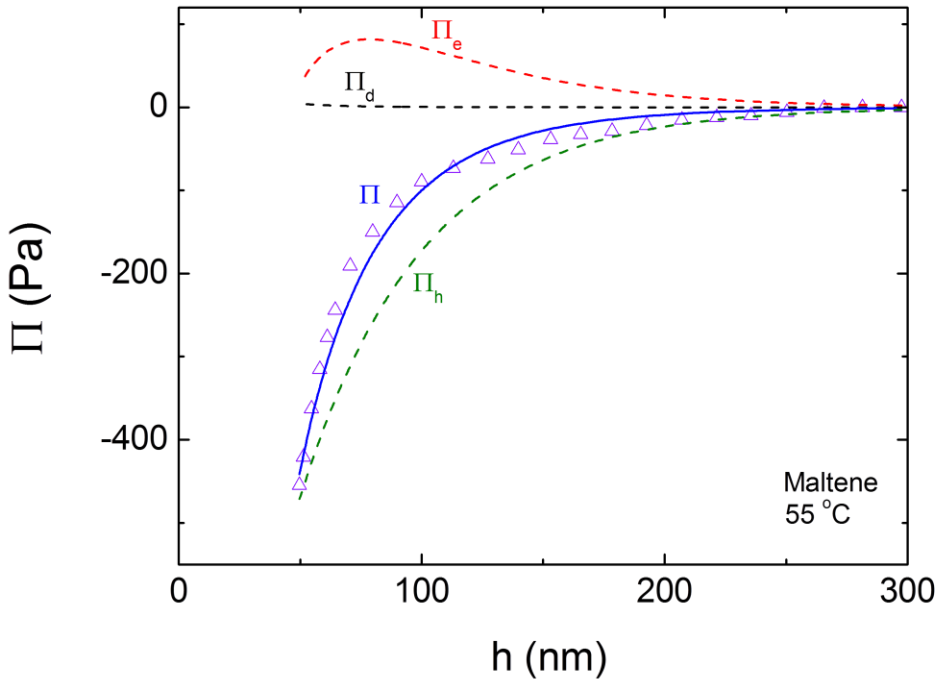

Figure 3.6 The disjoining pressure isotherm (Π(h)) obtained at the center of the wetting film of water formed on maltene at 55 °C. The triangles represent the experimental data presented in Figure 3.5. The solid line represents a fit to the extended DLVO theory, which includes contributions from: van der Waals force (Π_d) with a Hamaker constant of A_{132} = -1 x 10^{-20} J; electrostatic force (Π_e) with surface potential of ψ_1 = - 65 mV for maltene, surface potential of ψ_2 = - 26 mV for air bubble, and Debye length of κ^{-1} = 50 nm; and hydrophobic force (Π_h) with fitting parameters of C = -0.43 mN/m and D = 50 nm.

where C (= -0.4 mN/m) and D (= 50 nm), known as decay lengths, are the best fit parameters. The figure legend shows all other parameters used to construct the disjoining pressure isotherms.

The Π *vs*. h isotherms show that Π_h far exceeds in magnitude the sum of Π_e and Π_d, so that Π is net negative at all separations studied. The decay length of 50 nm is very large as compared to the hydrophobic forces measured between hydrophobic surfaces, partly because air bubbles in water are the most hydrophobic entity known to date.[47, 48] Air bubbles in water have an interfacial tension of 72 mN/m, while hydrocarbon oils have interfacial tensions of ~50 mN/m. Interfacial tensions are excellent measures of hydrophobicity.

b) Asphaltene

Figure 3.7 shows the disjoining pressure isotherms obtained at the center of the wetting film of water formed on asphaltene at 55 °C. As shown, $\Pi > 0$ indicating that asphaltene is hydrophilic. As suggested previously,[2] the sharp increase in Π may represent the repulsive steric disjoining pressure (Π_s). Thus, the extended DLVO theory may be written as follows,

$$\Pi = \Pi_d + \Pi_e + \Pi_s \qquad [3.13]$$

where

$$\Pi_s = \frac{kT}{s^3}\left[(2L/h)^{4/9} - (h/2L)^{3/4}\right] \qquad [3.14]$$

In Eq. [3.14], s represents the mean distance between grafted points of a polymer, and L is the length of the polymer tail. Eq. [3.14] was derived by de Gennes for the interaction between two

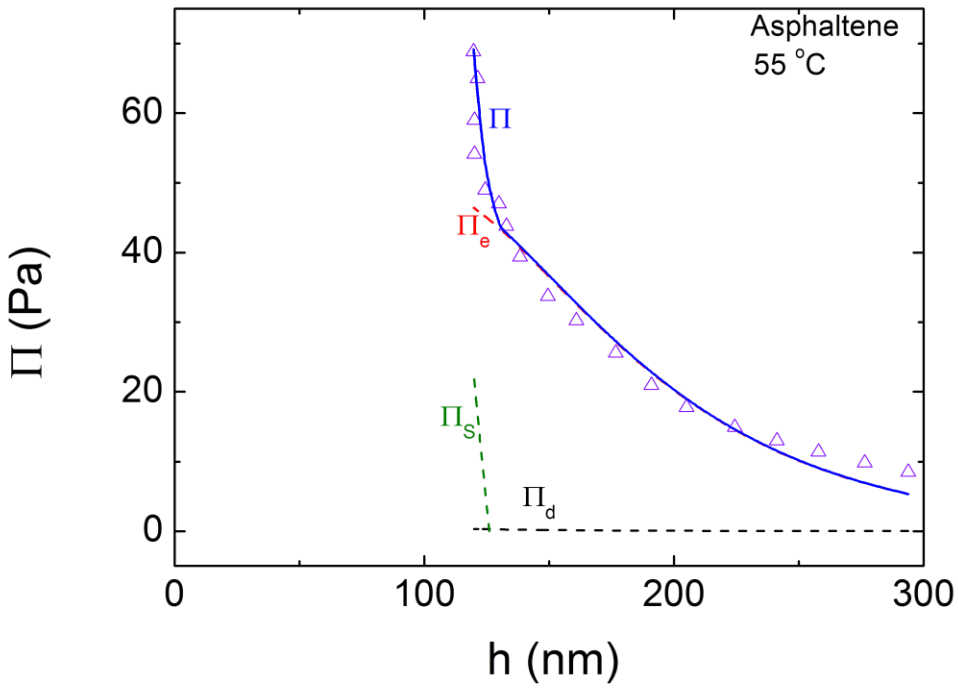

Figure 3.7 The disjoining pressure isotherm (Π(h)) obtained at the center of the wetting film of water formed on asphaltene at 55 °C. The triangles represent the experimental data presented in Figure 3.5. The solid line represents a fit to the extended DLVO theory, which includes contributions from: van der Waals force (Π_d) with a Hamaker constant of A_{132} = -1 x 10^{-20} J; electrostatic force (Π_e) with surface potential of ψ_1 = - 68 mV for asphaltene, surface potential of ψ_2 = - 26 mV for air bubble, and Debye length of κ^{-1} = 65 nm; and repulsive steric force (Π_s) between asphaltene polymers with a brush length of L = 63 nm and a grafting distance of s = 23 nm.

surfaces grafted by "brush-like" polymers.[49] The best-fit parameters used to fit the experimental data are presented in the figure legend.

c) Bitumen

Figure 3.8 shows the disjoining pressure isotherms for the TLF of water formed on bitumen at 55 °C. The extended DLVO theory that was used to represent the system included four different components:

$$\Pi = \Pi_d + \Pi_e + \Pi_s + \Pi_h \qquad [3.15]$$

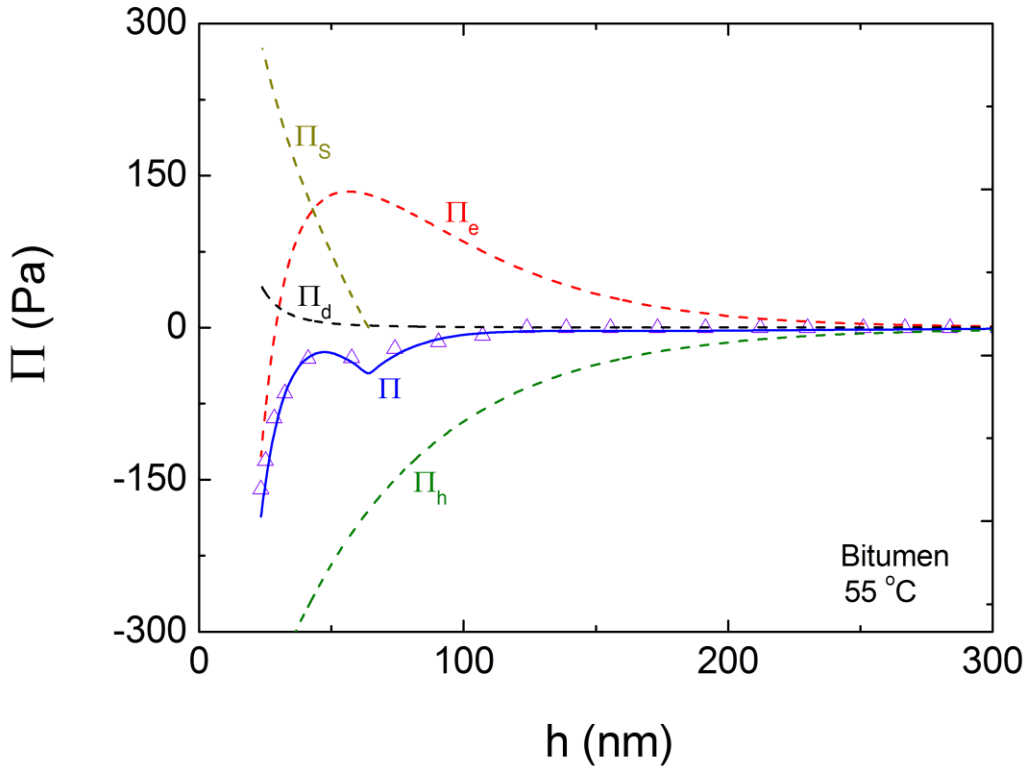

Figure 3.8 The disjoining pressure isotherm (Π(h)) obtained at the center of the wetting film of water formed on bitumen at 55 °C. The triangles represent the experimental data. The solid line represents a fit to the extended DLVO theory, which includes contributions from: van der Waals force (Π_d) with a Hamaker constant of A_{132} = -1 x 10^{-20} J; electrostatic force (Π_e) with surface potential of ψ_1 = - 57 mV for bitumen, surface potential of ψ_2 = - 30 mV for air bubble, and Debye length of κ^{-1} = 45 nm; repulsive steric force (Π_s) between bitumen polymers with a brush length of L = 32 nm and a grafting distance of s = 26 nm, and hydrophobic force (Π_h) with fitting parameters of C = -0.2 mN/m and D = 54 nm.

where the subscripts *d*, *e*, *s*, and *h* represent the dispersion, double-layer, steric, and hydrophobic disjoining pressures, respectively. The model parameters that were used to fit the experimental data are given as figure legends.

As shown in Chapter 2, disjoining pressure measurements were also conducted with bitumen substrates at other three different temperatures, *i.e.*, 22, 35 and 80 °C, and their disjoining pressure isotherms were constructed using the extended DLVO theories (Eq. [3.15]) with the

Table 3.1 Parameters used to fit the disjoining pressure of the wetting film of water formed on bitumen at different temperatures

T (°C)	A_{132} (J)	ψ_1 (mV)	ψ_2 (mV)	κ^{-1} (nm)	s (nm)	L (nm)	C (mN/m)	D (nm)
22	-1×10^{-20}	-50	-24	80	30	68.3	0	0
35	-1×10^{-20}	-55	-20	33	26	28.3	-0.12	47
55	-1×10^{-20}	-57	-30	45	26	32	-0.2	54
80	-1×10^{-20}	-110	-45	50	26	32	-1.32	55

fitting parameters shown in Table 3.1. The disjoining pressure component due to hydrophobic force (Π_h) have been obtained and plotted together in Figure 3.9. As shown, Π_h becomes increasingly negative (or strong) and longer-ranged at higher temperatures, which is consistent with the flotation data reported in the literature.[1] Further, this finding is in agreement with the contact angle data obtained on the thick films of bitumen immersed in water (Chapter 2, Figures 2.9 and 2.10).

That hydrophobic forces measured in the wetting films of bitumen becomes stronger with increasing temperature, as shown in Figure 3.9, is contrary to what has been reported previously by Yoon's group at Virginia Tech.[50, 51] The group conducted a series of AFM force measurements with silica and gold surfaces hydrophobized by different surfactant coatings. The results obtained with the gold and silica surfaces hydrophobized with *n*-hexadenane (C-16) thiol and octadecylchlorosilane (OTS), respectively, showed that hydrophobic forces increase with decreasing temperature, which is contrary to what has been observed in the present work with bitumen and presented in Figure 3.9.

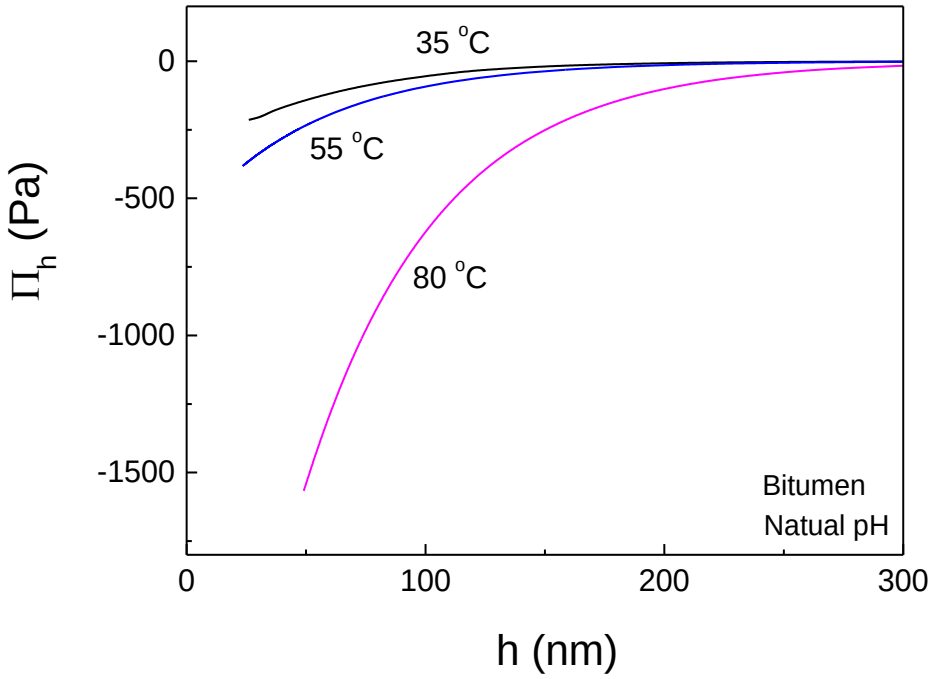

Figure 3.9 Hydrophobic disjoining pressure isotherms (Π_h) on bitumen at different temperatures in water of a natual pH of about 5.7.

A rigorous thermodynamic analysis of the AFM force data obtained previously by the Yoon group showed that the excess entropy (S^f) in the thin liquid films (TLFs) confined between hydrophobic surfaces decreases with decreasing film thickness, which has been attributed to the formation of H-bonded structures in the TLFs. The free energy of the water molecules in the TLFs confined between hydrophobic surfaces are higher than those in thick films, because much of the water molecules in the vicinity of hydrophobic surfaces cannot form H-bonds with the confining surfaces. The excess free energy is expended to form H-bonded structures, known as low density liquid (LDL).

It has been found also that the entropy decrease ($\Delta S^f < 0$) becomes more significant at lower temperatures, which indicates that water molecules can more readily form structures at lower

temperatures, which is consistent with our daily experiences that water forms H-bonded structures at lower temperatures (*i.e.*, ice).

It is well known that water molecules form low density liquid (LDL) in supercooled water.[52] More recent spectroscopic studies conducted using x-ray absorption spectroscopy (XAS) and x-ray Raman scattering (XRS) at Stanford University showed that LDL is also formed in bulk water at ambient temperatures.[53, 54] By monitoring the OH-vibrations of water molecules using the Raman and FTIR experiments, the Mallanace group at the University of Messina, Italy, showed that the population of LDL species at ambient temperatures are much higher than anticipated.[55, 56] According to Stillinger, water molecules behave similarly under supercooled conditions and in hydrophobic interactions,[52] suggesting that LDL can be more readily formed in the TLFs confined between hydrophobic surfaces at ambient temperature. In supercooled water, water molecules are prevented from forming ice by mechanical agitation or other external forces. Under this condition, they can form LDL to minimize free energy. In confined spaces, water cannot interact with the hydrophobic surfaces. One way to expand the excess free energy is to form LDL. Thus, the hydrophobic forces operating in colloid chemistry and mineral flotation originate from the structural changes of water in TLFs relative to the water structure in the bulk.

As has already been noted, the hydrophobic forces measured with gold and silica surfaces coated with C-16 thiol and OTS-coated surfaces decreased with increasing temperature, which is contrary to what has been observed with bitumen-coated surface in the present work. The AFM force measurements were carried out in narrow temperature ranges, *i.e.*, 10 to 40 °C, so that the chemistry of the hydrophobic surfaces would not change significantly with temperature. The only change that can occur over the narrow temperature range would be the water structure, or, rather, the tendency for low-density-liquid (LDL) to form in confined spaces.[50, 51] With bitumen, the

structure and properties of the substrate, *i.e.*, bitumen, can change significantly over the larger temperature range investigated in the present work, *i.e.*, 22 to 80 °C. After all, the bonding between hydrocarbons constituting bitumen was in liquid form; therefore, its structure can be more readily changed than the structure of a solid, such as gold or silica. It has been shown that the surface tension of bitumen decreases significantly with increasing temperature,[57] which is a manifestation of changing intermolecular bond energy. Surface tensions of solids do not change significantly over the narrow range of temperatures employed in the present work. In general, the lower the surface energy (or surface tension), the higher the hydrophobicity. Therefore, the increase in bitumen contact angle with temperature observed in the present work may be attributed to the decrease in surface free energy of bitumen, which corroborate well with the surface tension data noted above. Yoon's group showed also that the higher the contact angle, the stronger and longer-ranged the hydrophobic force.[41] Thus, there are two opposing factors affecting the hydrophobic forces in a bitumen flotation system. One is the contact angle, and the other is water structure. It appears that the former plays a more significant role than the latter.

Figure 3.10 compares the disjoining pressure components due to the steric forces present in the TLFs formed on bitumen at different temperatures. As shown, Π_s is maximum at 55 °C, followed by those obtained at 35 °C and 22 °C. The data seem to suggest that asphaltene polymers are more readily exposed at higher temperatures.

In Table 3.1, the Hamaker constant (A_{132}) for the asymmetric interaction between air bubble **1** and bitumen **2** in the medium of water **3** is predicted using the geometric mean combining rule

$$A_{132} = \sqrt{A_{131} A_{232}} \qquad [3.16]$$

where A_{131} and A_{232} are the Hamaker constants for symmetric interactions. From the values of $A_{131} = 3.7 \times 10^{-20}$ J and $A_{232} = 2.8 \times 10^{-21}$ J reported in the literature,[8, 58] one can obtain the value of A_{132}

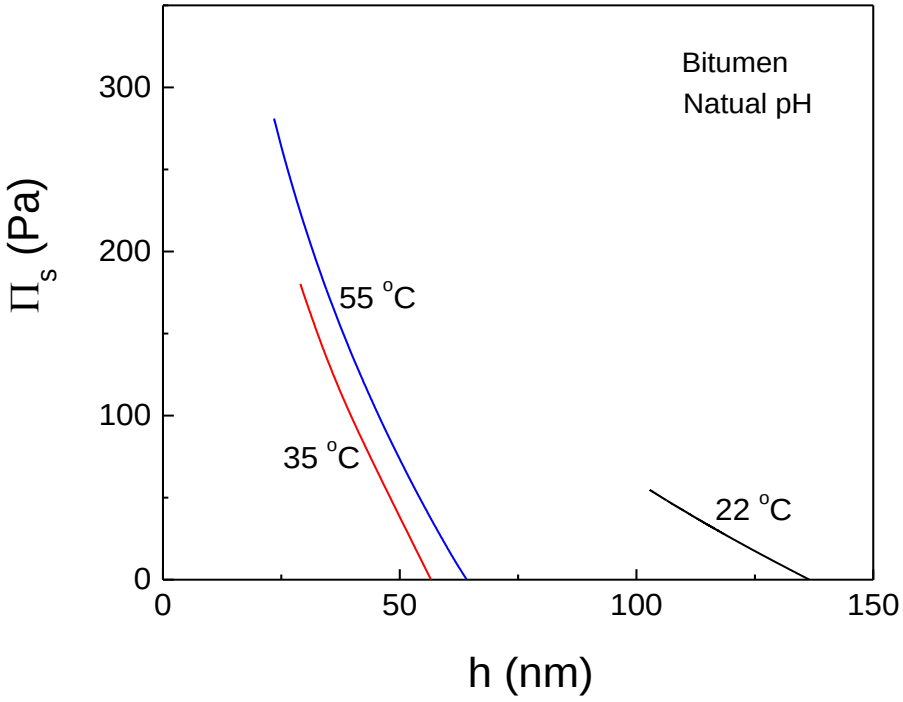

Figure 3.10 Steric disjoining pressure isotherms (Π_s) on bitumen at different temperatures in water of a natual pH of about 5.7.

= -1.0 × 10^{-20} J for the bitumen and bubble interaction, which is the same as used by Englert *et al.*[22] The ζ-potentials of the bitumen/water interface given in the table were obtained from the data reported by Dai *et al.*[59] and Liu *et al.*[60] The bitumen zeta potential used at 80 °C is more negative than those at lower temperatures, which is in agreement with Dai's findings[59] and other materials such as quartz,[61] sodium kaolinite,[61, 62] and others.[63] Zeta potentials of air bubble in water were close to the value reported by McShea *et al.*[64] The rest of the parameters in the table were best-fit parameters obtained on the basis of the experimental disjoining pressure isotherms. Better fit could have been obtained if the zeta potentials of bitumen and air bubbles were directly measured on the bitumen samples used in the present work at the relevant temperatures of interest. The zeta

potentials can be readily measured by electrokinetic methods, and the structural information on polymers can be measured using the dynamic light scattering, viscometric methods, and the small-angle neutron scattering (SANS) techniques.

3.3.4 Disjoining Pressure in Liberation

Unlike the oil sands in Utah, the sand grains in Canadian oil sands are thought to be surrounded by a thin film of water, known as connate water, as shown in Figure 3.11a. The first step toward extracting bitumen is to create a positive disjoining pressure in the innate water, *i.e.*, $\Pi > 0$. According to the extended DLVO theory discussed above, there are two ways to create a positive disjoining pressure. One is to increase the steric repulsion (Π_s), and the other is to increase the double-layer repulsion (Π_e). Both of these parameters are optimized by controlling temperature, pH, and electrolyte concentrations. At an elevated temperature, asphaltene can be more readily exposed to the surface of bitumen due to decreased viscosity. As shown in Table 2.1, the viscosity of Athabasca bitumen decreases by nearly three orders of magnitude as temperature increases from 20 to 75 °C. The presence of asphaltene polymers creates steric repulsion (Π_s) and

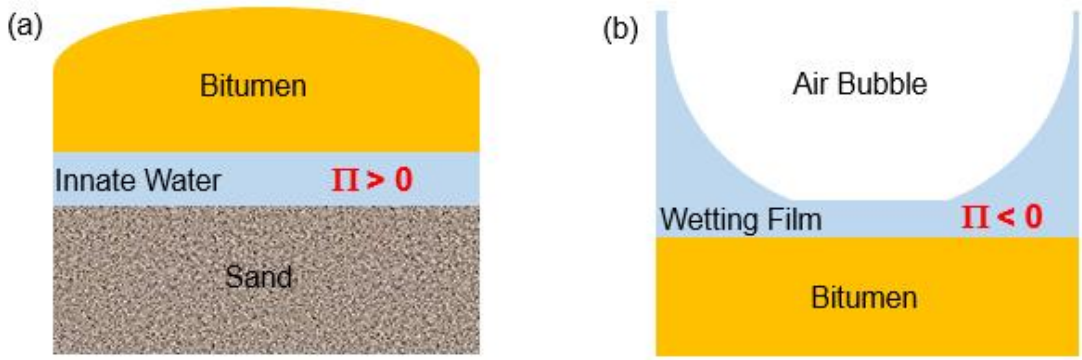

Figure 3.11 a) For liberation, it is necessary to create a positive disjoining pressure in the TLFs of water between bitumen and sand grains, *i.e.*, $\Pi > 0$; for air bubble-bitumen attachment, it is necessary to create negative disjoining pressures in the TLFs, *i.e.*, $\Pi < 0$.

hence a positive disjoining pressure. Further, an increase in pH should ionize the polar groups of the asphaltene polymers and, thereby, increase the negative surface charge and increase the repulsive electrostatic disjoining pressure (Π_e). In principle, any electrolyte in process water should be detrimental to bitumen liberation as it can cause the surface charge to decrease (*e.g.*, by Ca^{2+} ion adsorption) and the electrical double-layer to be compressed. However, the double-layer compression becomes discernable only at very high electrolyte concentrations.

Figure 3.11b shows that a bubble deforms when it encounters a bitumen surface in a hydrotransport pipeline. The deformation creates an excess pressure (p) in the film, causing the film to thin. At this point in the film thinning process, the excess pressure is solely dependent upon the radius R of the bubble and surface tension, *i.e.*, ($p_{cur} = 2\gamma/R$). As the film thinning continues and reaches a thickness range of ~250 to 300 nm, however, disjoining pressure (Π) comes into play. The film thins further if $\Pi < 0$. If $\Pi > 0$, however, film thinning stops when Π becomes equal to the curvature pressure (p_{cur}), because p becomes zero according to Eq. [3.2]. The film is stable at this equilibrium thickness (h_e); therefore, the contact angle (θ) becomes zero, and no flotation will occur. As shown in Eq. [3.10], $\theta > 0$ only when $\Pi < 0$ by virtue of the hydrophobic force present in the wetting film. Since the disjoining pressure in the film must be high to liberate bitumen, the hydrophobic force should be strong and long-ranged enough to create a negative disjoining pressure, which is a necessary condition for aeration. One way to increase the hydrophobic force is to increase the temperature for bitumen aeration. In mineral flotation, a collector is added to render the surface hydrophobic. In bitumen aeration, temperature is raised to increase contact angle and hence hydrophobic force as has been discussed in foregoing sections.

3.4 Summary

In the present work, the bitumen was separated into maltene and asphaltene in order to study the role of these two components in the interaction between bitumen and air bubble. The kinetics of thinning of the wetting films formed on bitumen, asphaltene, and maltene were monitored using the TFPB technique. The results showed that the kinetics decreased in the order of maltene, bitumen and asphaltene. The disjoining pressure in the wetting film was determined based upon the temporal and spatial profiles of the wetting films obtained using the modified TFPB method. It was found that $\Pi < 0$ on maltene and bitumen, while $\Pi > 0$ on asphaltene, indicating that asphaltene may serve as a kinetic barrier for bitumen aeration. Finally, the disjoining pressure data obtained in the present work were analyzed in view of the extended DLVO theories. Comparison of the disjoining pressure isotherms for maltene, bitumen, and asphaltene showed that the electrostatic and steric forces are responsible for the difficulties that may be encountered in bitumen-bubble interactions, while the hydrophobic force serves as the driving force for the fruitful interactions.

References

1. Masliyah, J.H., Z. Xu, and J.A. Czarnecki, *Handbook on Theory and Practice of Bitumen Recovery from Athabasca Oil Sands*, Kingsley Publishing Services, 2011.
2. Yoon, R.H., D. Guzonas, and B.S. Aksoy, *Role of Surface Forces in Tar Sand Processing*, in *Proceeding of the 1st UBC-McGill Bi-Annual International Symposium* Vancouver, BC, Canada, 1995.

3. Yoon, R.H. and Y.I. Rabinovich, *Role of Asphaltene in the Processing of Tar Sand*, in *Proceeding of the 3rd UBC-McGill Bi-Annual International Symposium*, CIM, Montreal, Quebec, Canada, 1999.

4. Wu, X., et al., *Interaction Forces between Bitumen Droplets in Water*, Langmuir. 15(16), p. 5244-5250, 1999.

5. Wu, X., et al., *Applications of colloidal force measurements using a microcollider apparatus to oil sand studies*, Colloids and Surfaces A: Physicochemical and Engineering Aspects. 174(1–2), p. 133-146, 2000.

6. Wu, X., T. Dabros, and J. Czarnecki, *Determining the Colloidal Forces between Bitumen Droplets in Water Using the Hydrodynamic Force Balance Technique*, Langmuir. 15(25), p. 8706-8713, 1999.

7. Laroche, I., et al., *Dynamic and Static Interactions between Bitumen Droplets in Water*, Journal of Colloid and Interface Science. 250(2), p. 316-326, 2002.

8. Liu, J., Z. Xu, and J. Masliyah, *Colloidal forces between bitumen surfaces in aqueous solutions measured with atomic force microscope*, Colloids and Surfaces A: Physicochemical and Engineering Aspects. 260(1), p. 217-228, 2005.

9. Liu, J., Z. Xu, and J. Masliyah, *Studies on bitumen-silica interaction in aqueous solutions by atomic force microscopy*, Langmuir. 19(9), p. 3911-3920, 2003.

10. Long, J., Z. Xu, and J. Masliyah, *On the role of temperature in oil sands processing*, Energy & fuels. 19(4), p. 1440-1446, 2005.

11. Zhao, H., et al., *Effect of divalent cations and surfactants on silica-bitumen interactions*, Industrial & engineering chemistry research. 45(22), p. 7482-7490, 2006.

12. Hogshead, C.G., et al., *Studies of bitumen− silica and oil− silica interactions in ionic liquids,* Energy & Fuels. 25(1), p. 293-299, 2010.

13. Liu, J., Z. Xu, and J. Masliyah, *Interaction forces in bitumen extraction from oil sands,* Journal of colloid and interface science. 287(2), p. 507-520, 2005.

14. Drelich, J., et al., *The role of gas bubbles in bitumen release during oil sand digestion,* Fuel. 74(8), p. 1150-1155, 1995.

15. Drelich, J., D. Leliński, and J.D. Miller, *Bitumen spreading and formation of thin bitumen films at a water surface,* Colloids and Surfaces A: Physicochemical and Engineering Aspects. 116(1), p. 211-223, 1996.

16. Gu, G., et al., *Effects of physical environment on induction time of air–bitumen attachment,* International Journal of Mineral Processing. 69(1), p. 235-250, 2003.

17. Gu, G., et al., *A novel experimental technique to study single bubble–bitumen attachment in flotation,* International Journal of Mineral Processing. 74(1), p. 15-29, 2004.

18. Wang, W., et al., *Attachment of individual particles to a stationary air bubble in model systems,* International Journal of Mineral Processing. 68(1–4), p. 47-69, 2003.

19. Gu, G., et al., *Hydrogen and Oxygen Bubble Attachment to a Bitumen Drop,* The Canadian Journal of Chemical Engineering. 82(4), p. 846-849, 2004.

20. Lelinski, D., et al., *Rate of bitumen film transfer from a quartz surface to an air bubble as observed by optical microscopy,* The Canadian Journal of Chemical Engineering. 82(4), p. 794-800, 2004.

21. Moran, K., J. Masliyah, and A. Yeung, *Factors affecting the aeration of small bitumen droplets,* The Canadian Journal of Chemical Engineering. 78(4), p. 625-634, 2000.

22. Englert, A., et al., *Interaction forces between a deformable air bubble and a spherical particle of tuneable hydrophobicity and surface charge in aqueous solutions,* Journal of colloid and interface science. 379(1), p. 121-129, 2012.

23. Ren, S., J. Masliyah, and Z. Xu, *Studying bitumen–bubble interactions using atomic force microscopy,* Colloids and Surfaces A: Physicochemical and Engineering Aspects. 444 p. 165-172, 2014.

24. Su, L., Z. Xu, and J. Masliyah, *Role of oily bubbles in enhancing bitumen flotation,* Minerals engineering. 19(6), p. 641-650, 2006.

25. Laskowski, J. and J. Kitchener, *The hydrophilic—hydrophobic transition on silica,* J. of Colloid and Interface Sci. 29(4), p. 670-679, 1969.

26. Pan, L., S. Jung, and R.H. Yoon, *A fundamental study on the role of collector in the kinetics of bubble–particle interaction,* International Journal of Mineral Processing. 106 p. 37-41, 2012.

27. Pan, L., S. Jung, and R.H. Yoon, *Effect of hydrophobicity on the stability of the wetting films of water formed on gold surfaces,* Journal of colloid and interface science. 361(1), p. 321-330, 2011.

28. Dickie, J.P. and T.F. Yen, *Macrostructures of the asphaltic fractions by various instrumental methods,* Analytical chemistry. 39(14), p. 1847-1852, 1967.

29. Lesueur, D., *The colloidal structure of bitumen: Consequences on the rheology and on the mechanisms of bitumen modification,* Advances in colloid and Interface Science. 145(1), p. 42-82, 2009.

30. Khadim, M.A. and M.A. Sarbar, *Role of asphaltene and resin in oil field emulsions,* Journal of Petroleum Science and Engineering. 23(3–4), p. 213-221, 1999.

31. Schramm, L.L. and R.G. Smith, *The influence of natural surfactants on interfacial charges in the hot-water process for recovering bitumen from the athabasca oil sands,* Colloids and Surfaces. 14(1), p. 67-85, 1985.

32. Schramm, L.L. and R.G. Smith, *Two classes of anionic surfactants and their significance in hot water processing of oil sands,* The Canadian Journal of Chemical Engineering. 65(5), p. 799-811, 1987.

33. Acevedo, S., X. Gutierrez, and H. Rivas, *Bitumen-in-Water Emulsions Stabilized with Natural Surfactants,* Journal of Colloid and Interface Science. 242(1), p. 230-238, 2001.

34. McLean, J.D. and P.K. Kilpatrick, *Effects of Asphaltene Solvency on Stability of Water-in-Crude-Oil Emulsions,* Journal of Colloid and Interface Science. 189(2), p. 242-253, 1997.

35. Yan, Z., J.A.W. Elliott, and J.H. Masliyah, *Roles of Various Bitumen Components in the Stability of Water-in-Diluted-Bitumen Emulsions,* Journal of Colloid and Interface Science. 220(2), p. 329-337, 1999.

36. Gao, S., et al., *Role of Bitumen Components in Stabilizing Water-in-Diluted Oil Emulsions,* Energy & Fuels. 23(5), p. 2606-2612, 2009.

37. Gu, G., et al., *Influence of water-soluble and water-insoluble natural surface active components on the stability of water-in-toluene-diluted bitumen emulsion,* Fuel. 81(14), p. 1859-1869, 2002.

38. Xu, Z. and R.H. Yoon, *A study of hydrophobic coagulation,* Journal of Colloid and Interface Science. 134(2), p. 427-434, 1990.

39. Scheludko, A. and D. Exerowa, Kolloid-Z. 165 p. 148, 1959.

40. Scheludko, A., Dokl. Bolg. Akad. Nauk. 24 p. 47, 1971.

41. Yoon, R.H. and S.A. Ravishankar, *Long-range hydrophobic forces between mica surfaces in dodecylammonium chloride solutions in the presence of dodecanol,* Journal of Colloid and Interface Science. 179(2), p. 391-402, 1996.

42. Derjaguin, B., *Theory of the stability of strongly charged lyophobic sols and the adhesion of strongly charged particles in solutions of electrolytes,* Acta Physicochim. USSR. 14 p. 633-662, 1941.

43. Verwey, E.J.W. and J.T.G. Overbeek, *Theory of the Stability of Lyophobic Colloids*, Elsevier, Amsterdam, 1948.

44. Derjaguin, B.V., *Friction and adhesion IV. The theory of adhesion of small particles.,* Kolloid Z. 69 p. 155-164, 1934.

45. Frumkin, A., *On the phenomena of wetting and the adhesion of bubbles I,* Zh. Fiz. Khim. 12 p. 337, 1938.

46. Yoon, R.H. and L. Mao, *Application of Extended DLVO Theory, IV: Derivation of Flotation Rate Equation from First Principles,* Journal of Colloid and Interface Science. 181(2), p. 613-626, 1996.

47. Yoon, R.H. and L. Wang, *Hydrophobic Forces in Foam Films,* in *Colloid Stability- The Role of Surface Forces - Part I,* T.F. Tadros, Editor, p. 161-186, Wiley-VCH, 2006.

48. Van Oss, C.J., *Interfacial Forces in Aqueous Media*, 2nd ed, CRC press, Taylor and Francis Group 2006.

49. De Gennes, P., *Polymers at an interface; a simplified view,* Advances in Colloid and Interface Science. 27(3), p. 189-209, 1987.

50. Wang, J., R.H. Yoon, and J.C. Eriksson, *Excess thermodynamic properties of thin water films confined between hydrophobized gold surfaces,* Journal of colloid and interface science. 364(1), p. 257-263, 2011.

51. Li, Z. and R.H. Yoon, *Thermodynamics of hydrophobic interaction between silica surfaces coated with octadecyltrichlorosilane,* Journal of colloid and interface science. 392 p. 369-375, 2013.

52. Stillinger, F.H., *Water revisited,* Science. 209(4455), p. 451-457, 1980.

53. Wernet, P., et al., *The structure of the first coordination shell in liquid water,* Science. 304(5673), p. 995-999, 2004.

54. Nilsson, A., et al., *X-ray absorption spectroscopy and X-ray Raman scattering of water and ice; an experimental view,* Journal of Electron Spectroscopy and Related Phenomena. 177(2–3), p. 99-129, 2010.

55. Mallamace, F., et al., *NMR evidence of a sharp change in a measure of local order in deeply supercooled confined water,* Proceedings of the National Academy of Sciences. 105(35), p. 12725-12729, 2008.

56. Mallamace, F., *The liquid water polymorphism,* Proceedings of the National Academy of Sciences. 106(36), p. 15097-15098, 2009.

57. Potoczny, Z.M., et al., *Surface Tension of Bitumen. I. Temperature Dependence,* AOSTRA Journal of Research. 1 p. 107-115, 1984.

58. Israelachvili, J.N., *Intermolecular and surface forces: revised third edition*, p. 266, Academic press, 2011.

59. Dai, Q. and K.H. Chung, *Bitumen—sand interaction in oil sand processing,* Fuel. 74(12), p. 1858-1864, 1995.

60. Liu, J., et al., *Bitumen–clay interactions in aqueous media studied by zeta potential distribution measurement,* Journal of colloid and interface science. 252(2), p. 409-418, 2002.

61. Ramachandran, R. and P. Somasundaran, *Effect of temperature on the interfacial properties of silicates,* Colloids and Surfaces. 21(0), p. 355-369, 1986.

62. Srinivasan, N.S., L.G. Spitzer, and L.G. Hepler, J. Can. Petr. Technol. 21(4), p. 25, 1982.

63. Somasundaran, P. and R.D. Kulkarni, *A new streaming potential apparatus and study of temperature effects using it,* Journal of Colloid and Interface Science. 45(3), p. 591-600, 1973.

64. McShea, J.A. and I. Callaghan, *Electrokinetic potentials at the gas-aqueous interface by spinning cylinder electrophoresis,* Colloid & Polymer Science. 261(9), p. 757-766, 1983.

Chapter 4

The Effect of Solution Chemistry on the Stability of Wetting Films on Bitumen

Abstract

The solution chemistry plays an important role in bitumen aeration. In this study, the effects of solution chemistry on the thinning of wetting films between bitumen and air bubble were studied. It was found that the thinning kinetics of wetting films decreased with increasing immersion time. The addition of electrolyte KCl compressed the double layer and increased the thinning kinetics. The presence of calcium and magnesium ions did not show significant effects on the thinning kinetics when 1 mM KCl was present. In addition, the effect of approach speed of air bubble to bitumen surface was investigated. It was found that dimples were formed at high approaching speeds. There existed a critical film thickness, above which the wetting film thinned faster at higher approaching speeds and below which the film thinned faster at lower approaching speeds.

4.1 Introduction

Properties of the thin liquid films (TLFs) formed between particles, bubbles, and drops control their interactions with each other. In Athabasca bitumen flotation in Canada, air bubbles collide with bitumen droplets and create wetting films between them. If the TLFs are unstable, bitumen droplets coalesce, attach to air bubbles, and float. In contrast, no flotation is possible if

the TLFs are stable. Thus, the stability of wetting films is of critical importance in bitumen flotation, and is strongly dependent on the chemistry of the flotation system, which includes factors such as temperature, pH, electrolyte concentration, the presence of fines, *etc.*

The effect of processing temperature on bitumen extraction has been studied extensively.[1-7] It has been reported that bitumen recovery does not significantly change in the range of 50 to 80 °C, but sharply decreases with decreasing temperatures below 35 °C (see Chapter 2).

The solution pH is another critical operating parameter, which controls the surface charges of the particles in bitumen slurry. As early as 1920s, in the Clark's Hot Water Extraction Process, chemicals such as NaOH and Na_2CO_3 were added to the oil sands slurry to increase the solution pH to achieve satisfactory bitumen recovery.[8] It was found that there was an optimal concentration of reagent to obtain maximum bitumen recovery.[9] Sanford and Seyer[10] found that the role of NaOH addition was to derive natural surfactants by ionizing organic acids in the bitumen. However, a subsequent study indicated that only a small fraction of NaOH was needed to produce sufficient natural surfactants needed for bitumen flotation, and that the bulk of added NaOH reacted with polyvalent metal carbonates, clays and sulfates contained in the oil sands.[11] One study also produced a report that increasing slurry pH favors bitumen detachment (or liberation) from sand grains.[4] Specifically, the zeta potential of the bitumen surface in an aqueous solution becomes more negative with increasing pH.[4, 12, 13] After the pH had reached 8, the zeta potential leveled off. Moreover, the zeta potential of an asphaltene surface becomes increasingly negative as the pH is increased.[14-17] Force measurements conducted by AFM showed that the repulsive force between bitumen-silica, asphaltene-silica, bitumen-bitumen and asphaltene-asphaltene in an aqueous solution increased with increasing pH.[14, 18-21]

Divalent cations such as Ca^{2+} and Mg^{2+} ions are always present in a bitumen extraction system. Calcium ions can be introduced into a bitumen extraction system through gypsum, which is added as a process aid to form consolidated tailings in the recycling of process water from tailings.[22] The presence of Ca^{2+} ions could decrease the absolute values of the negative zeta potentials of bitumen and clay surfaces due to their adsorption on these surfaces.[13, 18, 23] A sizable number of studies also confirmed that the presence of calcium and magnesium ions has a detrimental effect on bitumen recovery.[11, 18, 24, 25] However, Kasongo *et al*.[23] found that calcium alone appears to have a marginal effect on bitumen recovery. When both calcium and montmorillonite were present, however, bitumen recovery decreased sharply. In support of Kasongo's findings, Gu *et al.*[26] reported that calcium and fine solids had a synergic effect on the induction time of air-bubble attachment. The researchers proposed that when calcium ions are combined with fine solids, the adsorbed positive calcium ions on fines would interact with negative carboxylic groups on bitumen surfaces, acting as a ''binder'' between bitumen and fine solids. A coating of fine solids on a bitumen surface changes its wettability from hydrophobic to more hydrophilic in nature, thereby reducing bitumen-bitumen coalescence and air bubble-bitumen attachment.

Although earlier studies have advanced our knowledge of bitumen extraction from oil sands, we still do not fully understand the stability of the wetting films formed between bitumen and air bubbles. The present study was designed to fill that knowledge gap by investigating the various factors that impact the thinning of the wetting films of water formed on bitumen. Specifically, a bubble-against-plate (BAP) apparatus was used to measure the kinetics of the thinning of wetting films of water formed between bitumen and bubble under different conditions. Optical interference patters (Newton rings) were recorded using a high-speed camera and then

analyzed offline to calculate the film thickness, which changed with time at different radial positions of the film. The results will be useful in elucidating the mechanisms involved in bitumen aeration.

4.2 Experimental

4.2.1 Materials

A sample of bitumen (99 wt%) was provided by Suncor Energy, Inc. Reagent grade toluene (>99.5% purity) was purchased from Spectrum Chemical Mfg. Corp. Anhydrous $CaCl_2$ (99%, Alfa Aesar) and $MgCl_2$ (99%, Alfa Aesar), and KCl (99%, Alfa Aesar) were used to study the effect of electrolyte on the film thinning. Diluted hydrochloric acid and NaOH were used to adjust solution pH. Millipore ultrapure water with a resistivity of 18.2 MΩ·cm was obtained using a Direct Q3 water purification system. Silicon wafers (100 crystal planes, University Wafer) were used as the substrates for coating bitumen. Sulfuric acid (H_2SO_4, 98% purity, VMR international) and hydrogen peroxide (H_2O_2, 29.0–32.0% purity, Alfa Aesar) were used to clean the silicon substrates.

4.2.2 Preparation of Bitumen-coated Surfaces

Silicon wafers were first oxidized in an oxidation furnace at 1070 °C for ~40 min using wet oxidation procedure. The oxidized silicon wafers were then cut into 12x12 mm pieces and used as substrates for bitumen, asphaltene, and maltene. Before the coating, the silicon substrates were put in an ultrasonic bath of water for ~1 hr and then cleaned by immersing in a Piranha solution (3:7 by volume of H_2O_2/H_2SO_4) at 120 °C for 1 hr, followed by rinsing with an adequate amount of ultrapure water and pure nitrogen (N_2) blow-drying. The silicon substrate was placed in a spin-coater (Laurell, WS-400-6NPP), rinsed with toluene, and then spun at 6,000 rpm for 30 s to dry off the toluene. When the substrate was free of toluene, a small amount of (2 or 3 drops) of a bitumen-in-toluene solution (2.5 mg/mL) was placed on the substrate and let it stand for 10 s. The

substrate was then spun at 3,500 rpm for 20 s before placing another drop of the bitumen solution and continuing spinning for additional 10 s. The spinning continued for an additional 1 minute at 6,000 rpm to evaporate the solvent and obtain a smooth and uniform bitumen coating. The spin-coated bitumen was then placed in a particulate matter-free laminar hood for ~30 min to ensure maximum removal of toluene from the coating.

4.2.3 Measurement of Film Thinning Kinetics

In the TFPB technique described in previous chapters, a small volume of liquid is used to measure the thickness of wetting films. Also, the experimental procedure is complex and delicate. The objective of the present work is to study the effect of solution chemistry on the stability of thin liquid films, for which it would be desirable to use larger volumes of liquids. Figure 4.1 shows the bubble against plate (BAP) apparatus designed and constructed in the present work for this purpose. In a given experiment, a solution of known ionic composition is placed in a rectangular

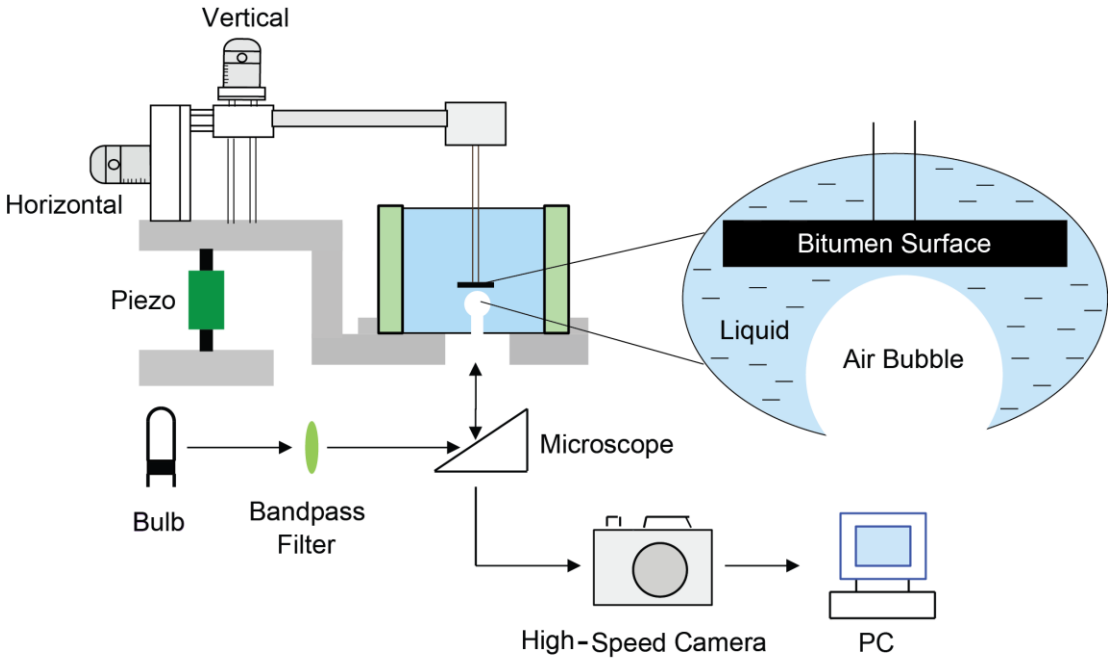

Figure 4.1 Schematic representation of the bubble-against-plate (BAP) apparatus used to monitor the film thinning kinetics of wetting films.

Plexiglas cell with dimensions of 38x38x14 mm. The bottom plate of the cell is thick enough to fixate a short glass tubing (~1.8 mm OD) at the center. Once a bubble of ~3 mm diameter is formed on the tip of the glass tubing by means of an air-tight syringe, a flat silicon plate (9x9x0.5 mm) coated with bitumen is brought close to the bubble surface within a distance of 15 μm. The bubble is then moved upward by means of the piezoelectric crystal at an approach velocity of 0.2 μm/sec. As the film thickness is reduced, optical interference patters (Newton rings) begin to appear. The Newton rings are recorded as a function of time by means of a high-speed camera using the same optical system employed for the TFPB system. The recorded Newton rings are analyzed off-line to determine the changes in film thickness (h) as a function of time (t) and radial distance (r). In the present work, all experiments have been carried out at room temperature, *i.e.*, ~22 °C.

4.3 Results and Discussion

4.3.1 Effect of Immersion Time

Figure 4.2 shows the results of the film thickness measurements conducted using the bubble against plate (BAP) apparatus shown in Figure 4.1. The measurements were conducted after immersing bitumen-coated silicon plates for different periods of time, *i.e.*, 5, 15, 30, and 60 min. As shown, the kinetics of film thinning decreased with increasing immersion time, indicating that the bitumen surface becomes less hydrophobic at longer immersion times. The results show also that the equilibrium film thickness (h_e) increased with increasing immersion time; h_e increased from 118 nm to 156 nm when the immersion time was increased from 5 min to 1 h. Note, however, that neither the thinning kinetics nor the equilibrium thickness increased further after 30 min of immersion time, indicating that 30 min is sufficient for the bitumen film to reach an equilibrium with water at room temperature. This finding is in agreement with the work conducted by Liu, *et al.*[19]

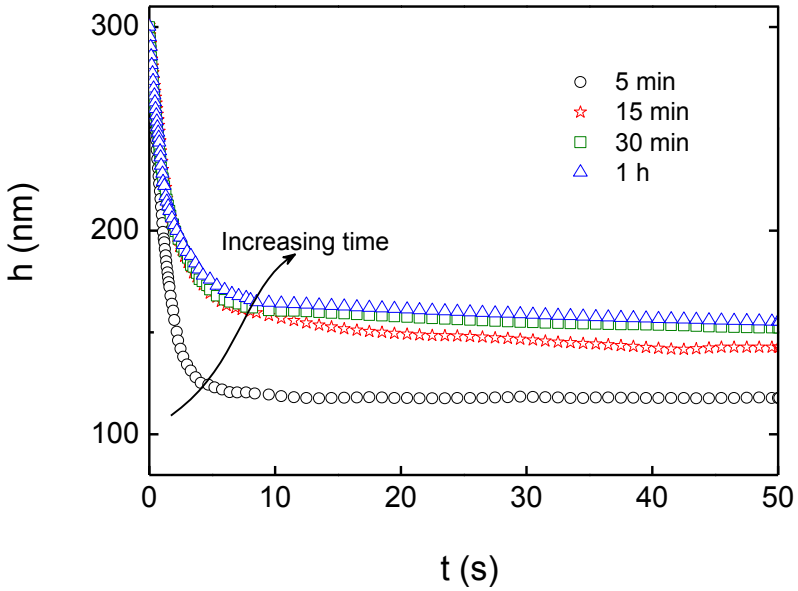

Figure 4.2 Thinning kinetics of the wetting films formed on bitumen at different immersion times in water at pH 8.4 to 7.5.

The time-dependent behavior of bitumen may be attributed to the slow kinetics of the polar groups of the asphaltene and resin, *e.g.*, carboxyl, amide, thiol, and hydroxyl groups,[27] migrating through the polymeric matrix at room temperature. When a bitumen surface is exposed to air, molecules in bitumen lie collapsed on the surface.[12] Upon exposure to water, the molecules swell, as indicated by the increase in h_e, and the polar groups migrate toward the bitumen/water interface, as evidenced by the slow film thinning kinetics. The slow kinetics of the 'swelling' and the migration of polar species may be due to the high viscosity of bitumen at room temperature. At higher temperatures, the kinetics of migration are faster, and the equilibrium thickness can be reached faster. The results presented in Figure 4.2 are consistent with the general observation that the surface chemistry of bitumen in contact with water is time-dependent.[18-20]

4.3.2 Effect of Electrolyte KCl

Figure 4.3 shows the effect of KCl on the thinning kinetics of the wetting films formed on bitumen. The experiments were conducted at a natural pH of about 5.7 and room temperature (~22 °C). In the absence of KCl, the wetting film thinned slowly and reached a thickness of 153 nm in 50 s. The film did not rupture. In the presence of 1 mM KCl, the film thinned faster and ruptured within 9 s at a critical film thickness (h_{cr}) of 34 nm.

As shown in the foregoing section, the bitumen surface is negatively charged in water due to the exposure of the negatively-charged polar groups on the surface, with its zeta potential being around -60 mV.[13] The air bubble surface is also negatively charged with different values of negative zeta potential reported in the literature.[28-31] Therefore there exists a repulsive electrostatic force between bitumen and air bubble, creating a positive disjoining pressure and thus causing the thinning rate to decrease and stop after reaching the equilibrium thickness.

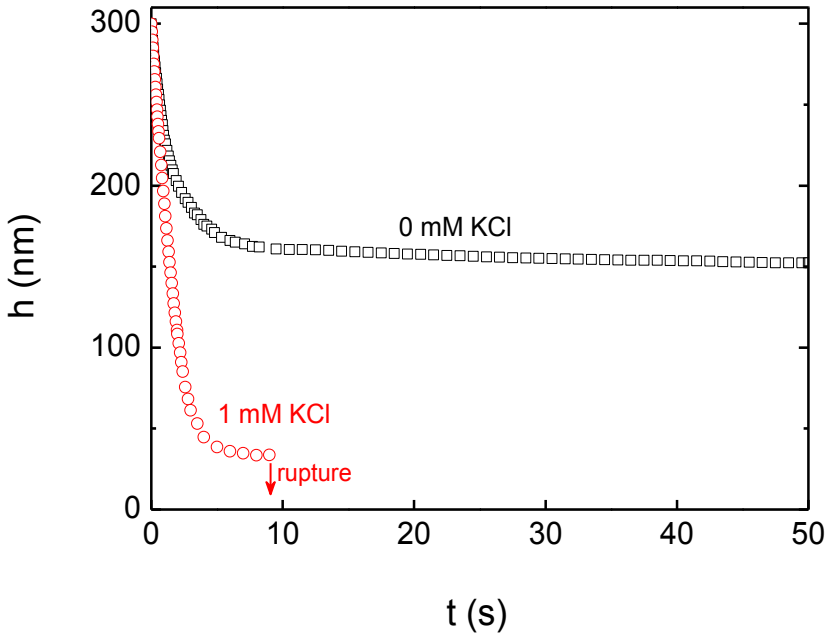

Figure 4.3 Effect of KCl on the thinning kinetics of the wetting films formed on bitumen in aqueous solution of pH 8.4 to 7.5 and at 22 °C.

In the presence of KCl, the electrical double-layers at the bitumen/water and air/water interfaces are compressed, causing the positive disjoining pressure to decrease. There are two consequences of the double-layer compression: one is to increase the kinetics of film thinning, and the other is to decrease the film thickness, both of which are clearly manifested in Figure 4.3. As the film thickness becomes thinner, the film is subjected to a stronger hydrophobic force, which is the major destabilizing force for wetting films, and therefore ruptures.

4.3.3 Effect of Solution pH

Figure 4.4 shows the effect of solution pH on the kinetics of film thinning in 1 mM KCl solution. As shown, the kinetics of film thinning decreased with increasing pH. The pH adjustments were made by adding aliquots of HCl and NaOH solutions. At pH < 5, the film ruptured within less than 3 s, while at pH ~8, the film was stable for as long as 9 s before it finally ruptured. These values are close to what has been reported earlier.[12] In general, the film rupture or induction time for bitumen flotation is orders of magnitude longer than observed in mineral

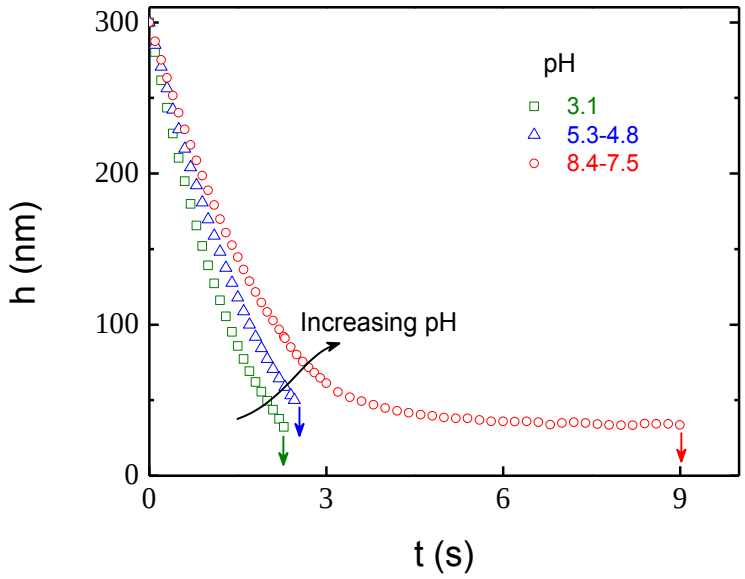

Figure 4.4 Effect of solution pH on the thinning kinetics of the wetting films formed on bitumen in a 1 mM KCl solution. The short arrows indicate the critical rupture thicknesses (h_{cr}) of the wetting films.

flotation, which has been attributed to the exposure of asphaltene on a bitumen surface. As has already been noted, the polar groups of asphaltene include carboxyl, amide, thiol, and hydroxyl groups, which are more readily ionized at higher pHs, giving rise to an increased electrostatic repulsive force. At the same time, the thickness of the asphaltene layer tend to increase with increasing pH, causing stronger steric repulsion. Both of these forces contribute to the increased stability of the wetting films formed on bitumen and hence to the slower kinetics of film thinning at higher pHs.

4.3.4 Effect of Calcium Ions

Figure 4.5 shows the changes in the thickness of wetting films between the bitumen surface and air bubble in 1 mM KCl solution at different $CaCl_2$ concentrations. When the calcium concentration was increased from 0 to 1 mM, the kinetics of film thinning slightly increased. As the concentration was further increased to 10 mM, however, the kinetics decreased. The initial increase in kinetics may be attributed to the likelihood that the Ca^{2+} ions react with the carboxylate

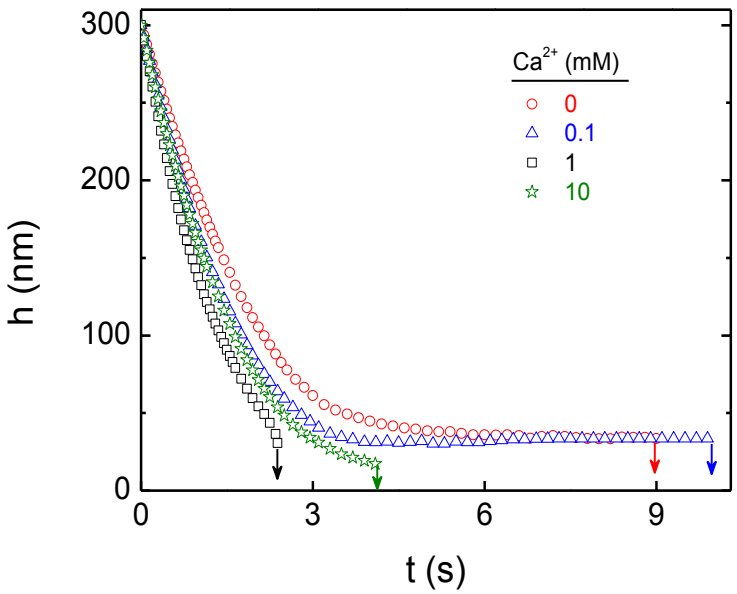

Figure 4.5 Effect of Ca^{2+} ions on the thinning kinetics of the wetting films formed on bitumen in a 1 mM KCl solution at pH 8.4 to 7.5.

groups ($RCOO^-$) of the asphaltene and, thereby, reduce the negative surface charge and hence the positive disjoining pressure. At 10 mM calcium concentration, it is possible that calcium hydroxyl or carbonate species adsorb on the surface, rendering the bitumen surface hydrophilic. In general, the critical rupture thickness decreased with increasing calcium concentration, as shown in Figure 4.5, which may be attributed to the likelihood that in the presence of Ca^{2+} ions the wetting films become thinner, subjecting the film to stronger hydrophobic forces. Overall, the changes in the film thinning kinetics and the critical rupture thickness at different calcium concentrations were not significant compared to other factors.

4.3.5 Effect of Magnesium Ions

Figure 4.6 shows the effect of $MgCl_2$ concentration on the thinning kinetics of the wetting films formed on bitumen in 1 mM KCl solution at pH 8.4-7.5. As shown, the addition of Mg^{2+} ions had a relatively small effect on the kinetics of film thinning but a relatively large effect on rupture

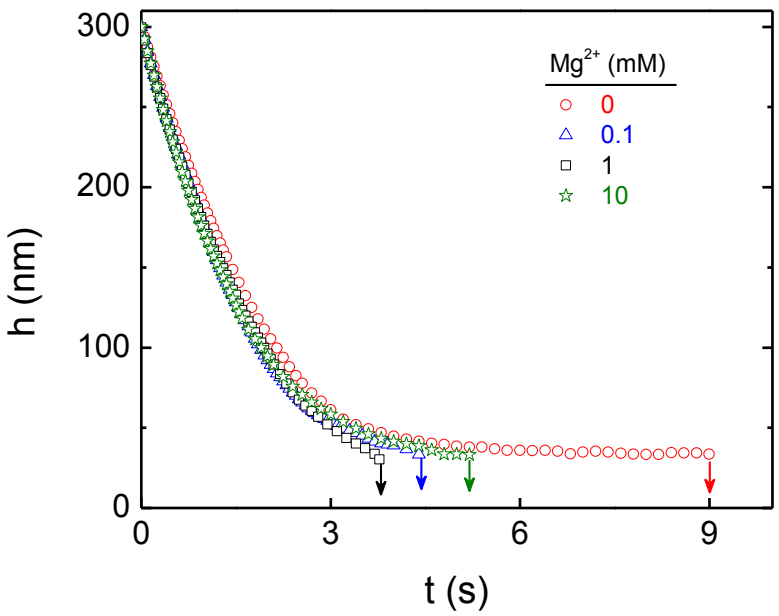

Figure 4.6 Effect of Mg^{2+} ions on the thinning kinetics of the wetting films formed on bitumen in a 1 mM KCl solution at pH 8.4 to 7.5.

time. The rupture time decreased substantially with increasing concentration of Mg^{2+} ions in solution, which may also be attributed to the decrease in the electrostatic repulsion.

Masliyah, *et al*.[3] studied the effect of Mg^{2+} and Ca^{2+} ions on laboratory flotation, and showed that the effect was marginal. Thus, the results obtained in the present work is consistent with the work of Masliyah *et al*. A detrimental impact was observed, however, with some ores in the presence of montmorillonite clay.

4.3.6 Effect of Approaching Speed on Film Thinning

Much of the study conducted in the present work was to study the surface chemistry variables. However, the interaction force between bubble and bitumen should also be affected by the hydrodynamic force. To better understand the role of the hydrodynamic force, the velocity of the bubble approaching a flat bitumen surface was varied during the film thickness measurement using the BAP apparatus (Figure 4.1). Figure 4.7 compares the temporal and spatial profiles of the wetting films formed at approach velocities of 0.2 and 4.6 μm/s in a 1 mM KCl solution with natural pH of about 5.7. At the lower approaching velocity, the film thinned slowly and ruptured at the critical film thickness (h_c) of 40 nm in 2.78 s. At the higher approaching speed, the film

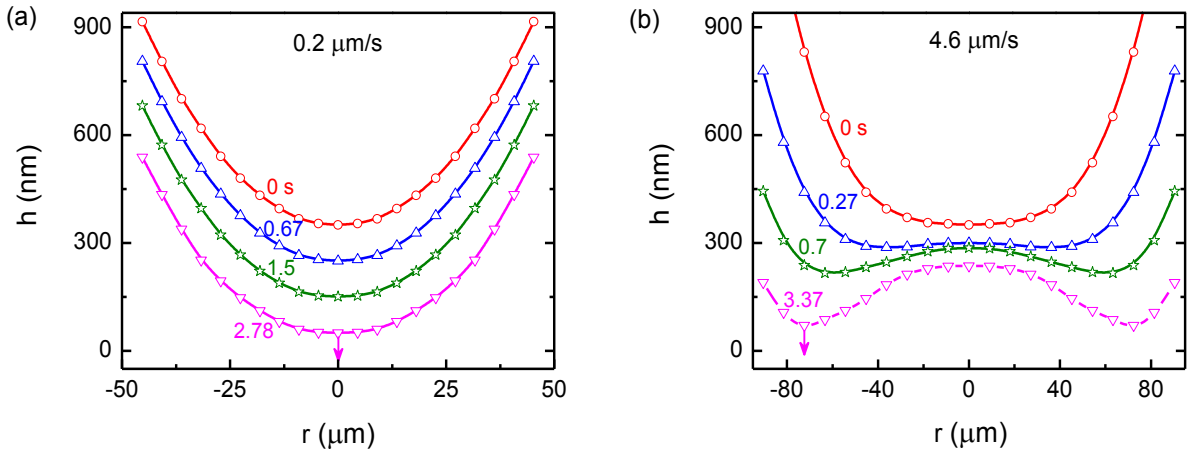

Figure 4.7 Temporal and spatial profiles of the wetting films formed bitumen in a 1 mM KCl solution at two different approach speeds: a) 0.2 and b) 4.6 μm/s.

became flat initially and then began to form a dimple after 0.27 s. At longer thinning times, the dimple became increasingly convex, forming a well-defined barrier rim at r = 73 μm. At 3.37 s, the film ruptured catastrophically at the rim, with a rupture thickness of 70 nm. Similar observations were made on hydrophobic surfaces by Pan *et al.*[32]

In Figure 4.8, the closest separation distances between bubble and bitumen have been plotted as a function of time at the two different approach speeds employed in the present work, *i.e.*, 0.2 and 4.6 μm/s. Also shown in the figure is a plot of film thicknesses at the center of the dimpled film. Initially, the dimpled film thinned faster than the non-dimpled film. After ~1.7 s, the non-dimpled film began to thin faster and ruptured before the dimpled film did. Does this mean that less turbulence or weaker hydrodynamic force is better for bitumen aeration? It is difficult to answer this question on the basis of a single set of experiments. In principle, dimpled films should

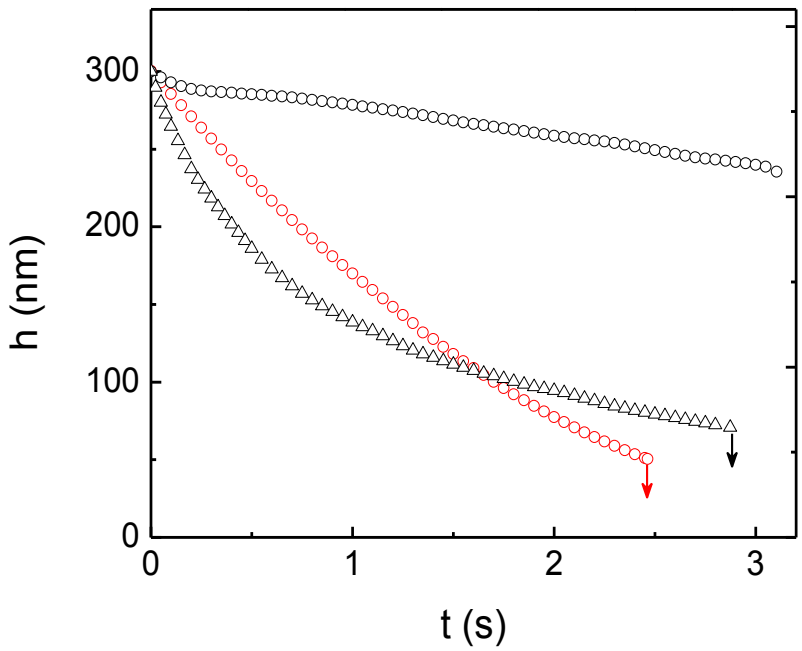

Figure 4.8 Comparison of the thinning kinetics obtained for dimpled and non-dimpled wetting films in a 1 mM KCl solution. Black triangles represent the minimum film thickness of the dimpled film, *i.e.*, at the rim; black circles represent the film thicknesses at the center of the dimpled films; and red circles, the minimum film thicknesses of the non-dimpled films, *i.e.*, at the center.

thin more slowly because they have larger film radii than non-dimpled films, as shown in Figure 4.7. On the other hand, the film thinning kinetics should also depend on the magnitude of the hydrodynamic force applied. Thus, there may be an optimum hydrodynamic force that can give the fastest film thinning kinetics. Further investigation is needed to find optimum hydrodynamic conditions for bitumen aeration.

4.4 Summary

In this study, the effects of solution chemistry on the thinning of wetting films formed between bitumen and air bubble were studied. It was found that the kinetics of film thinning decreased with increasing immersion time. In the presence of an electrolyte (KCl), the kinetics increased due to double-layer compression. In the presence of KCl in the solution, the addition of divalent cations such as Ca^{2+} and Mg^{2+} ions did not change the thinning kinetics significantly.

In addition, the effect of approach speed of air bubble to bitumen surface was investigated. It was found that dimples were formed at high approach speeds, which is commonly observed with other wetting and foam films. In general, film thinning rate is increased due to increased hydrodynamic pressure; however, its effect is more significant on the rim of a film where the curvature (or Laplace) pressure is higher than at the center of the film and hence the dimple formation.

References

1. Long, J., Z. Xu, and J. Masliyah, *On the role of temperature in oil sands processing,* Energy & fuels. 19(4), p. 1440-1446, 2005.

2. Long, J., et al., *Effect of Operating Temperature on Water-Based Oil Sands Processing,* The Canadian Journal of Chemical Engineering. 85(5), p. 726-738, 2007.

3. Masliyah, J., et al., *Understanding Water‐Based Bitumen Extraction from Athabasca Oil Sands,* The Canadian Journal of Chemical Engineering. 82(4), p. 628-654, 2004.

4. Dai, Q. and K.H. Chung, *Bitumen—sand interaction in oil sand processing,* Fuel. 74(12), p. 1858-1864, 1995.

5. Schramm, L., et al., *Temperature effects from the conditioning and flotation of bitumen from oil sands in terms of oil recovery and physical properties,* Journal of Canadian Petroleum Technology. 42(8), p. 55-61, 2003.

6. Ding, X., *Effects fo Divalent Ions, Illite Clays and Temperature on Bitumen Recovery*, in *Department of Chemical and Materials Engineering*, University of Alberta, Edmonton, AB, 2006.

7. Zhou, Z., et al., *Assessment of Bitumen Re c overy from the Athabasca Oil Sands Using a Laboratory Denver Flotation Cell,* The Canadian Journal of Chemical Engineering. 82(4), p. 696-703, 2004.

8. Clark, K. and D. Pasternack, *Hot Water Seperation of Bitumen from Alberta Bituminous Sand,* Industrial & Engineering Chemistry. 24(12), p. 1410-1416, 1932.

9. Sanford, E.C., *Processibility of athabasca oil sand: Interrelationship between oil sand fine solids, process aids, mechanical energy and oil sand age after mining,* The Canadian Journal of Chemical Engineering. 61(4), p. 554-567, 1983.

10. Sanford, E.C. and S. F.A., *Processability of Athabasca Tar Sand Using a Batch Extraction Unit: The Role of NaOH,* CIM Bull. 72(803), p. 164-169, 1979.

11. Smith, R.G. and L.L. Schramm, *The influence of mineral components on the generation of natural surfactants from Athabasca oil sands in the alkaline hot water process,* Fuel Processing Technology. 30(1), p. 1-14, 1992.

12. Yoon, R.H., D. Guzonas, and B.S. Aksoy, *Role of Surface Forces in Tar Sand Processing,* in *Proceeding of the 1st UBC-McGill Bi-Annual International Symposium* Vancouver, BC, Canada, 1995.

13. Liu, J., et al., *Bitumen–clay interactions in aqueous media studied by zeta potential distribution measurement,* Journal of colloid and interface science. 252(2), p. 409-418, 2002.

14. Abraham, T., et al., *Asphaltene-silica interactions in aqueous solutions: direct force measurements combined with electrokinetic studies,* Industrial & engineering chemistry research. 41(9), p. 2170-2177, 2002.

15. Parra-Barraza, H., et al., *The zeta potential and surface properties of asphaltenes obtained with different crude oil/n-heptane proportions,* Fuel. 82(8), p. 869-874, 2003.

16. González, G., et al., *Electrokinetic characterization of asphaltenes and the asphaltenes-resins interaction,* Energy & fuels. 17(4), p. 879-886, 2003.

17. Vega, S.S., et al., *The zeta potential of solid asphaltene in aqueous solutions and in 50: 50 water+ ethylene glycol (v/v) mixtures containing ionic surfactants,* Journal of Petroleum Science and Engineering. 69(3), p. 174-180, 2009.

18. Liu, J., Z. Xu, and J. Masliyah, *Studies on bitumen-silica interaction in aqueous solutions by atomic force microscopy,* Langmuir. 19(9), p. 3911-3920, 2003.

19. Liu, J., Z. Xu, and J. Masliyah, *Colloidal forces between bitumen surfaces in aqueous solutions measured with atomic force microscope,* Colloids and Surfaces A: Physicochemical and Engineering Aspects. 260(1), p. 217-228, 2005.

20. Yoon, R.H. and Y.I. Rabinovich, *Role of Asphaltene in the Processing of Tar Sand*, in *Proceeding of the 3rd UBC-McGill Bi-Annual International Symposium*, CIM, Montreal, Quebec, Canada, 1999.

21. Liu, J., et al., *Colloidal interactions between asphaltene surfaces in aqueous solutions,* Langmuir. 22(4), p. 1485-1492, 2006.

22. Consortium, F.T.F., A.D.o.E.O. Sands, and R. Division, *Advances in oil sands tailings research*, Alberta Department of Energy, Oil sands and Research Division, 1995.

23. Kasongo, T., et al., *Effect of clays and calcium ions on bitumen extraction from athabasca oil sands using flotation,* The Canadian Journal of Chemical Engineering. 78(4), p. 674-681, 2000.

24. Speight, J.G. and S.E. Moschopedis, *Factors affecting bitumen recovery by the hot water process,* Fuel Processing Technology. 1(4), p. 261-268, 1978.

25. Takamura, K. and R.S. Chow, *A mechanism for initiation of bitumen displacement from oil sand*, Journal of Canadian Petroleum Technology. 22(06), 1983.

26. Gu, G., et al., *Effects of physical environment on induction time of air–bitumen attachment,* International Journal of Mineral Processing. 69(1), p. 235-250, 2003.

27. Lesueur, D., *The colloidal structure of bitumen: Consequences on the rheology and on the mechanisms of bitumen modification,* Advances in colloid and Interface Science. 145(1), p. 42-82, 2009.

28. Yoon, R.-H. and J.L. Yordan, *Zeta-potential measurements on microbubbles generated using various surfactants,* Journal of Colloid and Interface Science. 113(2), p. 430-438, 1986.

29. McShea, J.A. and I. Callaghan, *Electrokinetic potentials at the gas-aqueous interface by spinning cylinder electrophoresis,* Colloid & Polymer Science. 261(9), p. 757-766, 1983.

30. Li, C. and P. Somasundaran, *Reversal of bubble charge in multivalent inorganic salt solutions—Effect of magnesium,* Journal of Colloid and Interface Science. 146(1), p. 215-218, 1991.

31. Creux, P., et al., *Specific Cation Effects at the Hydroxide-Charged Air/Water Interface,* The Journal of Physical Chemistry C. 111(9), p. 3753-3755, 2007.

32. Pan, L., S. Jung, and R.H. Yoon, *A fundamental study on the role of collector in the kinetics of bubble–particle interaction,* International Journal of Mineral Processing. 106 p. 37-41, 2012.

Chapter 5

Summary and Future Work

5.1 Research Revisits

Flotation is the major separation process used for the recovery of bitumen from oil sands. The process involves two steps, bitumen liberation and aeration. The aeration step involves bubble attachment on bitumen, followed by engulfment of the bubble by the bitumen drop. In the present work, the kinetics of aeration (or bubble-bitumen interaction) have been studied. Most of the work focused on the measurement of disjoining pressures of the water films of thickness h formed on bitumen and on its hydrophobic and hydrophilic components, *i.e.*, maltene and asphaltene. This was accomplished using a modified thin film pressure balance (TFPB) and a new bubble against plate (BAP) apparatus developed in the present work. Both were equipped with an optical microscope, microinterferometry, and a high-speed video camera. The nano-scale images provided information on the kinetics of film thinning in vertical directions, *i.e.*, $\partial h/\partial t$ and spatial variation in radial directions, *i.e.*,$\partial h/\partial r$, which are then used to determine the disjoining pressures (Π) in TLFs.

It is believed that the results of the present study have improved the understanding of the complex mechanisms involved in bubble-bitumen interactions, which is very different from the bubble-mineral and bubble-coal interactions. With improved understanding, it is now possible to develop a bitumen flotation model and a computer simulator that can have short-term industrial applications.

The major research conclusions and suggested future work are presented below.

5.2 Conclusions

It has been found that the film thinning rates increased in the order of asphaltene, bitumen, and maltene, suggesting that the hydrophobicity of the substrates increases in the same order.

The experimental work has been carried out at temperatures ranging from 22 to 80 °C to better understand the mechanisms involved in film thinning in the hot-, warm-, and cold-water processing of bitumen. In general, the kinetics of film thinning increased with temperature, indicating that the higher the temperature, the faster the film thinning and, hence, faster the aeration kinetics. The results show also that the film thinning kinetics is sufficiently high at temperatures as low as 35 °C. At lower temperatures, however, the film thinning and aeration kinetics are too slow to warrant efficient flotation recovery. These results are consistent with the industrial experience as reported in the literature.

The kinetic information on film thinning has then been used to determine the disjoining pressure (Π) in the wetting films. The results show that $\Pi < 0$ on maltene and bitumen, while $\Pi > 0$ on asphaltene. These results suggest that asphaltene may serve as a kinetic barrier for bubble-bitumen interactions. In this regard, controlling asphaltene chemistry is important for the success of bitumen flotation under various operating conditions.

The disjoining pressure data obtained in the present work have been analyzed in view of the extended DLVO theory, which includes contributions from the electrical double-layer force, van der Waals force, hydrophobic force, and steric force that are present in the wetting films formed between air bubble and bitumen. It has been found that the negative disjoining pressure ($\Pi < 0$) due to the hydrophobic force increases with increasing temperature, which agrees well with the contact angles measured on thick films of bitumen. These results are also in agreement with

the industrial flotation practice. The disjoining pressure isotherms, established using the extended DLVO theory, show also that steric force increases with increasing temperature.

The dynamic contact angle measurements conducted on bitumen show that, initially, contact angles are small but subsequently increase above 90^{o}, obviously due to the changes in the interfacial tensions involved. It appears that the changes in interfacial tensions are brought about by the diffusion of maltene from underneath the asphaltene layer formed on the surface of bitumen, causing an increase in the surface hydrophobicity of bitumen. When the asphaltene layer is saturated with maltene, an oily substance begins to coat the bubble surface. Simple thermodynamic calculations based on the acid-base theory suggest that the asphaltene saturated with maltene, rather than maltene, is more likely to coat the bubble surface. In effect, asphaltene is acting as a spreading agent for maltene. Based on the data obtained in the present work, a model for the bubble-bitumen interaction and subsequent engulfment has been proposed. The information obtained in the present work will be useful for developing a bitumen flotation model and a computer simulator that may be useful for industrial application near term.

5.3 Original Contribution

1. The present work represents the first measurement of disjoining pressure in the wetting films of water formed on bitumen.
2. It has been established that the kinetics of the thinning of the wetting films formed on bitumen and its components, *i.e.*, asphaltene and maltene, increased with temperature in the order of asphaltene, bitumen and maltene.
3. The disjoining pressure (Π) in the wetting films of water deceases with increasing temperature in the order of asphaltene, bitumen and maltene.
4. Bitumen is aerated when the disjoining pressure is negative, *i.e.*, $\Pi < 0$.

5. The disjoining pressure of the water films formed on asphaltene is positive, *i.e.*, $\Pi > 0$, which in turn stabilizes bitumen-in-water emulsions and prevents bitumen from aeration.
6. The bitumen droplets acquire hydrophobicity by diffusion of maltene into the layer of asphaltene exposed on the surface.
7. Air bubble on bitumen is coated by asphaltene, or the bubble is engulfed into bitumen, in which asphaltene helps the free energy of spreading to be negative, *i.e.*, $\Delta G_s < 0$. Thus, asphaltene acts effectively as a spreading agent for maltene on bubble surface.

5.4 Future Work

5.4.1 Studies of the Film Thinning Kinetics Using a New Cell

In the present work, the modified thin film pressure balance (TFPB) technique has been used to study the temperature effect on the thinning of wetting films of water on bitumen and its components. There are two limitations associated with this technique due to the design of the glass cell used to form a wetting film: 1) only a small amount of water (less than 0.1 mL) is in contact with the surface of interest; 2) the surface under investigation has to be flat.

In industry, bitumen is in contact with large reservoirs of aqueous solutions and are suspended in the solutions as droplets. Earlier photomicrographic studies show that rising bitumen droplets in a continuous pilot plant were approximately spherical under good processing conditions.[1, 2] Hence, a new experimental set-up is suggested to study the thinning of wetting films of water formed between bitumen and air bubble. It will be useful to modify the bubble-against-plate (BAP) apparatus described in Chapter 4 by replacing the flat bitumen substrate with a bitumen droplet. The new set-up is shown schematically in Figure 5.1. It will be useful to study the effects of temperature, bubble size, bitumen doplet size, approach speed, and solution chemistry (*e.g.*, pH, Ca^{2+}, Mg^{2+}, clays) on the thinning of the wetting film of water on bitumen.

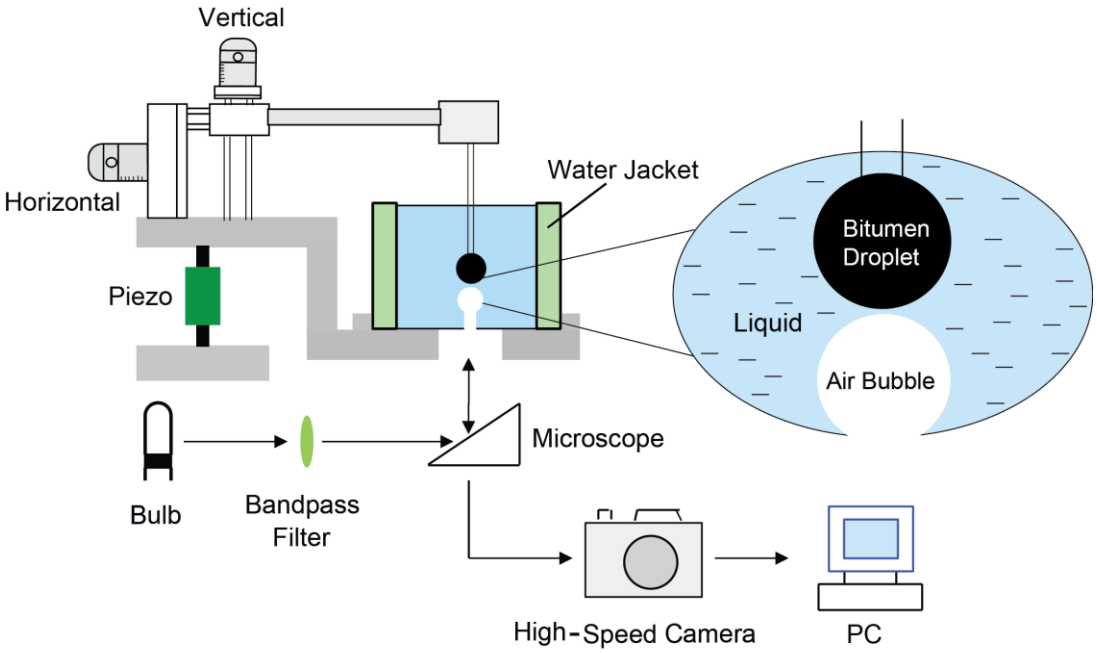

Figure 5.1 New experimental set-up designed for the study of the thinning of wetting film of water on bitumen.

In the TFPB technique, bitumen substrate was exposed to air before contacting the water in the cell and this is inevitable. In this way, it is possible that submicroscopic air bubbles might form on bitumen surface since the water contact angle on bitumen surface is high (~90°). With the new cell, one can generate a bitumen droplet *in situ*, *i.e.*, in the aqueous solution without contacting air before measurements, and *ex situ*, *i.e.*, in the air and then bring the droplet into the solution, and then compare the two sets of data to see whether the possibly adsorbed air on the bitumen surface plays a role in the bitumen-bubble attachment. The comparison would be useful to analyze the hydrophobic force in the bitumen aeration.

It is also suggested to do the measurements in KCl or NaCl solutions for convenient theoretical analysis afterwards. Under a given concentration of KCl or NaCl, it is easy to calculate the Debye length needed to determine the disjoining pressure due to the electrostatic force. Real

commercial processing water used for bitumen extraction in plants contains more than 20 mM NaCl.[3, 4]

5.4.2 Measurement of the Length of the Asphaltene Tails in an Aqueous Solution

In Chapter 3, the theoretical analysis about the disjoining pressure isotherm based on the extended DLVO theory was conducted by fitting the experimental data, where the length of the adlayer (L) of polymers present in bitumen was estimated for the sake of best fitting. It is useful to experimentally measure the adlayer length of polymers on bitumen, asphaltene, and maltene surfaces, respectively, in an aqueous solution under different conditions (*i.e.*, different temperature, pH, electrolyte concentration, *etc.*), in order to 1) confirm experimentally the exposure of asphaltene on bitumen surface by the comparison of the results obtained on above there surfaces; 2) use these values in the fitting process to better understand the hydrophobic force between bitumen and air bubble.

The polymer adlayer length can be conveniently measured using dynamic light scattering technique, also known as photo correlation spectroscopy (PCS), where the hydrodynamic diameter of polymer-covered particles is compared with that of bare particles.[5] Viscometric methods can also be used to determine the polymer tail length.[6] Small angle neutron scattering (SANS) method can be used to determine the polymer segment density distribution.[7]

5.4.3 Measurement of Surface Tension of Maltene and Maltene/water Interfacial Tension at Different Temperatures

As mentioned earlier in Chapter 2, there's lack of data about the surface tension of maltene and interfacial tension between maltene and water at different temperatures. It is therefore recommended to measure those in the future work. The results would be useful for the calculation

of spreading coefficient for the spreading of maltene onto air bubbles and hence provide insights on the mechanisms of the engulfment of bitumen over air bubbles.

There are a number of methods to measure surface or interfacial tension, such as Wilhelmy plate method, pendant drop method, Du Noüy ring method, *etc.*

5.4.4 Thermodynamic Studies on Surface Tension Components of Bitumen and Its Components

There is also lack of data about the surface tension components, *i.e.*, acidic, basic, dispersion, for bitumen, maltene, and asphaltene. Determination of these components would provide useful information to the understanding of the bitumen-air attachment and the engulfment.

5.4.5 Aeration Studies in Micron Size

In the present work, the radius of the air bubble used in the TFPB or BAP technique is around 2 mm, which is much larger than their actual sizes in industry. It was reported that in bitumen recovery process the mean diameter of air bubble in a pilot plant was 216 ± 140 μm, and that of bitumen droplet was about 280 ± 140 μm.[1, 2] It is preferable to do the experiments using bubbles in the size range of that in the pilot plant. It should be noted that although the mean bubble size fell in the mentioned range, bubbles as large as 1000 μm and as small as < 100 μm were also observed.[2] Moran *et al.*[4] used a micropipette technique to study the interaction between bitumen droplets and air bubbles at the 10 μm scale, roughly 10 to 40 μm in diameter.

References

1. Houlihan, R.N., *Unpublished results*, Syncrude Canada Ltd, Edmonton, 1976.
2. Stevenson, P., *Froth Flotation of Oil Sand Bitumen*, in *Foam engineering: fundamentals and applications*, John Wiley & Sons, West Sussex, United Kingdom, 2012.

3. Allen, E.W., *Process water treatment in Canada's oil sands industry: I. Target pollutants and treatment objectives,* Journal of Environmental Engineering and Science. 7(2), p. 123-138, 2008.
4. Moran, K., J. Masliyah, and A. Yeung, *Factors affecting the aeration of small bitumen droplets,* The Canadian Journal of Chemical Engineering. 78(4), p. 625-634, 2000.
5. Baker, J.A. and J.C. Berg, *Investigation of the adsorption configuration of polyethylene oxide and its copolymers with polypropylene oxide on model polystyrene latex dispersions,* Langmuir. 4(4), p. 1055-1061, 1988.
6. Gans, C., et al., *Viscometric determination of the statistical segment length of wormlike polymers,* Polymer. 39(17), p. 4155-4158, 1998.
7. Fleer, G.J., et al., *Polymers at interfaces,* Chapman & Hall, London, 1993.